Fisheries and Oceans Canada | Pêches et Océans Canada
Ecosystems and Oceans Science | Sciences des écosystèmes et des océans

Canadian Science Advisory Secretariat (CSAS)

Research Document 2020/037

Maritimes Region

Optical, Chemical, and Biological Oceanographic Conditions on the Scotian Shelf and in the Eastern Gulf of Maine during 2018

B. Casault, C. Johnson, E. Devred, E. Head, A. Cogswell, and J. Spry

Fisheries and Oceans Canada
Bedford Institute of Oceanography
1 Challenger Drive, PO Box 1006
Dartmouth, Nova Scotia B2Y 4A2

September 2020

Canada

Foreword

This series documents the scientific basis for the evaluation of aquatic resources and ecosystems in Canada. As such, it addresses the issues of the day in the time frames required and the documents it contains are not intended as definitive statements on the subjects addressed but rather as progress reports on ongoing investigations.

Published by:

Fisheries and Oceans Canada
Canadian Science Advisory Secretariat
200 Kent Street
Ottawa ON K1A 0E6

http://www.dfo-mpo.gc.ca/csas-sccs/
csas-sccs@dfo-mpo.gc.ca

ISSN 1919-5044

Correct citation for this publication:

Casault, B., Johnson, C., Devred, E., Head, E., Cogswell, A., and Spry, J. 2020. Optical, Chemical, and Biological Oceanographic Conditions on the Scotian Shelf and in the Eastern Gulf of Maine during 2018. DFO Can. Sci. Advis. Sec. Res. Doc. 2020/037. v + 66 p.

Aussi disponible en français :

Casault, B., Johnson, C., Devred, E., Head, E., Cogswell, A., et Spry, J. 2020. Conditions océanographiques optiques, chimiques et biologiques du plateau néo-écossais et de l'est du golfe du Maine en 2018. Secr. can. de consult. sci. du MPO, Doc. de rech. 2020/037. vi + 70 p.

TABLE OF CONTENTS

ABSTRACT

Ocean nutrient and plankton conditions on the Scotian Shelf and in the eastern Gulf of Maine were assessed in the context of continued mainly warmer than normal surface and near bottom ocean temperatures in 2018, a pattern that started in 2010, and in light of increasing stratification. Overall in 2018, deep nutrient inventories were lower than normal over the entire region of interest, continuing a pattern that started three (for nitrate) to five (for phosphate and silicate) years ago. Anomalies of surface nitrate were negative at the high frequency sampling stations (Halifax-2 and Prince-5) and in the eastern part of the region (Cabot Strait and Louisbourg sections) and positive in the central (Halifax section) and western (Browns Bank section) part. Surface phosphate and silicate anomalies were negative over the entire region. Anomalies of the amplitude and magnitude of the spring phytoplankton bloom, and of the water-column integrated chlorophyll *a*, a proxy for phytoplankton biomass, were mostly positive or near zero in the eastern Scotian Shelf and Cabot Strait, and negative in the central and western Scotian Shelf. Observations in 2018 provide additional evidence for a persistent plankton community change in recent years with lower abundance of large phytoplankton (diatoms), especially in summer, as observed at Halifax-2. Zooplankton biomass and *Calanus finmarchicus* abundance also continued to be mainly lower than normal, while non-copepod abundance was mainly high. The abundance of Arctic *Calanus*, a cold water zooplankton indicator, continued to be lower than normal on the Scotian Shelf, a trend that started in 2013. Above normal abundances of offshore copepods on the Scotian Shelf, particularly *Oithona atlantica* as observed at Halifax-2, suggest a greater influence of offshore waters in recent years. Changes in phytoplankton and zooplankton communities observed in recent years suggest changes in prey fields for planktivorous fish, birds, and mammals and could be associated with changes in the fate of primary and secondary production in the ecosystem.

The Bedford Basin surface temperatures were warmer than normal for 8 of 12 months in 2018, with the warmest September of the time series. Conversely, November and December were the coolest since 2003 and 2007, respectively. The Compass Station phosphate to nitrate ratio continued to match a new regime that has emerged since 2011, likely in response to declining soluble phosphate inputs associated with sewage treatment advancements and Federal laws controlling acceptable phosphate concentrations in detergents.

The 2017 Continuous Plankton Recorder (CPR) data, as reported here, indicate that the annual averages for the Phytoplankton Colour Index (PCI) were close to normal for the Eastern Scotian Shelf (ESS) and Western Scotian Shelf (WSS), while diatom and dinoflagellate abundances were lower, as seen at Halifax-2. Monthly values indicated a late, intense short spring bloom (WSS), as also observed at Halifax-2 in 2017. *Calanus* I–IV (mostly *C. finmarchicus* CI–IV) levels were higher than (ESS) or near (WSS) normal, while *C. finmarchicus* CV–VI levels were near normal (ESS, WSS). Annual abundances of *C. finmarchicus* have been low since 2011 at Halifax-2. The decreases are in CVs in summer/fall, with CPR observations suggesting they are in the sub-surface population. Among the other taxa, most 2017 annual mean abundances were near the 1992–2015 averages, except for *C. hyperboreus* CIII–VI and hyperiid amphipods (higher on ESS) and euphausiids (lower on WSS).

INTRODUCTION

The Atlantic Zone Monitoring Program (AZMP) was implemented in 1998 to enhance Fisheries and Oceans Canada's (DFO's) capacity to understand, describe, and forecast the state of the marine ecosystem (Therriault et al. 1998). The AZMP derives its information on the marine environment and ecosystem from data collected at a network of sampling locations (fixed point, high frequency sampling stations, cross-shelf sections, ecosystem trawl surveys) in each DFO region (Québec, Gulf, Maritimes, and Newfoundland), sampled at a frequency of twice-monthly to once-annually. The sampling design provides basic information on the variability in physical, chemical, and biological properties of the Northwest Atlantic continental shelf on annual and inter-annual scales. Ecosystem trawl surveys and cross-shelf sections provide information about broad-scale environmental variability (Harrison et al. 2005) but are limited in their seasonal coverage. High frequency sampling stations complement the broad-scale sampling by providing more detailed information on annual changes in ocean properties. In addition, the North Atlantic Continuous Plankton Recorder (CPR) survey provides monthly sampling along commercial shipping routes between Reykjavik and the New England coast, via the Scotian Shelf (SS). The CPR sampling extends a dataset started in 1960, allowing present-day observations to be set within a longer time frame. This report provides an assessment of the distribution and variability of nutrients and plankton on the SS and in the eastern Gulf of Maine (GoM), focusing on conditions observed during 2018. It complements assessments for the physical environment of the Maritimes Region (e.g., Hebert et al. 2020) and for the state of the Canadian Northwest Atlantic shelf system as a whole (DFO, 2019).

The SS is located in a transition zone influenced by both sub-polar waters, mainly flowing into the region from the Gulf of St. Lawrence and the Newfoundland Shelf, and warmer offshore waters. The deep-water properties of the western SS exhibit significant shifts in temperature, reflecting changes in the source of deep slope water to the shelf between cold, lower nutrient Labrador Slope Water, and more nutrient rich warm Slope Water that can be driven by changes in large-scale atmospheric pressure patterns (Petrie, 2007). Temperature and salinity on the SS are also influenced by heat transfer between the atmosphere and ocean, local mixing, precipitation, and runoff from land. Changes in the physical pelagic environment influence both plankton community composition and annual biological production cycles, with implications for energy transfer to higher trophic level production. The status of nutrients and plankton in the region in 2018 are reported here in the context of warmer conditions in the marine environment observed in recent years.

METHODS

To the extent possible, sample collection and processing conform to established standard protocols (Mitchell et al. 2002). Non-standard measurements or derived variables are described below.

MISSIONS

AZMP-DFO Maritimes Region sea-going staff participated in three missions (one ecosystem trawl survey and two seasonal cross-shelf oceanographic surveys) during the 2018 calendar year, in addition to day trips to the two high frequency sampling stations. A total of 292 hydrographic station occupations were performed with net samples collected at 215 of the stations (Table 1).

High Frequency Sampling Stations

The Halifax-2 (HL2) and Prince-5 (P5) high frequency sampling stations (Figure 1) were sampled 20 and 12 times, respectively, in 2018, similar to sampling frequencies achieved in recent years. There was no sampling in January at HL2.

The standard sampling suite for the high frequency sampling stations includes the following:

- a Conductivity, Temperature, Depth (CTD; measured using a Sea-Bird instrument) profile with dissolved oxygen, fluorescence, and Photosynthetically Active Radiation (PAR),
- Niskin water bottle samples at standard depths for nutrient analyses, salinity and oxygen calibration, and chlorophyll and accessory pigments analyses,
- Niskin water bottle samples for phytoplankton enumeration,
- vertical ring net tows (202 µm mesh net) for zooplankton biomass (wet and dry weights) and abundance, and
- Secchi depth measurement for light attenuation when possible.

Shelf Sections

The four primary sections (Cabot Strait [CSL]; Louisbourg [LL]; Halifax [HL]; Browns Bank [BBL]; Figure 1), and a number of ancillary sections/stations (gray markers in Figure 2) were sampled in spring and fall (Table 1). Results from the ancillary sections/stations are not reported here.

The standard sampling suite for the section stations is the same as for the high frequency sampling stations as listed above, but phytoplankton are not enumerated. In addition to the standard suite of analyses from water samples, particulate organic carbon is performed at standard depths.

Ecosystem Trawl Surveys

AZMP-DFO Maritimes Region participated in only one primary ecosystem trawl survey in 2018. The usual winter survey on the western SS and Georges Bank (GB) was cancelled due to ship availability. Moreover, the summer survey on the SS and the eastern GoM was shortened in duration and spatial coverage with all sampling occurring west of longitude 63°W (Figure 3). The summer survey was led by the DFO Maritimes Science Population Ecology Division with AZMP participation.

The sampling suite for the ecosystem trawl survey stations includes the measurements listed above for the high frequency sampling stations, but the standard set of water bottle sampling depths is more limited, and vertical ring net tows (202 µm mesh net) are collected at only a subset of stations (Table 1 and Figure 3).

The sum of nitrate and nitrite is reported here as “nitrate.” For the summer ecosystem trawl survey, bottom nitrate concentrations were interpolated on a three-minute latitude-longitude grid using optimal estimation (Petrie et al. 1996) to generate maps of bottom properties within the ecosystem trawl survey strata. The interpolation method uses the three nearest neighbours, with data near the interpolation grid point weighted proportionately more than those farther away. The weighting scheme is described in Petrie and Dean-Moore (1996), with horizontal length scales of 30 km, a vertical length scale of 15 m (for depth <50 m) or 25 m (for depths between 50 and 500 m). Bottom oxygen concentrations were optimally interpolated using the same technique as for nitrate. Oxygen concentrations were measured using a CTD-mounted oxygen sensor, which was calibrated against oxygen concentrations measured by Winkler

titration. Anomalies of bottom oxygen are not presented here, as the quality of oxygen data collected prior to 2015 is under review.

Table 1. Atlantic Zone Monitoring Program sampling missions in the Maritimes Region in 2018.

Group	Location	Mission ID	Dates	# Hydro Stations	# Net Stations
Ecosystem Trawl Survey	Scotian Shelf	TEL2018-023	Jul 14–28	84	16
Seasonal Sections	Scotian Shelf	HUD2018-004	Apr 08–23	83	74
	Scotian Shelf	HUD2018-030	Sep 16–Oct 05	100	100
High Frequency Stations	Halifax-2	BCD2018-666	Jan 01–Dec 31	20(13)[1]	20(13)[1]
	Prince-5	BCD2018-669	Jan 01–Dec 31	12	12
			Total:	*292*	*215*

[1]Total station occupations, including occupations during trawl surveys and seasonal sections (dedicated occupations with mission ID as listed at left are in parentheses).

GEAR DEPLOYMENT

Conductivity, Temperature, Depth

The CTD is lowered to a target depth within 2 m of the bottom.

Standard depths for water samples include:

- High frequency sampling stations:

1. HL2: 1, 5, 10, 20, 30, 40, 50, 75, 100, 140 m,
2. P5: 1, 10, 25, 50, 95 m.

- Seasonal sections: near-surface, 10, 20, 30, 40, 50, 60, 80, 100, 250, 500, 1000, 1500, 2000 m, near-bottom (depths sampled are limited by bottom depth).
- Ecosystem trawl surveys: 5, 25, 50 m, and near bottom when possible.

Net Tows

Ring nets of a standard 202 µm mesh are towed vertically from near bottom to surface at approximately 1 m s^{-1}. In deep offshore waters, the maximum tow depth is 1000 m. Samples are preserved in buffered formalin and analyzed according to the protocol outlined in Mitchell et al. (2002).

DERIVED METRICS

Mixed Layer and Stratification Indices

Two simple indices of the vertical physical structure of the water column are computed:

1. The mixed layer (ML) depth is determined from CTD observations as the minimum depth where the density gradient is equal to or exceeds 0.01 kg m^{-4}.

2. The stratification index (SI) is calculated as:

$$SI\ (kg\ m^{-4}) = (\sigma_{t\text{-}50} - \sigma_{t\text{-}zmin})/(50 - z_{min})$$

where $\sigma_{t\text{-}50}$ and $\sigma_{t\text{-}zmin}$ are interpolated values of density (σ_t) at 50 m and z_{min}, the minimum depth of reliable CTD data, which is typically around 1 or 2 m and always less than approximately 5 m.

Optical Properties

The optical properties of seawater (attenuation coefficient [K_d], euphotic depth [Z_{eu}]) are derived from *in situ* light extinction measurements using a rosette-mounted PAR meter and Secchi disk, according to the following procedures:

1. The downward vertical attenuation coefficient for PAR ($K_{d\text{-}PAR}$) is estimated as the slope of the linear regression of $\ln[E_d(z)]$ versus depth z (where $E_d(z)$ is the value of downward irradiance at depth z) in the depth interval from minimum depth to approximately 50 m. The minimum depth is typically around 2 m, although the calculation is sometimes forced below that target when near-surface PAR measurements appear unreliable.
2. The value of the light attenuation coefficient $K_{d\text{-}Secchi}$ from Secchi disc observations is found using:

$$K_{d\_secchi}\ (m^{-1}) = 1.44 / Z_{sd}$$

where Z_{sd} is the depth (in m) at which the Secchi disc disappears from view (Holmes, 1970).

Estimates of the euphotic depth (Z_{eu}) are obtained using the following expression:

$$Z_{eu}\ (m) = 4.6 / K_d$$

Vertically Integrated Variables

Integrated chlorophyll and nutrient inventories are calculated over various depth intervals (e.g., 0–100 m for chlorophyll, and 0–50 m and 50–150 m for nutrients) using trapezoidal numerical integration. When the maximum depth at a given station is shallower than the lower depth limits noted above, the inventories are calculated by setting the lower integration limit to the maximum depth at that station (e.g., 95 m for P5). Data at the surface (0 m) is taken as the closest near-surface sampled value. Data at the lower depth is taken as:

1. the interpolated value when sampling is below the lower integration limit; or
2. the closest deep water sampled value when sampling is shallower than the lower integration limit.

Phytoplankton Taxonomic Groups

Phytoplankton abundance and taxonomic composition at the high frequency sampling stations are estimated from pooled aliquots of water collected in the upper 100 m using the Utermöhl technique (Utermöhl, 1931).

SATELLITE REMOTE SENSING OF OCEAN COLOUR

Near-surface chlorophyll *a* is estimated from ocean colour data collected by the Sea-viewing Wide Field-of-view Sensor (SeaWiFS) satellite[1] launched by the National Aeronautics and Space Administration (NASA) in late summer 1997, the Moderate Resolution Imaging Spectroradiometer (MODIS) "Aqua" sensor[2] launched by NASA in July 2002 and the Visible Infrared Imaging Radiometer Suite (VIIRS) sensor[3] launched by NASA and the National Oceanic and Atmospheric Administration (NOAA) in October 2011. Here, SeaWiFS data from January 1998 to December 2007, MODIS data from January 2008 to December 2011 and VIIRS data from January 2012 to December 2018 are combined to construct composite time series of surface chlorophyll in selected sub-regions in the Maritimes Region (Cabot Strait [CS], Eastern Scotian Shelf [ESS], Central Scotian Shelf [CSS], Western Scotian Shelf [WSS], Lurcher Shoal [LS], Georges Bank [GB]; Figure 4). The OCx (x = 4, 3M and 3V for SeaWIFS, MODIS, and VIIRS, respectively) band-ratio algorithms are used to derive chlorophyll *a* concentration from remote sensing reflectance as described in O'Reilly et al. (1998) with coefficients of the algorithms for each sensors accessible on NASA's OceanColor Web chlorophyll-a website (accessed on October 2, 2019). Basic statistics (mean, standard deviation) are extracted from semi-monthly composites for the purpose of visualizing the annual cycle and the inter-annual variability of surface chlorophyll for the sub-regions. Characteristics of the spring bloom are estimated from weekly satellite data using the shifted Gaussian function of time model (Zhai et al. 2011). Four metrics are computed to describe the spring bloom characteristics: start date (day of year), cycle duration (days), magnitude (the integral of chlorophyll concentration under the Gaussian curve), and amplitude (maximum minus the background chlorophyll concentration).

ANNUAL ANOMALIES SCORECARDS

Scorecards of key indices, based on normalized, seasonally-adjusted annual anomalies, represent physical, chemical, and biological observations in a compact format. Annual estimates of water column inventories of nutrients, chlorophyll and the mean abundance of key zooplankton species or groups at both the high frequency sampling stations and as an overall average along each of the four standard sections are based on general linear models (R Core Team, 2019) of the form:

$$Density = \alpha + \beta_{YEAR} + \delta_{MONTH} + \varepsilon$$ for the high frequency sampling stations, and

$$Density = \alpha + \beta_{YEAR} + \delta_{STATION} + \gamma_{SEASON} + \varepsilon$$ for the sections.

Density is in units of m^{-2} (or L^{-1} for microplankton abundance), α is the intercept and ε is the error. For the high frequency sampling stations, β and δ are categorical effects for year and month, respectively. For the sections, β, δ *and* γ take into account the effect of year, station and season, respectively.

[1] Information about SeaWiFS sensor can be found on the NASA's OceanColor Web SeaWiFS webpage (accessed on December 2, 2019).

[2] Information about the MODIS sensor can be found on the NASA's OceanColor Web MODIS webpage (accessed on December 2, 2019).

[3] Information about the VIIRS sensor can be found on the NASA's OceanColor Web VIIRS-SNPP webpage (accessed on December 2, 2019).

This approach is also used to calculate annual seasonal estimates of zooplankton indices (i.e., zooplankton biomass and *Calanus finmarchicus* abundance) for the individual sections (spring and fall) and the ecosystem trawl surveys (winter and summer) (e.g., Figures 25–28). In this case, a reduced model including the year and station effects is fitted to the seasonal data subsets. For the ecosystem trawl surveys data, the station term corresponds to the subset of strata that have been sampled in at least ten years since 1999.

Density in terms of zooplankton or phytoplankton abundance is log-transformed [$log_{10}(n+1)$] to normalize the skewed distribution of the observations, and one is added to the *Density* term to include observations for which the value equals zero. Integrated inventories of nutrients, chlorophyll and zooplankton biomass are not log-transformed. An estimate of the least-squares means based on type III sums of squares (Lenth et al. 2019) is used as the measure of the overall year effect.

Annual anomalies are calculated as the deviation of an individual year from the mean of the annual estimates over the period 1999–2015, and expressed either in absolute units or as normalized quantities (i.e., by dividing by the standard deviation of the annual estimates over the same period).

A standard set of indices representing anomalies of nutrient availability, phytoplankton biomass, and the abundance of dominant copepod species and groups (*C. finmarchicus*, *Pseudocalanus* spp., total copepods, and total non-copepods) are produced in each of the AZMP regions, including the Maritimes. To visualize Northwest Atlantic shelf scale patterns of environmental variation, a zonal scorecard including observations from all of the AZMP regions is presented in DFO's science advisory report (DFO, 2019).

ACCESS TO DATA PRODUCTS

Data products presented in Figures 6, 8, 10, 11, 15–18, 21–30 are published on the Government of Canada's Open Government website; a link to the data is available on request to the corresponding author. Chlorophyll semi-monthly estimates and climatologies presented in Figure 19 are available at the DFO Maritimes SeaWiFS FTP website, MODIS FTP website and VIIRS FTP website (all accessed on December 2, 2019).

BEDFORD BASIN MONITORING PROGRAM

The Compass Station (44° 41' 37" N, 63° 38' 25" W) has been occupied weekly as part of the Bedford Basin Monitoring Program since 1992 (Li, 2014). Regular occupations consist of a CTD equipped with a standard suite of sensors (accessed on December 2, 2019) and a vertical net tow for zooplankton identification and enumeration using AZMP protocols. Water samples are collected in Niskin bottles for a variety of analyses (accessed on December 2, 2019) at 2, 5, 10 and 60 m depths. Only zooplankton samples from 1999–2002 and 2012–2017 have been analyzed and archived in a local database; thus, only the CTD sensor and bottle observations are reported in this summary of 2018 conditions.

For ease of interpretation, surface conditions are expressed as the mean conditions at 2, 5 and 10 m. There is a strong seasonal agreement between these depths for the physical and chemical conditions being measured and generally a minor difference in magnitude.

CONTINUOUS PLANKTON RECORDER

The Continuous Plankton Recorder (CPR) is an instrument towed by commercial ships that collects plankton at a depth of approximately 7 m on a long continuous ribbon of silk (approximately 260 µm mesh). The position on the silk corresponds to the location of the

different sampling stations. CPR data are analyzed to detect differences in the surface indices of phytoplankton (colour and relative numerical abundance of large taxa) and zooplankton relative abundance for different months, years or decades in the northwest Atlantic. The indices are used to indicate relative changes in concentration over time (Richardson et al. 2006). The sampling methods from the first surveys in the northwest Atlantic (1960 for the continental shelf) to the present are exactly the same so that valid comparisons can be made between years and decades.

The tow routes between Reykjavik and the GoM are divided into eight regions: WSS, ESS, the south Newfoundland Shelf, the Newfoundland Shelf and four regions in the northwest Atlantic sub-polar gyre, divided into 5 degree of longitude bins (Figure 5). Only CPR data collected on the SS since 1992 are reported here, since these are comparable to AZMP survey results, which date back to 1999. CPR data collected in all regions and all decades (i.e., including the four regions in the sub-polar gyre east of 45° W) are presented in annual Atlantic Zone Offshore Monitoring Program reports (e.g., Yashayaev et al. 2016). In 2017, there was CPR sampling during 10 months on the WSS and ESS.

Monthly abundances of 14 taxa [log10(N+1) transformed] and the phytoplankton colour index (PCI), a semi-quantitative measure of total phytoplankton abundance, are calculated by averaging values for all individual samples collected within either the WSS or ESS region for each month and year sampled. The examined taxa include: the PCI, diatoms and dinoflagellates (phytoplankton), four groups of *Calanus* species/stages, three representative small copepod taxa, two macrozooplankton taxa and three acid-sensitive taxa.

It should be noted that in 2018 the Sir Alister Hardy Foundation for Ocean Science (SAHFOS), the organization that used to run the CPR survey in the North Atlantic, merged with the Marine Biological Association of the UK. The contract was transferred and is continuing with no interruption or changes. Also, in 2018 the format of the sampling time data supplied was changed for the entire dataset, so that sampling times do not reflect local solar cycles, as they used to, but are UTC values. Climatological seasonal cycles are obtained by averaging monthly averages for 1992–2015, and these are compared with values in the months sampled in 2017. Details are presented for three indices of phytoplankton abundance and for the *Calanus* I–IV and *C. finmarchicus* V–VI taxa. Annual abundances and their anomalies are calculated only for years during which there were 8 or more months of sampling, with no gaps of 3 or more consecutive months: conditions that were met in both regions in 2017.

OBSERVATIONS

MIXING AND OPTICAL PROPERTIES

At HL2, the ML is deepest and SI lowest during the winter months when surface heating is weak and wind-driven mixing is strong (Figure 6). The ML shoals in the spring to minimum values from June to August and deepens in the last four months of the year. Similarly, SI increases in the spring to maximum values in August and September and then declines during the fall months. Since SI is calculated using a reference depth of 50 m, low values of the SI typically concur with ML depths deeper than 50 m. Conversely, shallow ML depths (<50 m) correspond to higher SI values that are determined by the strength of the pycnocline below the ML.

In 2018, MLs at HL2 followed the typical seasonal pattern although values were generally shallower than normal throughout the year. The most important departures from the normal conditions were observed in February, April, August, October and November, where the ML depths were shallower than normal by about 10 to 15 m, and in December, where the ML was deeper than normal by about 10 m. In a similar way, the SI also followed the typical seasonal

pattern with values close to normal throughout the year. As expected, the SI was lowest when the ML was deeper or around the 50 m depth, indicating well mixed conditions down to that depth level. The SI was highest in August, which coincided with the shallowest ML. The above normal stratification conditions in August are likely associated to warmer than normal air temperatures and high insolation conditions that prevailed in late July and early August 2018, and that likely resulted in increased surface heating of the water column.

At P5, the ML is typically deeper and more variable and stratification weaker than at HL2 due to strong tidal mixing. The SI normally remains low (below 0.01 kg m^{-4}) for most of the year and ML depths vary from nearly full depth (90 m) in winter to approximately 40 m in summer (Figure 6). In 2018, MLs at P5 were mostly close to normal or deeper than normal, especially in spring, summer and late fall. This also translated as below normal SI values during these periods. The deeper than normal ML observed in June was likely associated with the extensive flooding of the St. John river resulting in freshwater being mixed throughout the water column. SI was highest in August, which also coincided with the shallowest ML, similar to the pattern observed at HL2. This also is likely linked to warm and sunny meteorological conditions that prevailed at that time over most of the Maritimes Region. Note that the October ML depth at P5 was estimated from temperature only as problems were encountered with the conductivity sensor.

In 2018, wind observations at Halifax Airport, a proxy for HL2 station, indicated that the daily maximum wind gusts were mostly above normal throughout the year (Figure 7). Of particular interest was the decrease in wind speed observed in early February, which may have contributed to the increase in stratification (shallower than normal ML and higher than normal SI values observed at HL2 at that time). Similarly, comparatively lower wind speed conditions observed in August also likely contributed to the above normal stratification observed at HL2 at that time. Despite strong wind conditions recorded during the fall, only peak wind values in November appear to have translated into deeper than normal ML, suggesting that other factors (e.g., water intrusion) might have contributed to maintaining the water column stratified in October. Wind observations at Grand Manan, a proxy for P5, mainly followed the climatological pattern throughout the year. Periods of above normal wind speed conditions were observed in March and October without, however, translating into deeper mixing conditions, thus reinforcing the dominant role of tidal mixing in controlling the ML depth at P5. The shallowest ML and highest SI value observed at P5 in August could likely be linked to the lower wind speed conditions observed in August combined with favourable meteorological conditions.

Euphotic depths are generally deepest in the winter months and after the decline of the spring phytoplankton bloom, and they are shallowest during the period of the bloom when light attenuation in the water column is maximal (Figure 8). Z_{eu} depths based on PAR and Secchi disc measurements were mostly variable throughout the winter and spring at HL2 in 2018, and they were generally deeper than normal in summer and fall, especially. The shallowest Z_{eu} was observed in late March/early April, which coincided with the peak of the spring phytoplankton bloom. Conversely, the deepest Z_{eu} was observed in late April/early May, which coincided with the end of the spring phytoplankton bloom.

At P5, Z_{eu} depths are relatively constant year-round since the primary attenuator is non-living suspended matter due to tidal action and continental freshwater input (Figure 8). In 2018, both PAR-based and Secchi-based Z_{eu} were close to or shallower than normal despite lower than normal chlorophyll concentrations observed throughout the year at P5. The deeper than normal Z_{eu} observed in April and June can be associated, respectively, with the delayed start of the spring phytoplankton bloom and the significantly lower than normal surface chlorophyll concentrations observed in June.

NUTRIENTS

The primary dissolved inorganic nutrients (nitrate, silicate, phosphate) measured by the AZMP strongly co-vary in space and time (Petrie et al. 1999). For this reason and because the availability of nitrogen is most often associated with phytoplankton growth limitation in coastal waters of the Maritimes Region (DFO, 2000), this report focuses mainly on variability patterns for nitrate, with information on silicate and phosphate concentrations presented mainly to help interpreting phytoplankton taxonomic group succession at HL2 and P5.

High Frequency Sampling Stations

At HL2, the highest surface nitrate concentrations are observed in the winter when the water column is well mixed and primary production is low (Figure 9). Surface nitrate declines with the onset of the spring phytoplankton bloom, and the lowest surface nitrate concentrations are observed in the late spring through early fall. Deep-water nitrate concentrations are lowest in the late fall and early winter, and they increase from February to August, perhaps reflecting sinking and decomposition of the spring phytoplankton bloom (Petrie and Yeats, 2000).

At the end of 2017, the surface and bottom nitrate inventories were respectively below and above normal (Johnson et al. 2020). By early 2018, both the surface and bottom inventories had reached normal values (Figure 10), which is indicative of upward mixing during that time period. The surface nitrate fell below normal levels during spring, summer and early fall but bounced to above normal in late fall, which was most likely associated with water intrusion as the deep nutrients remained lower than normal and ML depths were mostly shallower than normal during the fall months. Surface nitrate depletion was slightly earlier than normal and coinciding with the onset of the spring phytoplankton bloom (Figure 9). Nitrate depletion conditions also extended deeper than normal in the water column during the spring and summer months, thus contributing to the lower than normal surface nitrate inventory as indicated by an overall negative anomaly (Figure 11). The deep nitrate inventory at HL2 in 2018 was variable in the winter and spring months, but it was below normal in the summer and fall (Figure 10). Pulses of nitrate input were observed in the winter and spring, but the overall bottom nitrate replenishment in the summer months was lower (less intense and shorter in time) than normal, thus contributing to the lower than normal bottom nitrate inventory as reflected by an overall negative anomaly (Figure 11). In parallel with the nitrate conditions, both the surface and deep silicate and phosphate inventories were also below normal at HL2 in 2018 (Figure 11).

The nitrate dynamics at P5 differs considerably from that at HL2 because of the strong tidal mixing combined with the nitrate sources at that station originating mostly from river input and organic matter decomposition. These combined factors contribute to a lower nitrate replenishment of the deep water while maintaining a higher overall surface inventory compared to HL2. The highest nitrate concentrations are observed in the winter and late fall, when the water column is well mixed from surface to bottom (Figure 9). Nitrate concentrations start to decline in the upper water column when the spring phytoplankton bloom starts in April, and the lowest surface nitrate concentrations are typically observed in June and July.

The surface nitrate inventory at P5 in 2018 was mostly below normal in the spring and fall as a result of stronger, deeper and longer than average surface nitrate depletion, with lower than normal concentrations measured in the surface starting as early as mid February and extending beyond mid October when surface replenishment typically occurs (Figure 9). As a result, the overall anomaly for surface nitrate was negative (Figure 11). Similarly, the deep water nitrate inventory at P5 in 2018 was mostly normal or slightly below normal throughout the year (Figure 10) resulting in an overall negative anomaly (Figure 11). Note that the deep water nitrate inventory for the June sampling was not available as the deepest valid nitrate measurement was

taken at approximately 50 m. Again, in parallel with the nitrate conditions, both the surface and deep silicate and phosphate inventories were also below normal at P5 in 2018 (Figure 11).

Broad-scale Surveys

The highest nitrate concentrations on the sections are observed in the deep waters of the Scotian slope, CSL, and deep Emerald Basin (i.e., the deep HL3 station on the shelf portion of the Halifax section) in both spring and fall (Figure 12a and 12b). Surface nitrate concentrations on the sections in spring and fall are strongly dependent on the timing of the sampling relative to the timing of the spring and the fall phytoplankton blooms. In the spring of 2018 (Figure 12a), surface nitrate concentrations were low at all stations on the CSL and LL sections. Examination of the weekly composite images of surface chlorophyll concentrations (not shown here) suggests that spring phytoplankton bloom conditions in the ESS and CS regions had occurred about one and two weeks prior to the occupation of the LL and CSL sections, respectively. The low surface nitrate concentrations were, therefore, indicative of nutrient depleted water resulting from the phytoplankton bloom having occurred earlier. For the HL and BBL sections, low surface nitrate concentrations were observed at the inshore stations (1–5) but relatively higher concentrations were observed at the offshore stations (6–7). Again, the weekly composite surface chlorophyll images suggest that weak bloom conditions were occurring at the time of the occupation of HL and BBL, with lower, pre-bloom phytoplankton levels away from the coast. The large positive nitrate anomalies observed at the offshore stations (6–7) of HL and BBL are thus indicative of low phytoplankton nutrient uptake resulting in surface water not yet nutrient depleted. Spring anomalies of the deep nitrate in the 50–150 m range vary from mostly negative on the CSL section to mostly positive on the BBL section, although important cross-shelf variability is also observed on each section (Figure 12a). Despite high bottom nitrate concentrations (i.e., below 150 m) observed at all deep-water stations, spring anomalies in that depth range were mostly negative for all sections, with the exception of CSL.

In the fall of 2018, low surface nitrate concentrations were observed at all stations of all sections (Figure 12b). All sections were occupied in the second half of September 2018, and the low surface nitrate concentrations observed were mostly representative of pre-fall bloom conditions that precedes nutrients replenishment of surface water. Weekly composite surface chlorophyll images (not shown here) indicated fall bloom conditions having occurred in late September for CS and late October/early November for ESS, CSS and WSS. Anomalies of surface nitrate in the 0–50 m range were mostly negative or weakly negative at most stations of each section. In the 50–150 m range, fall anomalies were variable in sign for CSL, and they were mostly negative for the inshore stations but mostly positive for the offshore stations of HL and BBL. LL displayed an opposite pattern with positive anomalies inshore and negative anomalies offshore (Figure 12b). The highest nitrate concentrations were observed at the deep (i.e., below 150 m) stations of each section with CSL displaying positive anomalies at all stations. For HL and BBL, anomalies were mostly positive at the shelf break but mostly negative further away from the shelf break.

Overall, the annual anomalies of the surface nitrate inventory were negative on CSL and LL and positive on HL and BBL, which, as described above, can be explained by the relative timing of the spring and fall bloom conditions to the occupation of the sections. The annual anomalies of the deep nitrate inventory (i.e., 50–150 m) were negative on all sections in 2018 (Figure 11) as it has been mainly the case since 2016. The surface and deep silicate and phosphate inventories were also below normal at all sections in 2018, with annual anomalies of the deep silicate and phosphate having been mainly negative since 2013.

Due to vessel unavailability, sampling during the 2018 summer ecosystem trawl survey (second half of July) was restricted to locations west of parallel 63º W, which included the western SS,

the eastern GoM and the Bay of Fundy. Anomalies of bottom nitrate concentrations were predominantly negative (Figure 13) over most of the area covered, except for slightly positive anomalies near LaHave Bank and particularly at the shelf break, perhaps indicating the presence of warm nutrient-rich water at that location. Lower than normal bottom nitrate concentrations observed during the summer survey agree with the general pattern observed elsewhere (i.e., sections and fixed stations)

The lowest oxygen saturation levels are typically observed in deep basins and deep slope waters where nutrient concentrations are highest. In July 2018, bottom oxygen saturation values near or below 60% were observed mainly in LaHave Basin and in the slope water south of LaHave Bank (Figure 14) in the central and western part of the SS, respectively.

PHYTOPLANKTON

Although phytoplankton temporal and spatial variability is high in coastal and shelf waters, a recurrent annual pattern including a pronounced diatom dominated spring phytoplankton bloom and smaller secondary summer-fall blooms is observed across the SS. A bloom develops as phytoplankton growth outpaces losses such as grazing and sinking (Behrenfeld and Boss, 2014). Spring bloom initiation is thought to be regulated by the light environment of phytoplankton as well as temperature, starting when the water column stabilizes in late winter/early spring (Sverdrup, 1953). Bloom magnitude is thought to be regulated largely by nutrient supply, and bloom duration is regulated by nutrient supply and, secondarily, by loss processes such as aggregation-sinking and grazing by zooplankton (Johnson et al. 2012).

High Frequency Sampling Stations

In 2018, the timing of the spring bloom initiation at HL2 was normal but the duration was shorter than normal as shown by a rapid decline of chlorophyll concentrations following the peak intensity. The bloom intensity was higher than normal with the highest chlorophyll concentrations recorded in the 40–60 m depth range (Figure 15). Higher than normal chlorophyll concentrations at around 100 m depth observed in late March/early April (Figure 15) coincided with lower than normal nitrate concentrations at that depth and time of the year (Figure 9). The spring bloom was dominated by diatoms although flagellates were briefly higher than normal just prior to the peak bloom intensity (Figure 16). Although not reflected in the integrated chlorophyll inventory, subsurface chlorophyll maxima of relatively low intensity were observed throughout the spring, summer and fall. Weak fall bloom conditions were observed at the surface in late October at HL2 in 2018 (Figure 15). Overall, the integrated chlorophyll anomaly at HL2 in 2018 was slightly positive, owing mostly to the above normal chlorophyll concentrations measured at the peak of the spring bloom (Figure 17). The abundance anomaly of diatoms and dinoflagellates at HL2 was negative or slightly negative in 2018 and generally consistent with the trend started in 2009, while the abundance of ciliates and flagellates was above or near normal in 2018 (Figure 18). Apart from the period leading to the peak of the spring bloom, the abundance of phytoplankton was mostly slightly lower than normal throughout the year (Figure 16). The summer phytoplankton community composition indicated lower than normal relative abundance of diatoms and larger than normal levels of flagellates, which can possibly be linked to the subsurface phytoplankton activity observed throughout the summer. Ciliates were also relatively more abundant for a short period immediately following the peak of the spring bloom and remained slightly more abundant than normal throughout the summer and fall (Figure 16).

The start of the spring phytoplankton at P5 in 2018 was delayed by about a month (perhaps emphasized by the low temporal resolution of monthly sampling), and its intensity was lower than normal as shown by surface chlorophyll concentrations well below normal levels

(Figure 15). Surface chlorophyll concentrations remained lower than normal during the summer months until September where phytoplankton growth was observed below the surface at about 15 m depth, which was representative of a weak late summer bloom occurring one month later than normal. Chlorophyll concentrations remained low throughout the water column over the fall months (Figure 15). Phytoplankton abundance was mostly below or near normal throughout the year, with the exception of two very low abundance levels (Figure 16) recorded during the period of the weak spring bloom in May, and in August when the stratification was much shallower than normal. The phytoplankton community was predominantly composed of diatoms throughout the year and particularly during the May to July bloom period. A larger than normal relative abundance of flagellates was observed in September, coinciding with the observed pulse of phytoplankton biomass below the surface. Ciliates were also relatively more abundant than normal in November and December (Figure 16). Overall, the annual integrated chlorophyll anomaly at P5 in 2018 was negative as a result of weak spring bloom conditions and ensuing low summer chlorophyll concentrations (Figure 17).

The abundance anomaly of diatoms was negative at P5 in 2018 and mostly consistent with the pattern observed during the last ten years, while the abundance anomaly of dinoflagellates and ciliates was positive and consistent with the trend of the last eight years (Figure 18). The abundance of flagellates was slightly below normal due to their quasi-absence in the winter, spring, and summer months (Figure 18 and 16, respectively).

Broad-scale Surveys and Satellite Remote Sensing

Phytoplankton is assessed in a broad-scale sense in terms of the annual integrated chlorophyll inventory from *in situ* sampling on the core sections (Figure 17), the semi-monthly surface chlorophyll estimates from remote sensing (Figure 19), and the spring bloom metrics as fitted from the remote sensing chlorophyll estimates (Figure 20). The annual integrated chlorophyll inventory measured during the 2018 seasonal surveys indicated higher or near normal chlorophyll levels on the eastern sections (CSL, LL) and lower than normal levels on the western sections (HL, BBL) (Figure 17). A similar pattern was also observed in the amplitude and the magnitude of the spring bloom, with the highest positive anomalies in CS and ESS, and the lowest negative anomalies in CSS, WSS and GB (Figure 20). This suggests that the spring bloom magnitude (i.e., a combined measure of intensity and duration) is the main driver of the overall annual chlorophyll inventory. With the exception of GB, this east-west pattern is also shown in the semi-monthly surface chlorophyll estimates going from CS (longest duration with moderate amplitude), to ESS (largest amplitude and average duration), to CSS (average amplitude and duration), to WSS (low amplitude and short duration), and to LS (undiscernible spring bloom) (Figure 19a and 19b).

The semi-monthly surface chlorophyll estimates showed mostly near normal chlorophyll concentrations in all regions during the summer months following the spring bloom, and mostly lower than normal levels during the fall months (Figure 19a and 19b), with consequently lower than normal amplitudes of the fall bloom in all regions.

The normal spring bloom initiation time and shorter duration observed in the CSS sub-region were in agreement with those observed *in situ* at HL2 in 2018 (Figure 15, 19a). However, the amplitude of the bloom estimated from remote sensing data was significantly lower than its *in situ* counterpart due to the deep penetration of the spring bloom as indicated by maximum chlorophyll concentrations occurring below the optical depth of the satellite sensor.

The model fits of the spring bloom amplitude (Figure 20) are typically fairly consistent with the surface chlorophyll estimates (Figure 19a and b). However, inconsistencies in the other bloom metrics are often noticed as, for example, the bloom duration for CS in 2018 (overestimated) or

the bloom initiation for CSS in 2018 (underestimated). This indicates greater uncertainty of the model in detecting the initial increase and the decline of the surface chlorophyll in the context of variable spring blooms, with direct implications on the predicted bloom magnitude as it is a combined measure of intensity and duration.

The low surface chlorophyll annual variability in the tidally mixed LS sub-region is such that bloom conditions are hardly discernable (Figure 19b) and, therefore, the different bloom metrics should be interpreted with caution for that sub-region.

The semi-monthly surface chlorophyll estimates seem to suggest that the fall phytoplankton bloom in the SS sub-regions (i.e., ESS, CSS and WSS) have become less prevalent since 2012 (Figure 19a and 19b), which corresponds with the introduction of the VIIRS sensor. Further investigation is recommended in order to assess whether this phenomenon is real or due to sensor bias.

ZOOPLANKTON

High Frequency Sampling Stations

Zooplankton biomass is presented here in terms of the total wet biomass for zooplankton larger than 0.202 mm and the dry biomass for zooplankton in the size range of 0.202 mm to 10 mm. Consequently, the dry biomass estimates are a close representation of the mesozooplankton size class, while the wet biomass estimates can represent both mesozooplankton and macrozooplankton, including gelatinous plankton. However, as Figure 21 suggests, there is strong similarity in the annual variability pattern of dry and wet biomass at HL2 and P5 stations.

At HL2, zooplankton biomass and total abundance are typically lowest in January and February, and increase to maximum values in April, similar to the spring phytoplankton bloom peak timing, before declining to low levels again in the fall (Figure 21 and 22). In 2018, the zooplankton biomass and the total zooplankton abundance at HL2 were mostly variable (i.e., fluctuating around the climatological mean) in winter, spring and early summer, and below normal in late summer and fall. Overall, the annual mean biomass of mesozooplankton at HL2 in 2018 was below normal (Figure 17).

The zooplankton community was strongly dominated by copepods throughout the year at HL2 (Figure 22). A larger than normal relative abundance of the Cnidaria-Appendicularia group was observed slightly following the spring phytoplankton bloom (consisting mainly of unidentified Siphonophera) and during late fall (consisting mainly of *Aglantha digitale*). The presence of bivalves (Cladocerans-Bivalvia group) and unidentified Polychaeta and *Parasagitta* (Polychaeta-Chaetognatha group) also contributed to the slightly larger relative abundance of these groups as observed in June and July.

At the end of 2017, the abundance of *C. finmarchicus* at HL2 was slightly above normal and the copepodites stage V represented over 95% of the population (Johnson et al, 2020), which contrasts considerably from climatological values. By the beginning of 2018, the abundance of *C. finmarchicus* had dropped to below normal levels with copepodites stage V and VI each representing about 40% of the population (Figure 23). *C. finmarchicus* abundance at HL2 was also mainly lower than normal from spring until late fall (Figure 23). Spring production was slightly earlier than usual (Figure 23). The late summer was characterized by a lower relative abundance of copepodite stage IV and a higher relative abundance of stage CV, while the inverse was observed in the fall months (Figure 23). These changes in the late summer and fall *C. finmarchicus* population appear to be related to changes in water mass properties as discussed later in the document. Overall, the annual mean abundance of *C. finmarchicus* was below normal at HL2 in 2018 (Figure 17).

Since copepods represent the dominant fraction of the total zooplankton abundance, their abundance followed a very similar pattern as the total zooplankton with moderate variability in winter, spring and early summer, and below normal levels in late summer and fall (Figure 24a). The most abundant copepod found at HL2 was *Oithona similis,* which represented 40 to 60% of the total copepod abundance (Figure 24a) throughout the year. The higher than normal copepod abundance levels measured in March were due to high counts of mostly late nauplii stages of *Calanus* and to a lesser extent *Pseudocalanus* (grouped under Others) and, in June, to *Temora longicornis,* as shown in the higher than normal relative abundance of these taxa (Figure 24a). Other noticeable anomalies in the copepod community in 2018 were the lower than normal relative abundances of *Centropages* spp. in fall, the warm water copepod *Paracalanus* spp. in fall, and the deep-water copepod *Microcalanus* spp. and the cold species *Calanus hyperboreus* throughout most of the year. On the other hand, *Oithona atlantica* was relatively more abundant in winter and summer, and *Metridia lucens* was also more abundant in spring and summer but less abundant in fall (Figure 24a). Overall at HL2 in 2018, the annual mean abundance of *Pseudocalanus* spp. was slightly higher than normal, the total copepod abundance was below normal, and the non-copepod abundance was above normal, which, for the latter, has been the case in the last eight years (Figure 17).

At P5, zooplankton biomass and total abundance are typically lowest in January–May and increase to maximum values in July–September, lagging the increase in phytoplankton by about a month, before declining to low levels again in the late fall (Figure 21 and 22). In 2018, zooplankton biomass was lower than normal in winter, spring and fall, and variable during summer. Overall, the annual mean mesozooplankton biomass anomaly was negative in 2018 (Figure 17). The total zooplankton abundance remained at normal or slightly below normal levels throughout the year (Figure 22).

The zooplankton community at P5 was mostly dominated by copepods throughout the year, except for larger than normal relative abundance of other non-copepod groups (mainly unidentified Cirripedia, i.e., barnacles) during the spring, and larger than normal abundance of *Podon leuckartii* (Cladocera+Bivalvia group) during the summer (Figure 22).

The abundance of *C. finmarchicus* at P5 was mainly lower than normal throughout the year except for a few months with higher (June and July) or normal (September) abundances (Figure 23). Overall, the annual mean abundance of *C. finmarchicus* was below normal at P5 in 2018 (Figure 17). *Calanus finmarchicus* was completely absent from samples collected in January and August 2018, at which times a relatively large presence of stage CV would be expected (Figure 23).

The annual pattern of total copepod abundance at P5 in 2018 was similar to that of the total zooplankton abundance, as the zooplankton community is dominated by copepods (Figure 24b). The small copepod *Oithona similis* was the most abundant copepod, and its relative abundance was higher than normal in winter, spring and late fall. Higher than normal relative abundances were also observed for *Paracalanus* spp. and *Eurytemora herdmani* in fall and late summer, respectively. On the other hand, lower than normal relative abundances were observed for *Temora longicornis* in summer and for *Pseudocalanus* spp. in spring and summer (Figure 24b).

Overall at P5 in 2018, the annual abundance anomalies were negative for two dominant copepod taxa, *C. finmarchicus* and *Pseudocalanus* spp., and for total copepods and total non-copepods (Figure 17).

Broad-scale Surveys

The zooplankton biomass was lower than normal on all sections in both spring and fall 2018, except for the LL section where it was higher than normal in the fall. The positive fall anomaly on the LL section was driven mainly by high biomass measured at the shelf break station LL8, while biomass was low at the other stations on LL (Figure 25). As a result, the annual anomalies of the zooplankton biomass were negative on CSL, HL and BBL, but positive on LL, which continued a pattern of generally lower than normal zooplankton biomass as observed in recent years (Figure 17). The zooplankton biomass measured during the 2018 summer ecosystem trawl survey was also below normal, although this assessment may be biased due to the limited spatial coverage achieved on the survey (Figure 26).

The abundance of *C. finmarchicus* was lower than normal on all sections in both spring and fall 2018, except for the HL section where it was higher than normal in the fall. The slightly positive fall anomaly on the HL section was driven by the relatively high abundance of *C. finmarchicus* measured in Emerald Basin at station HL3 (Figure 27). On an annual basis, though, the resulting abundance anomalies for *C. finmarchicus* were negative on all sections and continued a pattern of generally lower than normal abundance as observed since 2011 for most sections (Figure 17). Similarly, the abundance of *C. finmarchicus* was also below normal during the 2018 summer ecosystem trawl survey (Figure 28).

The annual abundance anomaly for *Pseudocalanus* spp. was negative for HL but slightly positive or near zero for the other sections in 2018 (Figure 17). Negative annual anomalies for the total copepod abundance were observed on all sections in 2018, especially on HL, while the total non-copepod abundance was above or near normal on all sections (Figure 17). Among the ten most abundant non-copepod groups, abundance anomalies in 2018 were positive or near normal for eight groups (larvaceans, gastropods, chaetognaths, polychaetes, bivalves, echinoderms, Cirripedia, and amphipods), and they were negative for euphausiids and especially ostracods. The ostracods (deep water crustaceans) abundance was particularly strongly below normal for a fourth year in a row (Figure 29). Overall, though, this is in general agreement with the trend of higher abundance of non-copepods observed in recent years (Figure 17).

Indicator Species

Indicator species provide insights into the response of the copepod community to changes in water mass properties. Arctic *Calanus* species (*Calanus hyperboreus* and *Calanus glacialis*) were mostly less abundant than normal throughout the region in 2018. The only exception was on the Cabot Strait section where the positive anomaly was due to higher than normal abundance of *C. glacialis* in the spring sampling. With the exception of CSL, the lower than normal abundance of Arctic *Calanus* species is a continuation of the trend that started in 2012 (Figure 30). In contrast, warm offshore copepod species (*Clausocalanus* spp., *Mecynocera clausi*, and *Pleuromamma borealis*) were mostly more abundant than normal throughout the region in 2018. Negative anomalies were observed on CSL and BBL due mainly to the lower than normal abundance of *Clausocalanus* species at CSL in spring (no occurrence) and fall, and lower than normal abundance of *Mecynocera clausi* and *Pleuromamma* species at BBL, particularly in fall. Again, the mainly higher than normal abundance of warm offshore copepod species mostly continues a trend that started in 2012 (Figure 30). Abundance anomalies of warm shelf copepod species (the summer–fall copepods *Paracalanus* spp. and *Centropages typicus*) were positive throughout the region in 2018. Although a temporal pattern is difficult to discern in the abundance anomalies of the warm shelf species, the anomalies in 2018 appear to increase from east (CSL) to west (P5), perhaps indicative of a similar temperature gradient along the same path.

DISCUSSION

Ocean monitoring observations during 2018 indicate a continuation of plankton community changes that started around 2010 on the SS, associated with above-average ocean temperatures and strong sub-annual variability in the physical environment. Changes in the pelagic environment have been characterized by mainly negative anomalies of deep silicate and phosphate concentrations since 2013 and deep nitrate concentrations since 2016. Changes in the plankton community have been characterized by mainly negative anomalies in diatom and other large phytoplankton abundances since 2009, zooplankton biomass since 2010, *C. finmarchicus* abundance since 2011, and Arctic *Calanus* abundance since 2012, while abundance anomalies of warm offshore copepods and non-copepods have been mainly positive in the central and western part of the region since 2012.

In the Maritimes Region, the SS is characterized by a strong seasonal cycle of temperature and stratification associated with longitudinal and cross-shelf gradients resulting from cold fresh waters advected onto the inshore ESS from the Gulf of St. Lawrence in the northeast and the intrusion of warm and salty slope waters onto the WSS and CSS in the southwest (Hebert et al. 2020). Ocean temperatures on the SS and in the GoM have exhibited strong inter-decadal variability since the 1950s, with recent years (2010–2018) consistently warmer than the long term average over that period (Hebert et al. 2020). The Maritimes Region composite temperature index, which includes 18 ocean temperature time series from surface to bottom in several sub-regions, indicated that above average temperatures were recorded at almost all locations and all depths in 2018. Sea surface temperature anomalies were positive for most areas of the SS and the GoM in 2018 though lower than in 2016 and 2017. Sea surface temperatures were particularly warmer than normal during the months of August to October across the region, likely in response to above normal air temperatures recorded at all coastal sites in the SS and the GoM in the July–September period. Bottom temperatures measured during the summer ecosystem trawl survey were also above average in the WSS, the eastern GoM, and the Bay of Fundy. Ocean stratification, which has shown an increasing trend on the SS since the 1950s driven both by warmer temperatures and lower salinity, was slightly below the 1981–2010 average in 2018 (Hebert et al. 2020).

The nutrient environment on the SS is influenced directly or indirectly by water inputs from upstream, for example the Labrador Current and the outflow from the Gulf of St. Lawrence, as well as by intrusions of Slope Water and Gulf Stream meanders (Pepin et al. 2013). Surface nutrients display a strong seasonality associated with phytoplankton production with larger production typically associated with surface nutrient depletion. Deep nutrients, on the other hand, provide a better representation of the nutrient pool available for primary production. Pepin et al. (2013) reported below-average concentrations of all deep nutrients on the SS in the years leading to 2010, with a low level of variability that was deemed uncharacteristic for the area. Deep nutrients were below normal across the region in 2018, continuing a pattern of low concentrations observed over the last three to five years. The recent shift in deep nutrients inventory is likely linked to changes in shelf circulation as well as changes in the Gulf Stream transport. A decrease in the deep nutrient concentrations coupled with the observed increase in stratification on the SS (Hebert et al. 2020) could imply a lower productivity and potential impacts on the structure and functioning of the food web.

In ocean regions where annual-scale environmental variability is a dominant frequency, plankton life history, behavior and physiology provide adaptations that focus reproductive effort on favorable times of year and minimize exposure to risk at unfavorable times of year. However, unpredictable perturbations in the range of environmental seasonality and in seasonal timing can disrupt these adaptations (Greenan et al. 2008; Mackas et al. 2012). Large scale shifts in water mass boundaries also influence local plankton community composition (e.g., Keister et al.

2011). In the spring, the spring phytoplankton bloom develops under favourable conditions of increased insolation, warming temperature and water column stratification. However, Ross et al. (2017) observed spring blooms on the SS when stratification is at its lowest, water temperature at its coldest, and surface mixed layer still much deeper than the euphotic depth, which is in apparent contradiction of the critical depth hypothesis. Phytoplankton biomass declines after the bloom peak as grazing increases or growth becomes nutrient limited. In summer, sporadic occurrence of deep chlorophyll *a* maxima reflects intrusion of nutrient-rich deep water as a result of physical forcing.

The spring phytoplankton bloom at HL2 in 2018 was initiated in late February when the surface water temperature was near its minimum, which is not unusual for the CSS (Shadwick et al. 2011). The phytoplankton bloom was particularly intense in the 30–70 m layer due to a combination of a deeper than normal euphotic depth and an influx of warm and salty water likely carrying extra nutrients. The spring bloom was typically dominated by diatoms followed by a succession of dinoflagellates, as well as ciliates and flagellates for which the higher abundance is consistent with the pattern observed in the last six to ten years in the phytoplankton community at HL2. A shift toward smaller phytoplankton assemblages could be associated with warmer ocean conditions on the SS, as has been observed in other areas of the ocean (Doney et al. 2012). Episodic subsurface chlorophyll events were observed throughout the summer, although summertime biomass is typically dominated by small cell assemblages for which chlorophyll is a poor proxy of the phytoplankton biomass (Craig et al. 2015). These subsurface chlorophyll maxima follow the nitracline and occur at a depth where both light and nutrient can sustain new production. Ross et al. (2017) suggest that a subsurface phytoplankton layer made of small cells (nano- and picophytoplankton) is persistent throughout the summer and contributes to a significant portion of the annual primary production on the SS.

Strong tidal mixing at P5 affects the nutrient and phytoplankton dynamics in different ways. Mixing is responsible for the upward flux of nutrients toward the surface allowing high nutrient levels to be maintained throughout the year. Intense mixing also affects the turbidity of the water column resulting in euphotic depths that are much shallower than the mixed layer depth. As a result, primary production occurring in the surface layer is diluted down in the water column. The nutrient rich surface water also promotes the growth of diatoms, which overwhelmingly dominate the phytoplankton community structure at that station. The phytoplankton bloom at P5 in 2018 started to develop in early May in response to higher than normal light availability coupled with the gradual warming of the water column. A transient drop in phytoplankton biomass in June was likely due to freshwater input resulting from extensive flooding of the St. John river. The typical annual cycle observed at P5 suggest that temperature and light availability are critical variables regulating the start and the end of the phytoplankton growth period. Similar to HL2, the shift toward below normal abundance of diatoms and above normal abundance of dinoflagellates and ciliates is consistent with warmer than normal conditions observed at P5 since 2010 (Hebert et al. 2020).

Zooplankton biomass on the SS and in the eastern GoM is normally dominated by large, energy-rich copepods, mainly *C. finmarchicus*, which are important prey for planktivorous fish such as Herring and Mackerel, North Atlantic Right Whales, and other pelagic species. In 2018, the zooplankton community continued to be characterized by lower than normal abundances of *C. finmarchicus*, lower than normal zooplankton biomass, and higher than normal abundance of non-copepods across most of the region. Total copepods were also less abundant across the region in 2018. Shifts in the abundance of copepod groups that are indicators of water mass distributions in the region, including Arctic *Calanus* (mainly lower) and warm offshore copepods (mainly higher), in recent years are consistent with a greater influence of offshore water on the CSS and WSS. In contrast to more northern areas of the Canadian Northwest Atlantic shelf

system where abundances of *Pseudocalanus* spp., smaller spring–summer copepods that are also important prey for small fish, have increased coincident with declines in *C. finmarchicus* abundance (DFO, 2019), *Pseudocalanus* spp. were mixed in the Maritimes Region, with low abundances on the CSS and WSS. These observations reinforce the evidence of community change within the zooplankton population in general, and particularly within the copepod population with a shift toward lower dominance of *C. finmarchicus* in the region.

The population response of *C. finmarchicus* to environmental changes is complex due to interactions among transport by ocean circulation, annual primary production cycles, and the *Calanus* life history, which focuses reproductive effort on spring bloom production of diatoms and can include a period of late-juvenile-stage dormancy in deep water during less productive seasons. Winter abundance level of *C. finmarchicus* is an indicator of initial conditions for production, while late fall abundance level is an indicator of the overwintering stock for production in the following year.

At HL2, a drop in *C. finmarchicus* abundance coupled with a shift in *C. finmarchicus* composition from mostly CV to CIV–CVI stages between late 2017 (Johnson et al. 2020) and early 2018 suggest mortality losses in the overwintering stock and the emergence of adults from dormancy during that period. The active production period as characterized by the development of early stages CI–CIII was fairly synchronized with the spring phytoplankton bloom, and the high abundance of *C. finmarchicus* at the end of the spring bloom suggests that grazing pressure (i.e., top-down control) might have contributed to the earlier than normal end of the bloom in 2018. The post-bloom period was characterized by a succession of smaller copepods, with higher than normal relative abundance of *M. lucens* (mid April to mid August), *T. longicornis* (mid June to mid July), and *O. atlantica* (mid July to mid September), thus reinforcing a shift in copepods dynamics at HL2 and possibly on a broader scale. Changes in water properties influenced the *C. finmarchicus* dynamics at HL2 as shown by the unusual dominance of stage V in August/September likely associated with warm surface temperatures observed at that time, and by an unusual high relative abundance of stage CIV in the fall associated with cooler (at surface) and fresher (below 50 m) than normal water (Hebert et al. 2020). The overall abundance of *C. finmarchicus* at the end of 2018 was considerably lower than normal with a lower than normal combined proportion of late stage CV and CVI having entered dormancy period.

The overall abundance of *C. finmarchicus* at P5 is considerably lower than at HL2 throughout the year, which might suggest a different food web structure at that station. The *C. finmarchicus* abundance was extremely low (around 500 individuals/m^2) throughout the fall of 2017 resulting in a low overwintering stock (Johnson et al. 2020) and *C. finmarchicus* abundance level below the detection limit permitted by the analysis in early 2018. The start of the active production period in April coincided with the weak spring phytoplankton bloom, but the *C. finmarchicus* abundance only peaked about one month later than the maximum bloom intensity. As observed at HL2, grazing pressure in June (time of the highest *C. finmarchicus* abundance) might have contributed to the end of the spring bloom. *Calanus finmarchicus* was also absent from sampling in August, which coincided with a column-deep shift to warmer temperatures observed in August and September. This warming up of the water column also appeared to have resulted in higher relative abundance of *Eurytemora* as well as warm water *Centropages* and *Paracalanus* species. The overwintering stock of *C. finmarchicus* at P5 at the end of 2018 was low and mostly composed of late stage CV.

As warm ocean conditions persist in the Maritimes Region, there is increasing evidence of a shift in both phytoplankton and zooplankton communities away from the dominance of large phytoplankton cells and large, energy rich copepods like *C. finmarchicus* and toward smaller phytoplankton and copepod species and particle-feeding, opportunistic non-copepod species

such as larvaceans, pelagic gastropods, and thaliaceans. Since “classical” type food webs dominated by diatoms and *C. finmarchicus* are associated with higher transfer efficiency of energy to higher trophic level pelagic animals than are food webs dominated by small phytoplankton cells and small zooplankton taxa, this shift may indicate a change to less productive conditions for planktivorous fish, North Atlantic Right Whales, and pelagic-feeding seabirds in the Maritimes Region.

BEDFORD BASIN MONITORING PROGRAM

PHYSICAL CONDITIONS

Surface water temperature conditions in 2018 were near normal (+0.28 standard deviation [sd]) compared to the reference period 2000-2015 (Figure 31). Salinity, density and stratification annual conditions were also near normal. Monthly anomalies for surface temperature in 2018 were warmer than normal for 8 of the 12 months (Figure 32). Conditions from Feb–May were above normal, followed by a cooler than normal June. Jul–Oct were warmer than normal, with the warmest September of the time series (+2.21 sd) (Figure 32). Half way through October, a series of strong storms pushed through the region, ending 8 consecutive weeks of positive anomalies (Figure 33) and ushering in the coolest November and December since 2003 and 2007 respectively (-1.54 and -2.00 sd) (Figure 32).

Bottom conditions are generally stable within the basin unless otherwise perturbed by periodic intrusions of shelf water (Kerrigan et al. 2017). In 2018, temperature conditions at 60 m were the third warmest of the time series (Figure 34) and the warmest since 2012, and salinity and density were above normal for the first time since 2009. This ends the trend of negative or near normal annual bottom salinity and density anomalies going back to 2010 (Figure 34). These warmer than normal bottom conditions persisted throughout the year, with the warmest April on record for the time series (+2.13 sd) (Figure 35). Conditions at 60 m were the most saline since 2006 (+1.02 sd) (Figure 34) and remained above normal throughout the year (Figure 36).

NUTRIENTS AND PLANKTON CONDITIONS

Both surface and bottom annual anomalies for particulate organic carbon and nitrogen were below normal, and chlorophyll was at or slightly below normal (Figure 31 and 34). Surface nitrate and silicate annual anomalies ended their trend of negative values in 2018 (+0.50 and +0.11 sd) (Figure 31), while nitrite, ammonia, and phosphate remained below normal (-0.52, -0.55, and -1.17 sd). The conditions at 60 m were similar, with positive nitrate and silicate anomalies (+0.72 and +0.77 sd) and negative nitrite, ammonia and phosphate anomalies (-0.38, -0.94, and -0.61 sd) (Figure 34). Surface and bottom phosphate continues the trend of below average concentrations since 2010 (Figure 31 and 34), a phenomenon described previously in Johnson et al. (2020).

CONTINUOUS PLANKTON RECORDER

PHYTOPLANKTON

On the ESS and WSS, monthly PCI values and diatom abundances show the spring bloom occurring in March–April, with low values in summer (Figure 37). In fall and winter the PCI is low, but diatom abundance increases over the fall, remaining relatively high in winter. Dinoflagellate abundance shows no clear seasonal cycle in either region. In 2017, PCI monthly averages were generally close normal in both regions, but they were lower than normal in March and higher than normal in April. Diatom monthly abundances were unusually low in

January and February and between September and November on the WSS, but generally near normal on the ESS. The CPR observations for the WSS were they were generally consistent with *in situ* observations at Halifax-2 in 2017, where the spring bloom was found to be delayed, short and intense, and dominated by diatoms. Monthly dinoflagellate values in 2017 were close to normal for the first six month of the year and below normal (WSS) or variable (ESS) during the second.

Consistent with *in situ* observations at Halifax-2, annual abundance anomalies for diatoms and dinoflagellates were negative for the WSS and slightly negative for the ESS in 2017 (Figure 38). PCI annual anomalies were slightly positive for the WSS and ESS, possibly linked to the slightly positive anomaly for flagellate abundance at Halifax-2.

ZOOPLANKTON

CPR-derived climatological seasonal cycles for *Calanus* I–IV (mostly *C. finmarchicus*) and *C. finmarchicus* CV–VI have broad spring-summer (April–July) peaks in abundance on the WSS. On the ESS, there is a low level spring peak for *Calanus* CI–IV but not for *C. finmarchicus* CV–VI (Figure 39). In 2017, monthly abundances of *Calanus* CI–IV were above the 1992–2015 monthly averages in February–March on the WSS and in May–July on the ESS, and relatively low (fall) or close to normal in both regions during the other months. In both regions, *C. finmarchicus* CV–VI monthly abundances were mostly near normal but relatively low in September–November. The annual average abundance anomaly for *Calanus* CI–IV was positive for the ESS in 2017 but close to normal on the WSS, and *C. finmarchicus* CV–VI annual abundance anomalies were close to normal in both regions (Figure 38). Year-round *in situ* vertical net tow sampling at Halifax-2 has indicated low *C. finmarchicus* abundances compared with the 1999–2010 average values since 2011 (Johnson et al. 2020). This decrease is due to decreasing abundances of CVs, and since no such decrease is seen in the CPR levels of CV–CVI, it appears that it is occurring in the sub-surface portion of the CV population (Head et al. unpublished report[4]). This idea is further supported by the fact that the decrease in CV abundance is occurring mainly during the second half of the year, when most of the CVs are at depth.

Among the other taxa, most annual average abundances were near their 1992–2015 averages, except those for *C. hyperboreus* CIII–VI and hyperiid amphipods, which were higher than normal on the ESS, and those for euphausiids, which were lower than normal on the WSS.

ACID SENSITIVE ORGANISMS

In 2017, the annual average abundance anomalies of the three acid sensitive taxa (coccolithophores, foraminifera, and pteropods, mainly *Limacina* spp.) were near normal on both the ESS and the WSS (Figure 38), suggesting that these organisms have not been greatly affected by pH changes to date.

SUMMARY

- Observations in 2018 provided evidence that changes in the plankton community observed in recent years have persisted, perhaps as a response to change in nutrients availability and physical forcing. These changes are likely to alter the fate of production in the ecosystem,

[4] Head, E.J.H., Johnson, C.J., Pepin, P. 2019. Plankton monitoring in the Northwest Atlantic: a comparison of zooplankton data collected in Vertical Net Tows and by the Continuous Plankton Recorder on the Scotian and Newfoundland shelves, 1999–2016.

with negative impacts already observed in feeding habitat for specialized planktivores such as North Atlantic Right Whales.

- In 2018, both surface and deep silicate and phosphate inventories were mainly lower than average. This follows a trend since 2014 on the SS and since 2016 on the CSL section. Deep nitrate inventories were also below average across the region.
- Phytoplankton spring blooms observed with satellite remote sensing were well defined and fairly strong in the eastern part of the Maritimes Region (CS, ESS and CSS) but weaker in the western part (WSS, LS and GB). A deep, short and intense spring bloom, which would not be visible to the satellites, was again observed at HL2.
- Zooplankton biomass and *C. finmarchicus* abundance were mainly lower than average, while non-copepod abundance was mainly higher than average, continuing a pattern that started around 2011–2012.
- Copepod indicator species abundance patterns continued a trend that started in 2012 with warm-water offshore species more abundant than average and cold water immigrant species less abundant on the SS in 2018.
- In 2017, CPR observations indicated that annual average abundances for diatoms and dinoflagellates were lower than normal on the WSS and close to normal on the ESS, while the PCI was at near normal levels in both regions.
- In 2017, CPR observations indicated that annual abundance anomalies for the *Calanus* copepodite I–IV taxon (mostly *C. finmarchicus* CI–IV) were positive (ESS) or near normal (WSS), while *C. finmarchicus* CV–VI annual average abundances were near normal in both regions. Among the other taxa, *C. hyperboreus* CIII–VI and hyperiid amphipods abundances were higher than normal on the ESS, while euphausiids abundance was lower than normal on the WSS.
- Surface temperatures in Bedford Basin were warmer than normal throughout much of 2018 (8 of 12 months), with the warmest September in the time series; however, November and December surface temperatures were the lowest since 2003 and 2007, respectively, and the second lowest for both months over the time series.
- Average annual bottom temperatures in Bedford Basin were the third warmest of the time series and the warmest since record warm conditions in 2012.

ACKNOWLEDGEMENTS

The authors thank the sea-going staff of the Bedford Institute of Oceanography and St. Andrews Biological Station, the chief scientist on the ecosystem trawl survey mission, Don Clark, and the officers and crew of the Canadian Coast Guard ships *Hudson*, S*igma-T*, *Teleost*, *Viola M. Davidson*. Jay Barthelotte, Mélany Belzile, Robert Benjamin, Jay Bugden, Diana Cardoso, Carla Caverhill, Terry Cormier, Jennifer Field, Jack Fife, Jason Green, Adam Hartling, Dave Hebert, Flo Hum, Jeff Jackson, Matt Lawson, Chantelle Layton, Dave Levy, Kevin MacIsaac, Kevin Pauley, Cathy Porter, Tim Perry, Marc Ringuette, Jackie Spry, Peter Thamer and Dan Wood contributed to sample collection, sample analysis, data analysis, data management, and data sharing. Reviews by David Bélanger and Stéphane Plourde improved the manuscript.

REFERENCES CITED

Behrenfeld, M.J., and Boss, E.S. 2014. Resurrecting the Ecological Underpinnings of Ocean Plankton Blooms. Annu. Rev. Mar. Sci. 6: 167–194.

Craig, S.E., Thomas, H., Jones, C.T., Li, W.K., Greenan, B.J., Shadwick, E.H., and Burt, W.J., 2015. The effect of seasonality in phytoplankton community composition on CO2 uptake on the Scotian Shelf. J. Mar. Syst. 147:52–60.

DFO. 2000. Chemical and Biological Oceanographic Conditions in 1998 and 1999 – Maritimes Region. DFO Sci. Stock Status Rep. G3-03 (2000).

DFO. 2019. Oceanographic Conditions in the Atlantic Zone in 2018. DFO Can. Sci. Advis. Sec. Sci. Advis. Rep. 2019/034.

Doney, S.C., Ruckelshaus, M., Duffy, J.E., Barry, J.P., Chan, F., English, C.A., Galindo, H.M., Grebmeier, J.M., Hollowed, A.B., Knowlton, N., Polovina, J., Rabalais, N.N., Sydeman, W.J., and Talley, L.D. 2012. Climate change impacts on marine ecosystems. Annu. Rev. Mar. Sci. 2012. 4:11–37.

Greenan B.J.W., Petrie B.D., Harrison W.G., and Strain P.M. 2008. The onset and evolution of a spring bloom on the Scotian Shelf. Limnol. Oceanogr. 53.

Harrison, G., Colbourne, E., Gilbert, D., and Petrie, B. 2005. Oceanographic Observations and Data Products Derived from Large-scale Fisheries Resource Assessment and Environmental Surveys in the Atlantic Zone. AZMP/PMZA Bull. 4: 17–23.

Hebert, D., Pettipas, R., and Brickman, D. 2020. Physical Oceanographic Conditions on the Scotian Shelf and in the Gulf of Maine during 2018. DFO Can. Sci. Advis. Sec. Res. Doc. 2020/036. iv + 52 p.

Holmes, R.W. 1970. The Secchi Disk in Turbid Coastal Waters. Limnol. Oceanogr. 15(5): 688–694.

Johnson, C., Devred, E., Casault, B., Head, E., and Spry, J. 2020. Optical, Chemical, and Biological Oceanographic Conditions on the Scotian Shelf and in the Eastern Gulf of Maine in 2017. DFO Can. Sci. Advis. Sec. Res. Doc. 2020/002. v + 66 p.

Johnson, C., Harrison, G., Head, E., Casault, B., Spry, J., Porter, C., and Yashayaeva, I. 2012. Optical, Chemical, and Biological Oceanographic Conditions in the Maritimes Region in 2011. DFO Can. Sci. Advis. Sec. Res. Doc. 2012/071.

Keister, J.E., Di Lorenzo, E., Morgan, C.A., Combes, V., and Peterson, W.T. 2011. Zooplankton species composition is linked to ocean transport in the Northern California Current. Global Change Biol. 17: 2498–2511.

Kerrigan, E.A., Kienast, M., Thomas, H., and Wallace, D.W.R. 2017. Using oxygen isotopes to establish freshwater sources in Bedford Basin, Nova Scotia, a Northwestern Atlantic fjord. Estuar. Coast. Shelf. Sci. 199, pp. 96–04.

Lenth, R., Singmann, H., Love, J., Buerkner, P., and Herve, M. 2018. emmeans: Estimated Marginal Means, aka Least-Squares Means. R package version 1.3.4.

Li, W.K.W. 2014. The state of phytoplankton and bacterioplankton at the Compass Buoy Station: Bedford Basin Monitoring Program 1992–2013. Can. Tech. Rep. Hydrogr. Ocean Sci. 304.

Mackas, D.L., Greve, W., Edwards, M., Chiba, S., Tadokoro, K., Eloire, D., Mazzocchi, M.G., Batten, S., Richardson, A.J., Johnson, C., Head, E., Conversi, A., and Pelosi, T. 2012. Changing zooplankton seasonality in a changing ocean: Comparing time series of zooplankton phenology. Progr. Oceanogr. 97–100: 31–62.

Mitchell, M., Harrison, G., Pauley, K., Gagné, A., Maillet, G., and Strain, P. 2002. Atlantic Zonal Monitoring Program Sampling Protocol. Can. Tech. Rep. Hydrogr. Ocean Sci. 223.

O'Reilly, J.E., Maritorena, S., Mitchell, B. G., Siegel, D. A., Carder, K. L., Garver, S. A., Kahru, M., and McClain, C. R. 1998. Ocean Color Chlorophyll Algorithms for SeaWiFS. J. Geophys. Res. 103, 24937–24953.

Pepin, P., Maillet, G.L., Lavoie, D., and Johnson, C. 2013. Temporal trends in nutrient concentrations in the Northwest Atlantic basin. Ch. 10 (p. 127–150) In: Aspects of climate change in the Northwest Atlantic off Canada [Loder, J.W., G. Han, P.S. Galbraith, J. Chassé and A. van der Baaren (Eds.)]. Can. Tech. Rep. Fish. Aquat. Sci. 3045: x + 190 p.

Petrie, B. 2007. Does the North Atlantic Oscillation Affect Hydrographic Properties on the Canadian Atlantic Continental Shelf? Atmos. Ocean 45(3): 141–151.

Petrie, B., and Dean-Moore, J. 1996. Temporal and Spatial Scales of Temperature and Salinity on the Scotian Shelf. Can. Tech. Rep. Hydrogr. Ocean Sci. 177.

Petrie, B., and Yeats, P. 2000. Annual and Interannual Variability of Nutrients and Their Estimated Fluxes in the Scotian Shelf – Gulf of Maine Region. Can. J. Fish. Aquat. Sci. 57: 2536–2546.

Petrie, B., Drinkwater, K., Gregory, D., Pettipas, R., and Sandström, A. 1996. Temperature and Salinity Atlas for the Scotian Shelf and the Gulf of Maine. Can. Data. Rep. Hydrog. Ocean Sci. 171

Petrie, B., Yeats, P., and Strain, P. 1999. Nitrate, Silicate and Phosphate Atlas for the Scotian Shelf and the Gulf of Maine. Can. Tech. Rep. Hydrogr. Ocean Sci. 203.

R Core Team. 2019. R: A language and environment for statistical computing. R Foundation for Statistical Computing, Vienna, Austria.

Richardson, A.J., Walne, A.W., John, A.W.G., Jonas, T.D., Lindley, J.A., Sims, D.W., Stevens, D., and Witt, M. 2006. Using Continuous Plankton Recorder Data. Progr. Oceanogr. 68: 27–74.

Ross, T., Craig, S.E., Comeau, A., Davis, R., Dever, M., and Beck, M. 2017. Blooms and subsurface phytoplankton layers on the Scotian Shelf: Insights from profiling gliders. J Marine Syst, 172, 118–127.

Shadwick, E.H., Thomas, H., Azetsu-Scott, K., Greenan, B.J.W., Head, E., and Horne, E., 2011. Seasonal variability of dissolved inorganic carbon and surface water pCO2 in the Scotian Shelf region of the Northwestern Atlantic. Mar. Chem. 124, 23–37.

Sverdrup, H.U. 1953. On Conditions for the Vernal Blooming of Phytoplankton. J. Cons. Perm. Int. Explor. Mer. 18: 287–295.

Therriault, J.-C., Petrie, B., Pepin, P., Gagnon, J., Gregory, D., Helbig, J., Herman, A., Lefaivre, D., Mitchell, M., Pelchat, B., Runge, J., and Sameoto, D. 1998. Proposal for a Northwest Atlantic Zonal Monitoring Program. Can. Tech. Rep. Hydrogr. Ocean Sci. 194.

Utermöhl, von H. 1931. Neue Wege in der quantitativen Erfassung des Planktons. (Mit besondere Beriicksichtigung des Ultraplanktons). Verh. Int. Verein. Theor. Angew. Limnol., 5**,** 567–595.

Yashayaev, I., Head, E.J.H., Azetsu-Scott, K., Devred, E., Ringuette, M, Wang, Z., and Punshon, S. 2016. Environmental Conditions in the Labrador Sea during 2015. NAFO SCR Doc. 16/018. Serial N6559. 34 p.

Zhai, L., Platt, T., Tang, C., Sathyendranath, S., and Hernández Walls, R. 2011. Phytoplankton Phenology on the Scotian Shelf. ICES J. Mar. Sci. 68:781–791.

FIGURES

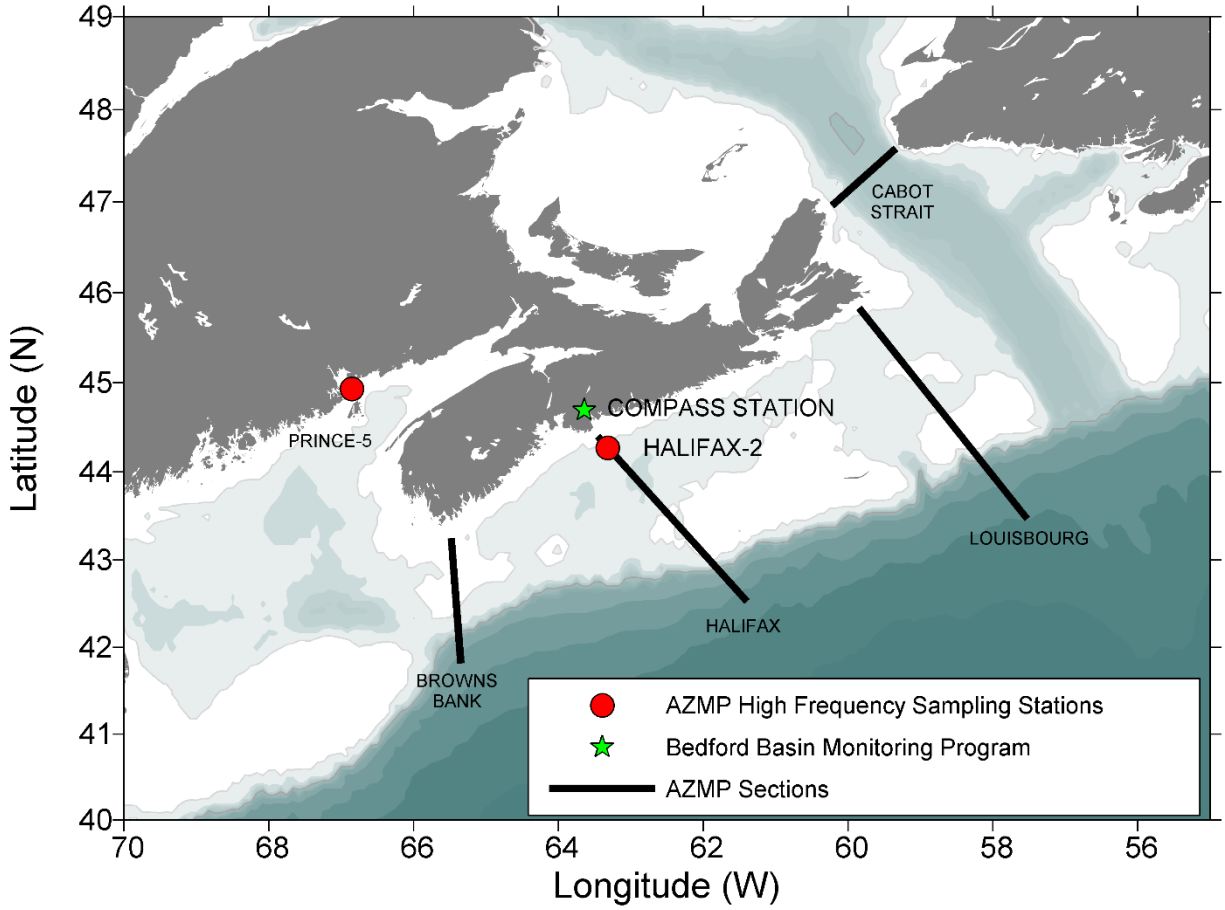

Figure 1. Map of primary sections (Cabot Strait [CSL]; Louisbourg [LL]; Halifax [HL]; Browns Bank [BBL]) and high frequency sampling stations (Halifax-2 [HL2]; Prince-5 [P5]) sampled in the DFO Maritimes Region. The Compass Station is sampled as part of the Bedford Basin Monitoring Program.

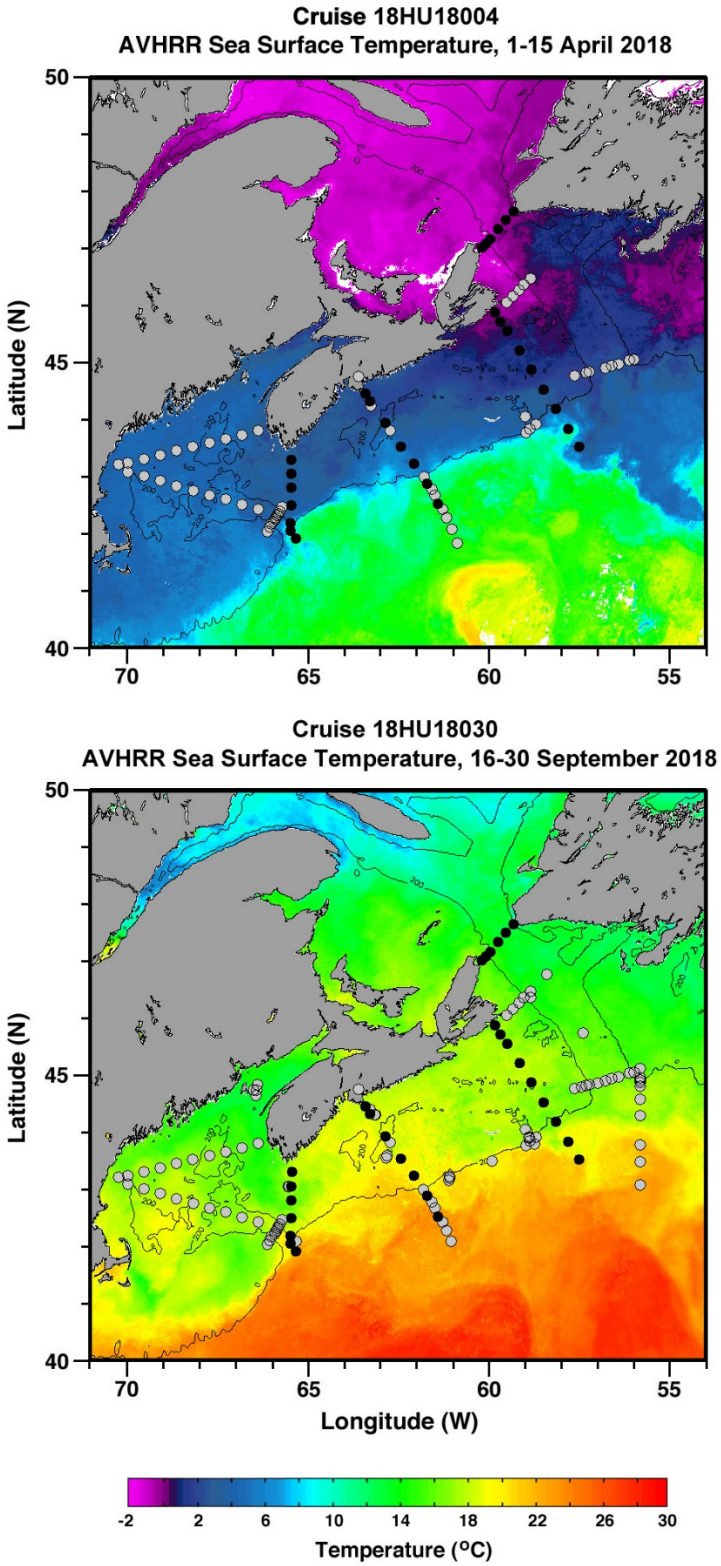

Figure 2. Stations sampled during the 2018 spring and fall surveys. Station locations are superimposed on sea-surface temperature composite images for dates close to the mission dates. Black markers indicate core stations, and gray markers indicate stations sampled for ancillary programs.

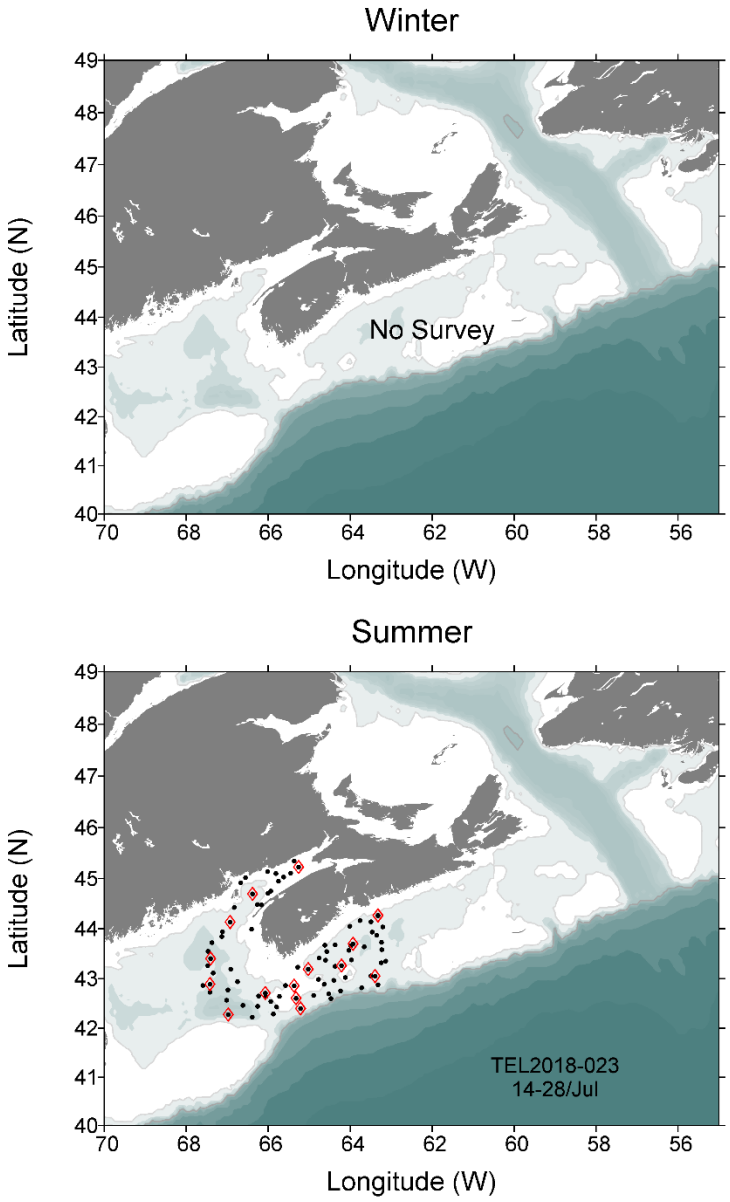

Figure 3. Stations sampled during primary Maritimes Region ecosystem trawl survey in 2018. Black solid markers are hydrographic stations; red open diamonds are stations where vertical nets tows were taken in addition to hydrographic measurements.

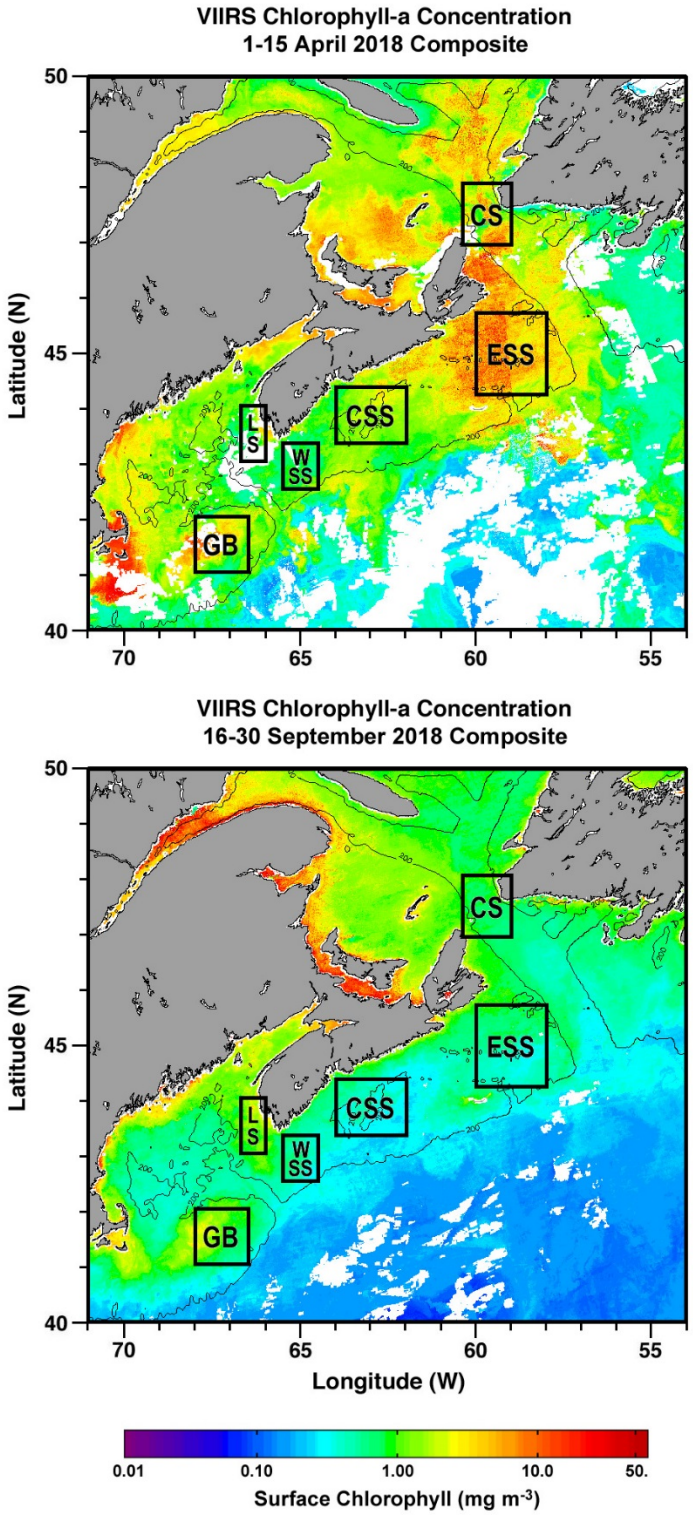

Figure 4. Statistical sub-regions in the Maritimes Region identified for spatial/temporal analysis of satellite ocean colour data. Sub-regions are superimposed on surface chlorophyll composite images for dates close to the mission dates. Cabot Strait [CS]; Eastern Scotian Shelf [ESS]; Central Scotian Shelf [CSS]; Western Scotian Shelf [WSS]; Lurcher Shoal [LS]; Georges Bank [GB].

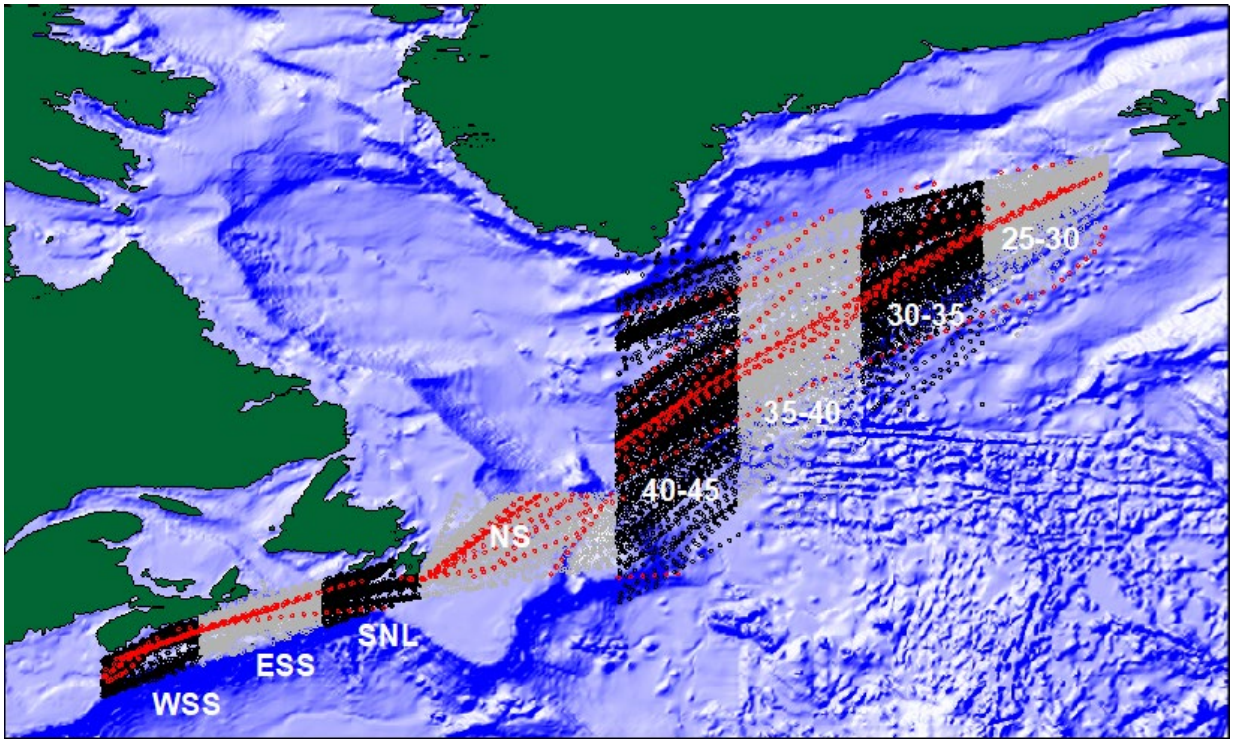

Figure 5. Continuous Plankton Recorder lines and stations 1957 to 2017. Stations sampled in 2017 are shown in red. Data are analysed by region. Regions are: Western Scotian Shelf (WSS), Eastern Scotian Shelf (ESS), South Newfoundland Shelf (SNL), Newfoundland Shelf (NS), and between longitudes 40–45°W, 35–40°W, 30–35°W, 25–30°W.

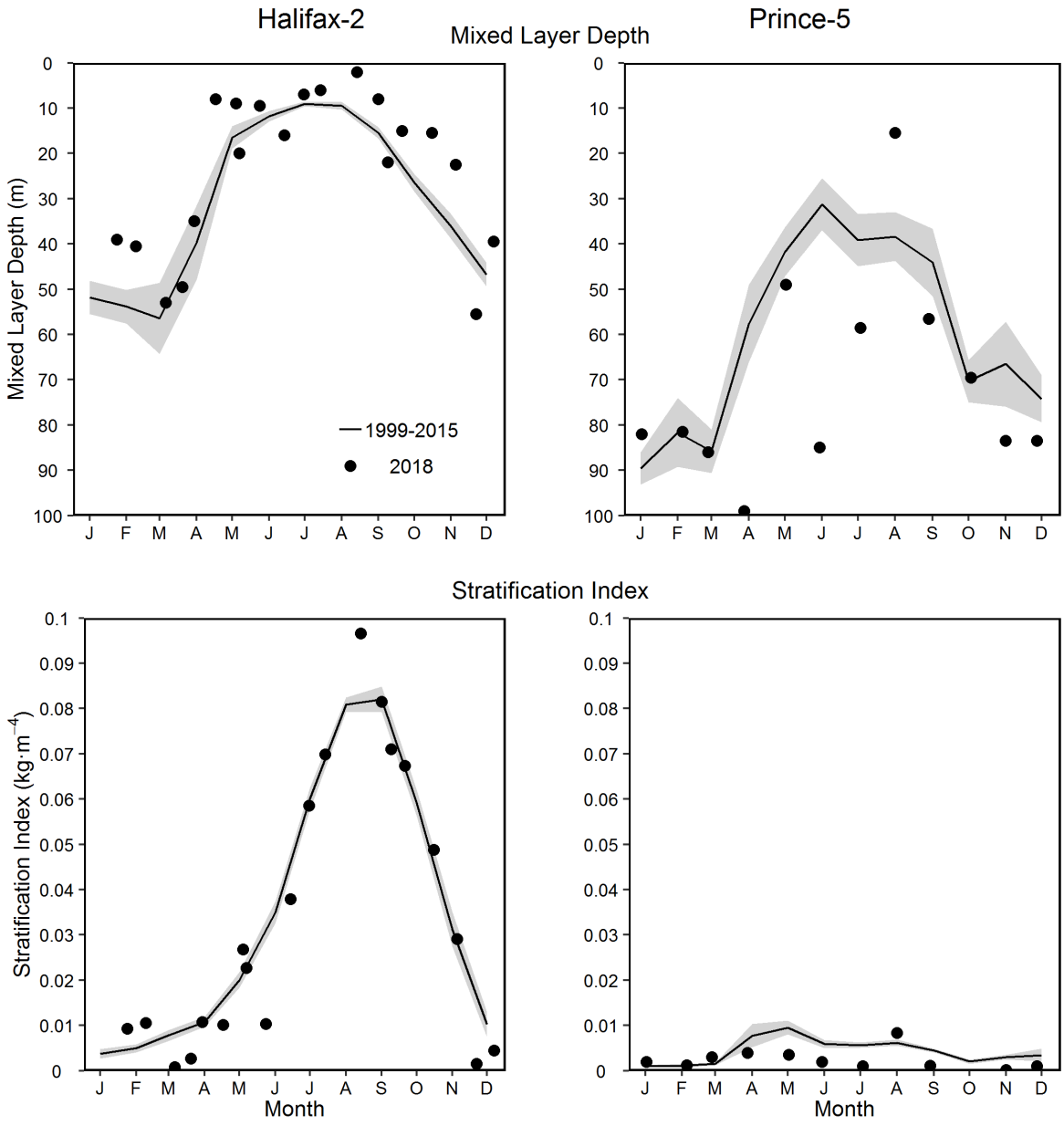

Figure 6. Mixing properties (mixed layer depth, stratification index) at the Maritimes high frequency sampling stations comparing 2018 data (solid circle) with mean conditions from 1999–2015 (solid line). The gray shaded area represents the standard error of the monthly means.

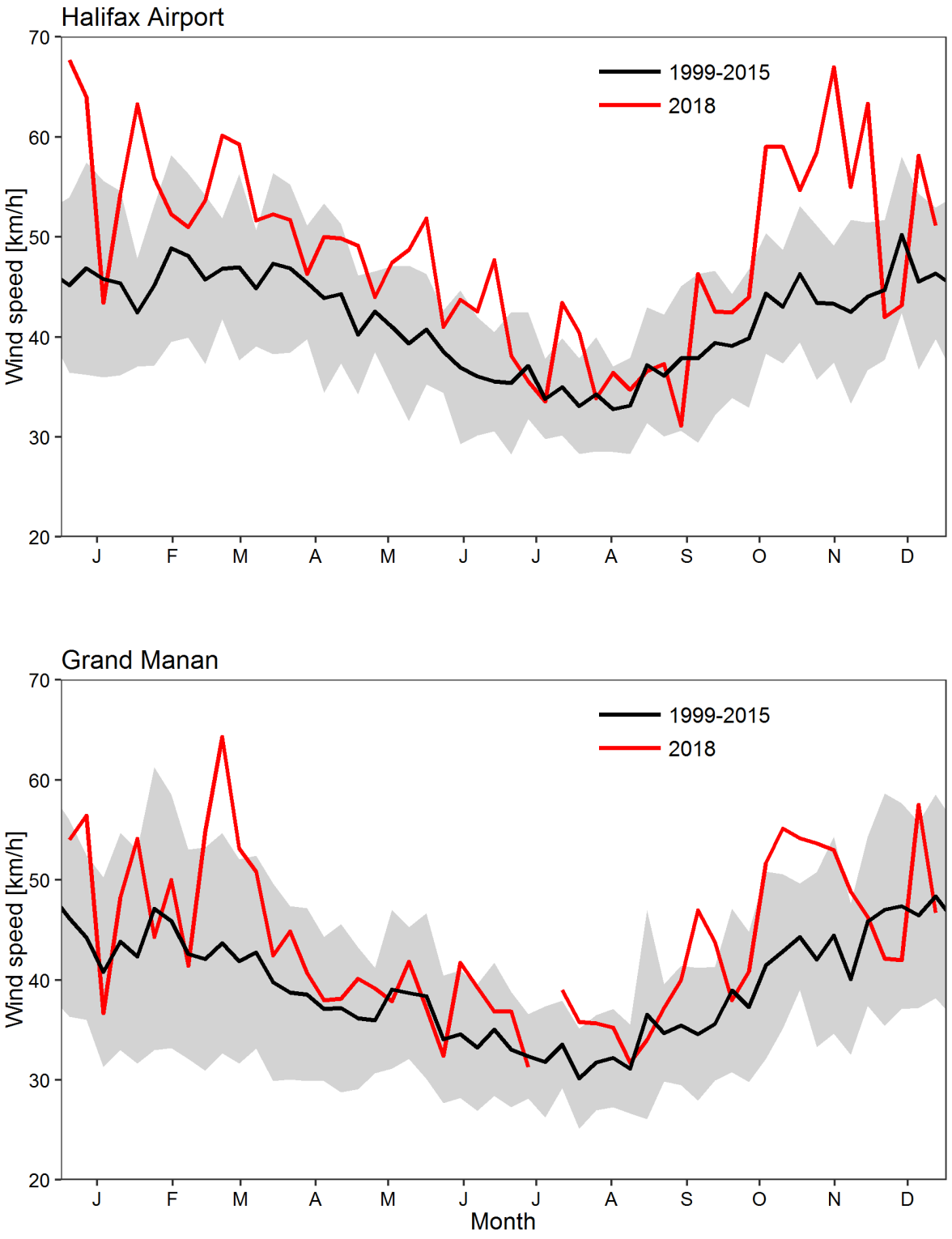

Figure 7. Mean daily maximum wind gust at Halifax International Airport (representative of wind conditions at Halifax-2) and Grand Manan Island (representative of wind conditions at Prince-5) for the year 2018 (red line) and the 1999–2015 climatology (black line). The gray shaded area represents the standard deviation to the climatology computed over 17 years.

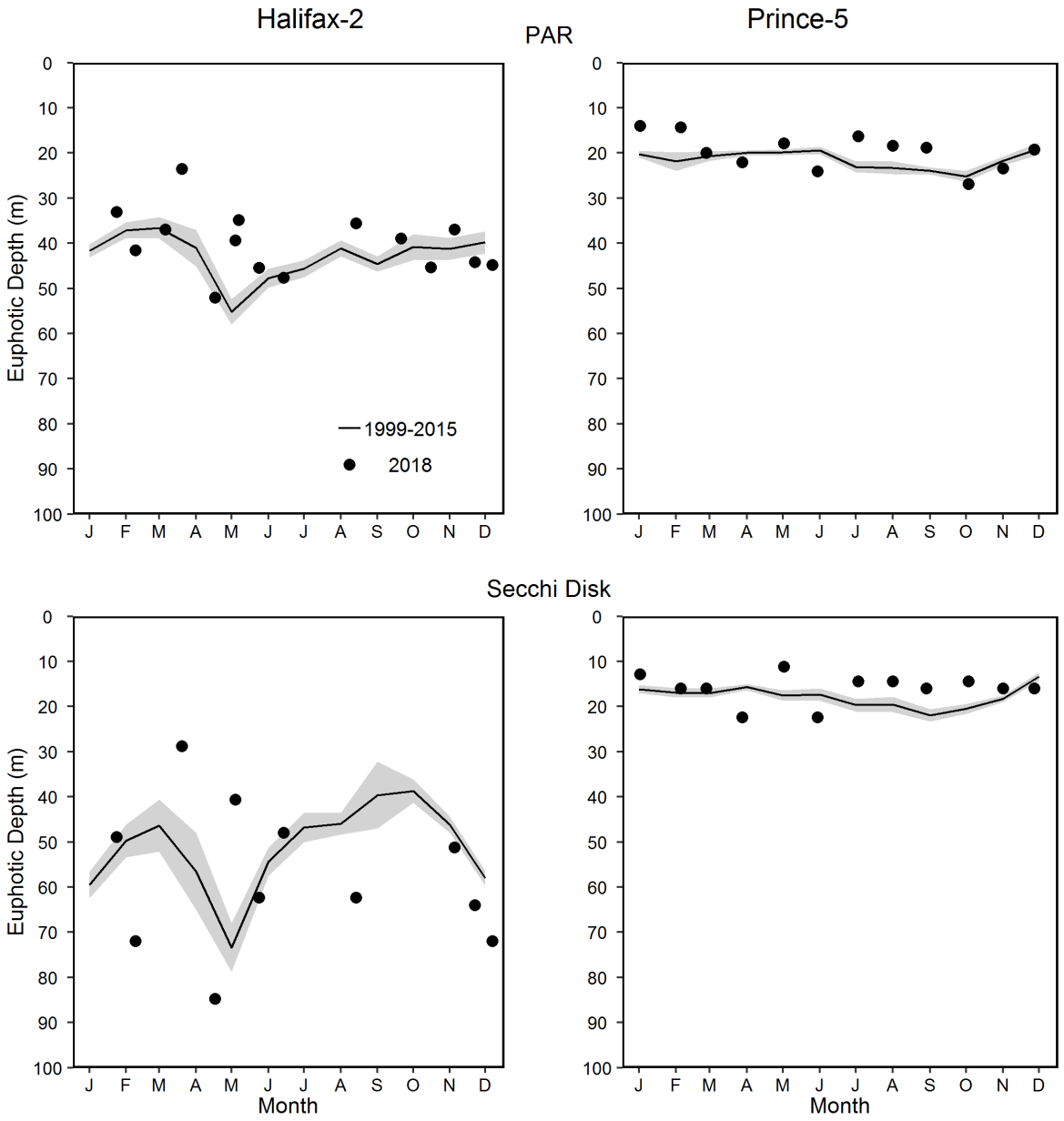

Figure 8. Optical properties (euphotic depth from PAR irradiance meter and Secchi disc) at the Maritimes high frequency sampling stations. Year 2018 data (solid circle) compared with mean conditions from 1999–2015 (solid line), except 2001–2015 for euphotic depth from PAR at Prince-5. The gray shaded area represents the standard error of the monthly means.

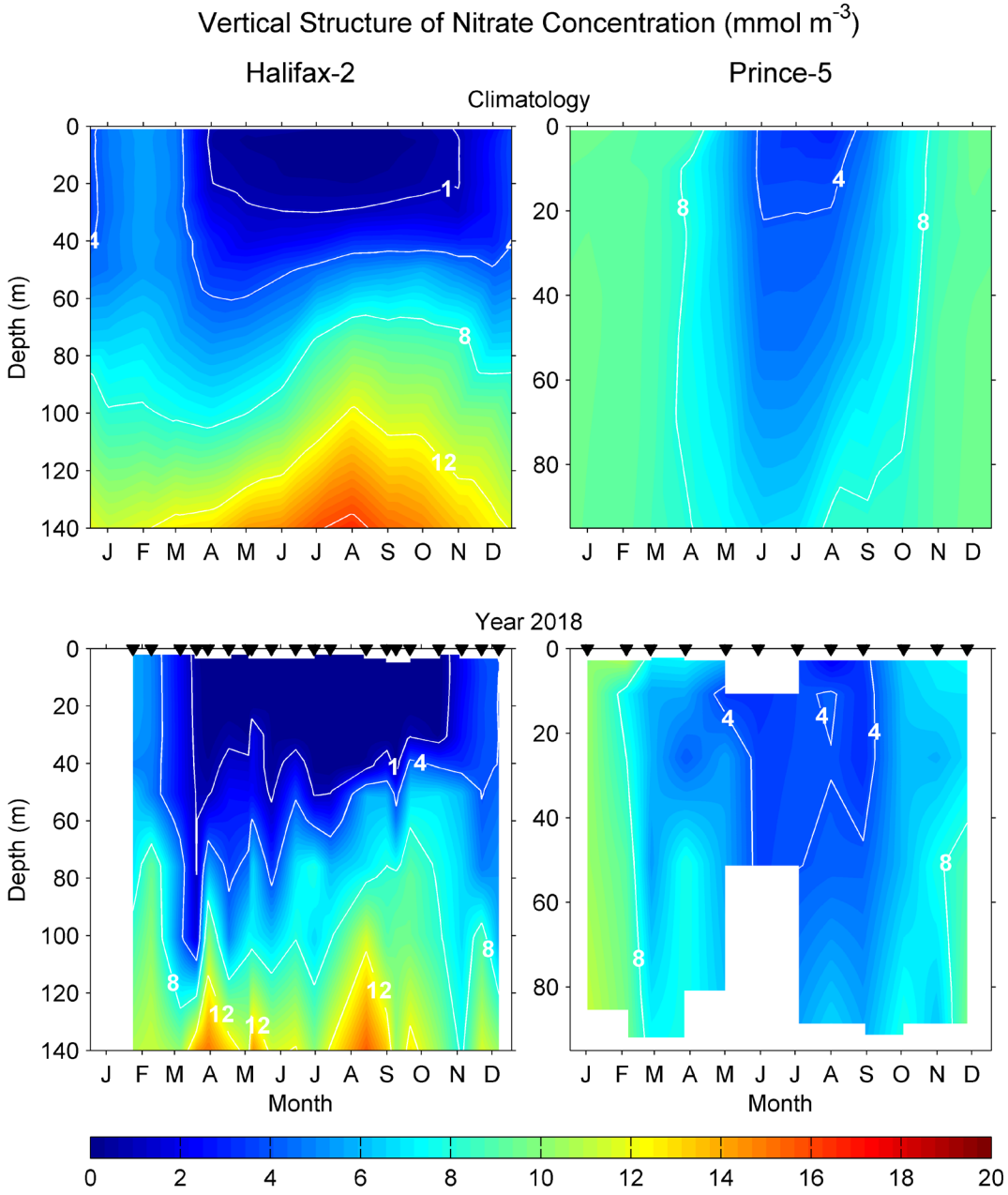

Figure 9. Comparison of annual changes in the vertical structure of nitrate concentrations (mmol m^{-3}) in 2018 (bottom panels) with climatological mean conditions from 1999–2015 (upper panels) at the Maritimes high frequency sampling stations. Black triangles in the bottom panels indicate sampling dates.

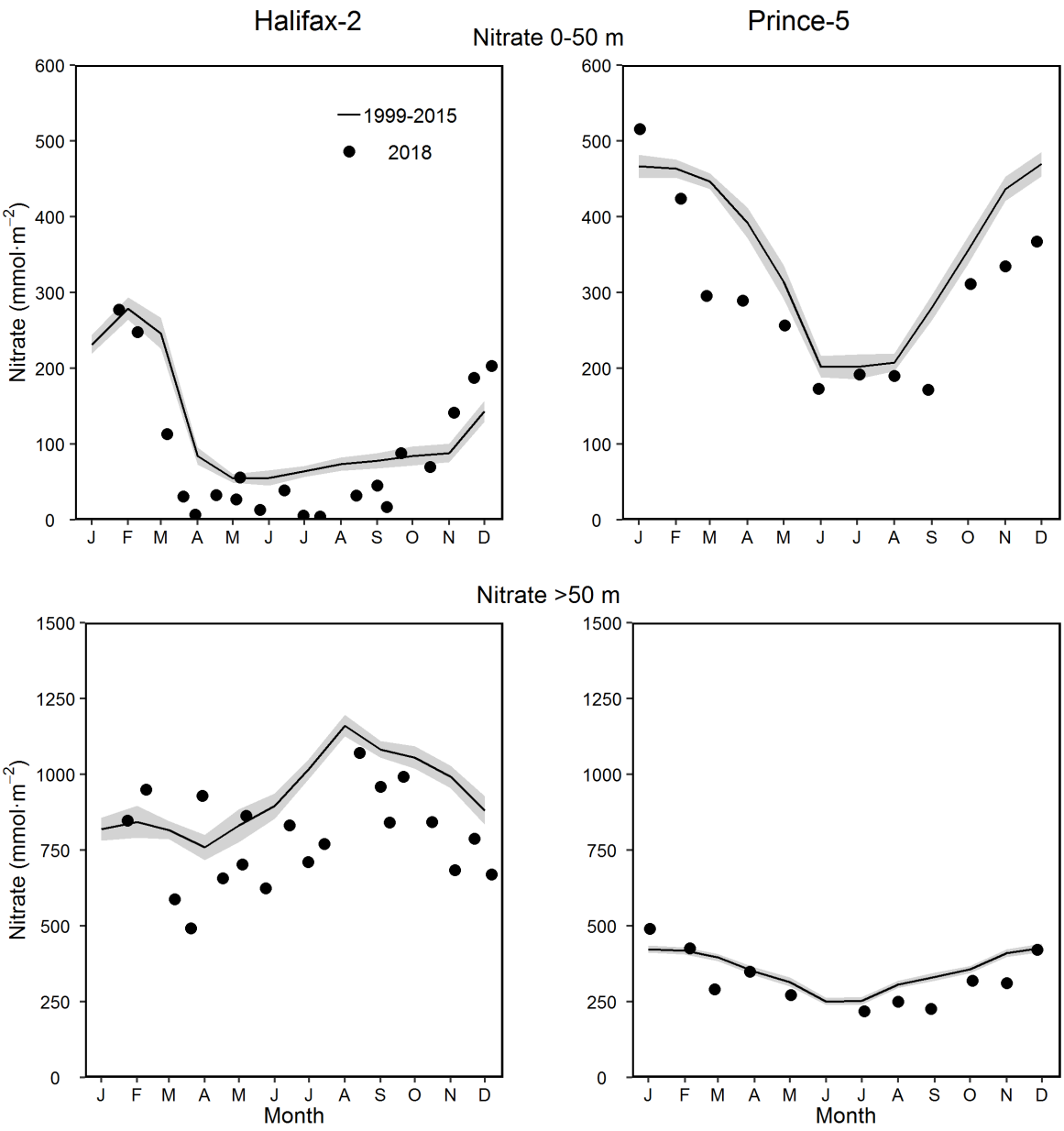

Figure 10. Comparison of 2018 (solid circle) data with mean conditions from 1999–2015 (solid line) at the Maritimes high frequency sampling stations. Upper panels: surface (0–50 m) nitrate inventory. Lower panels: deep (50–150 m for Halifax-2 and 50–95 m for Prince-5) nitrate inventory. The gray shaded area represents the standard error of the monthly means.

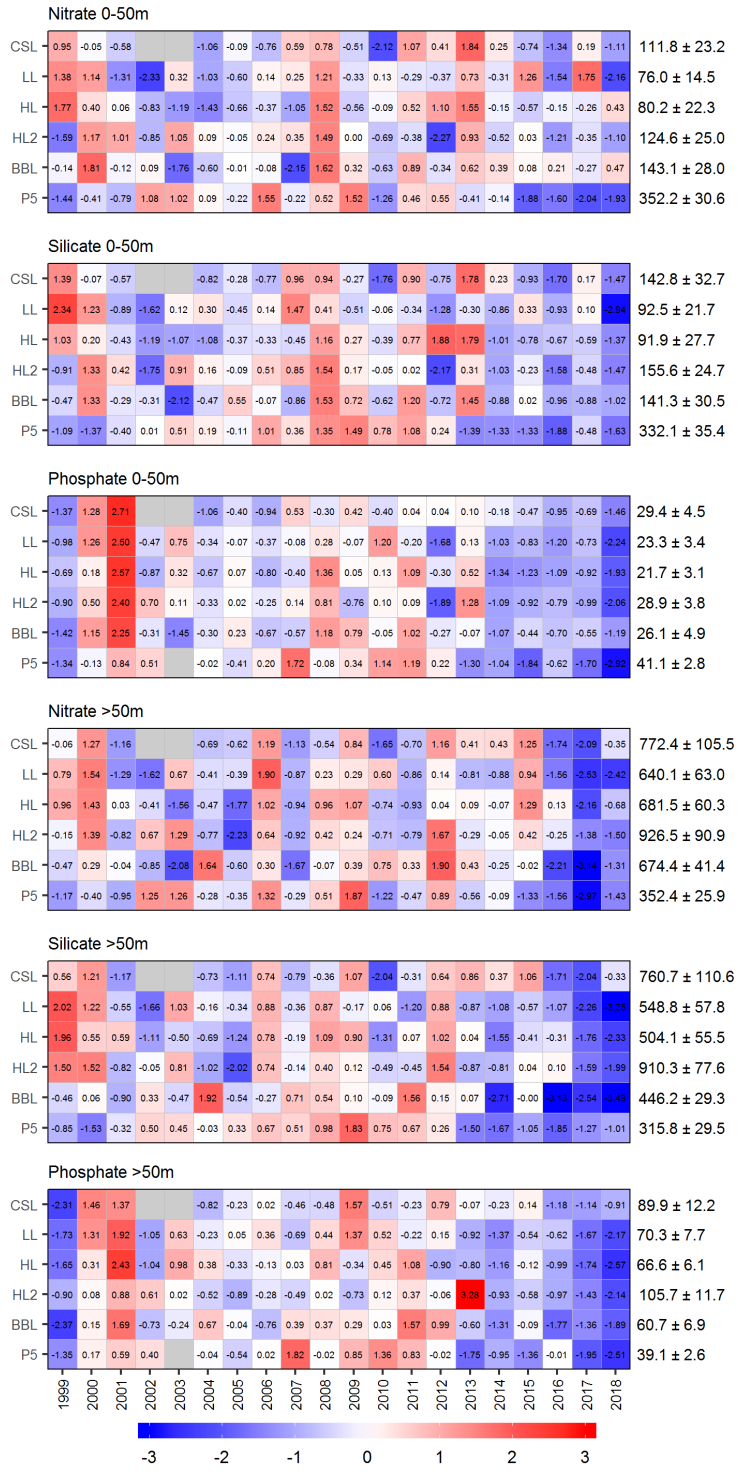

Figure 11. Annual anomaly scorecard for surface (0–50 m) and deep (>50 m) nitrate, silicate and phosphate inventories. Values in each cell are anomalies from the mean for the reference period, 1999–2015, in standard deviation (sd) units (mean and sd listed at right). A grey cell indicates missing data. Red (blue) cells indicate higher (lower) than normal nutrient levels. CSL: Cabot Strait section; LL: Louisbourg section; HL: Halifax section; HL2: Halifax-2; BBL: Browns Bank section; P5: Prince-5.

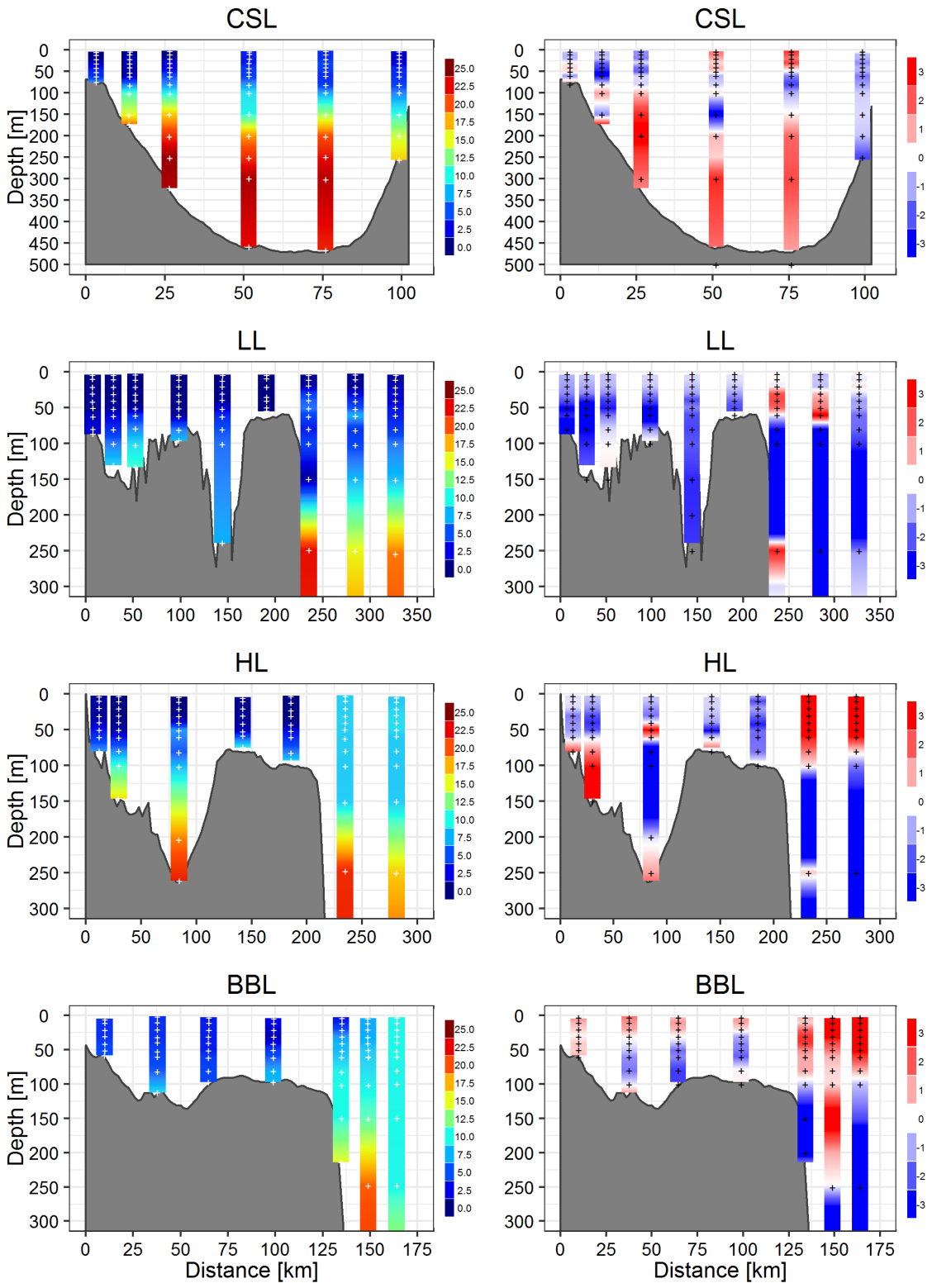

Figure 12a. Vertical profiles of nitrate concentration (mmol m^{-3}) (left panels) and their anomalies (mmol m^{-3}) from 1999–2015 conditions (right panels) on the SS sections in spring 2018. White markers on the left panels indicate the actual sampling depths for 2018. Black markers on the right panels indicate the depths at which station-specific climatological values were calculated. CSL: Cabot Strait section; LL: Louisbourg section; HL: Halifax section; BBL: Browns Bank section.

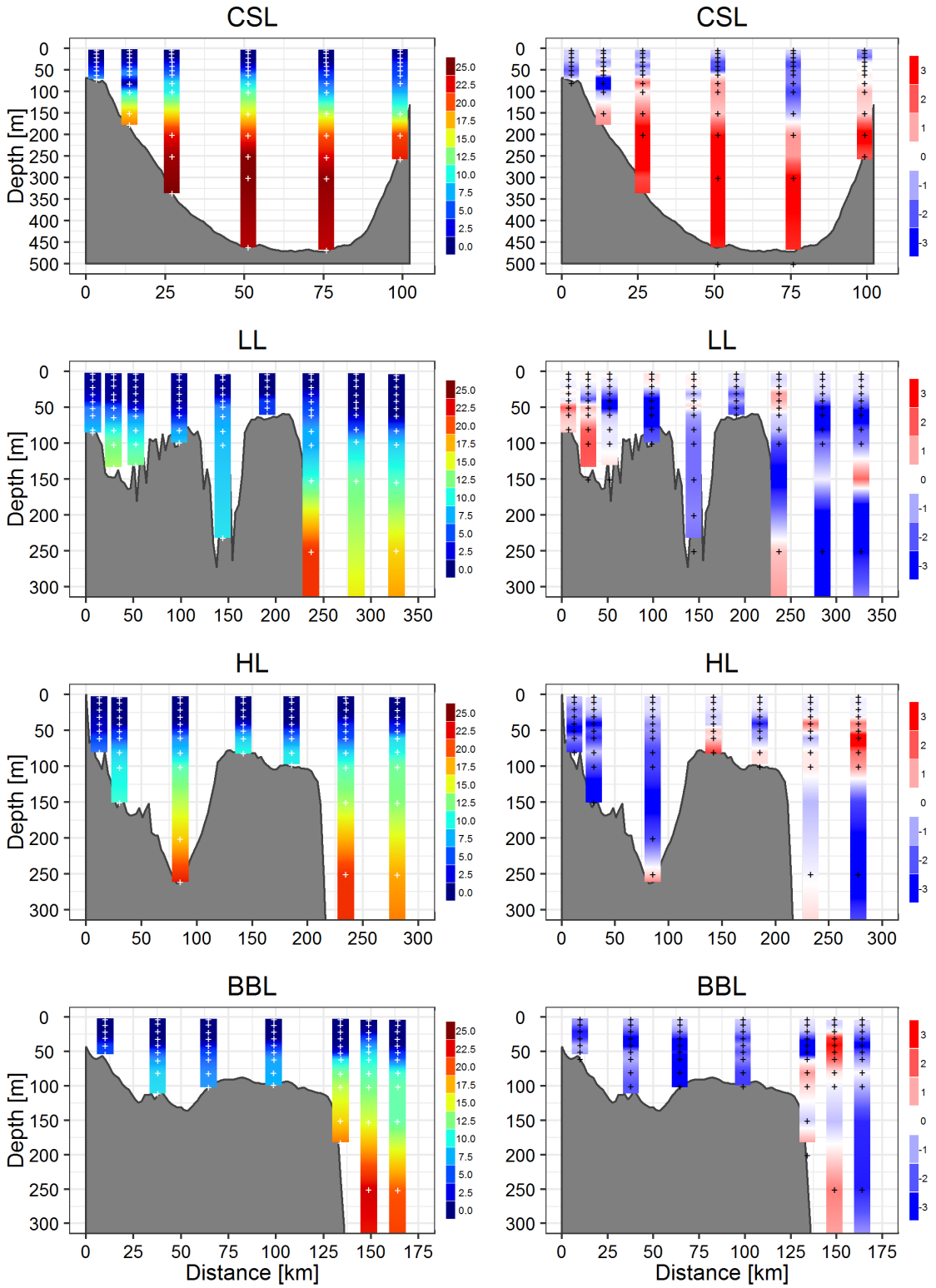

Figure 12b. Vertical profiles of nitrate concentration (mmol m^{-3}) (left panels) and their anomalies (mmol m^{-3}) from 1999–2015 conditions (right panels) on the SS sections in fall 2018. White markers on the left panels indicate the actual sampling depths for 2018. Black markers on the right panels indicate the depths at which station-specific climatological values were calculated. CSL: Cabot Strait section; LL: Louisbourg section; HL: Halifax section; BBL: Browns Bank section.

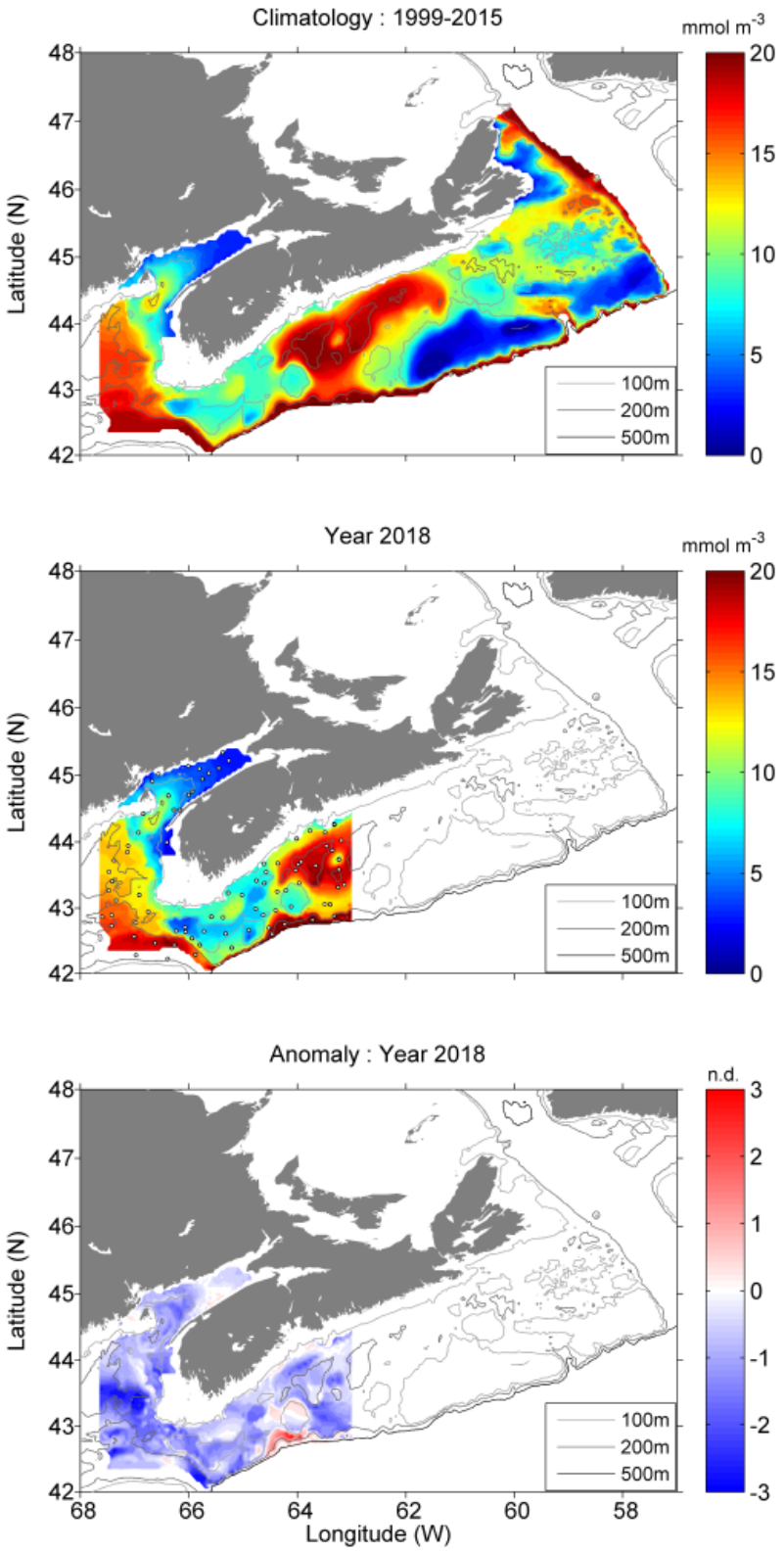

Figure 13. Bottom nitrate concentration during the annual summer ecosystem trawl survey: 1999–2015 climatology (upper panel), 2018 conditions (middle panel), and normalized anomalies from climatology (lower panel). Markers in middle panel represent the 2018 sampling locations. nd = no dimensions.

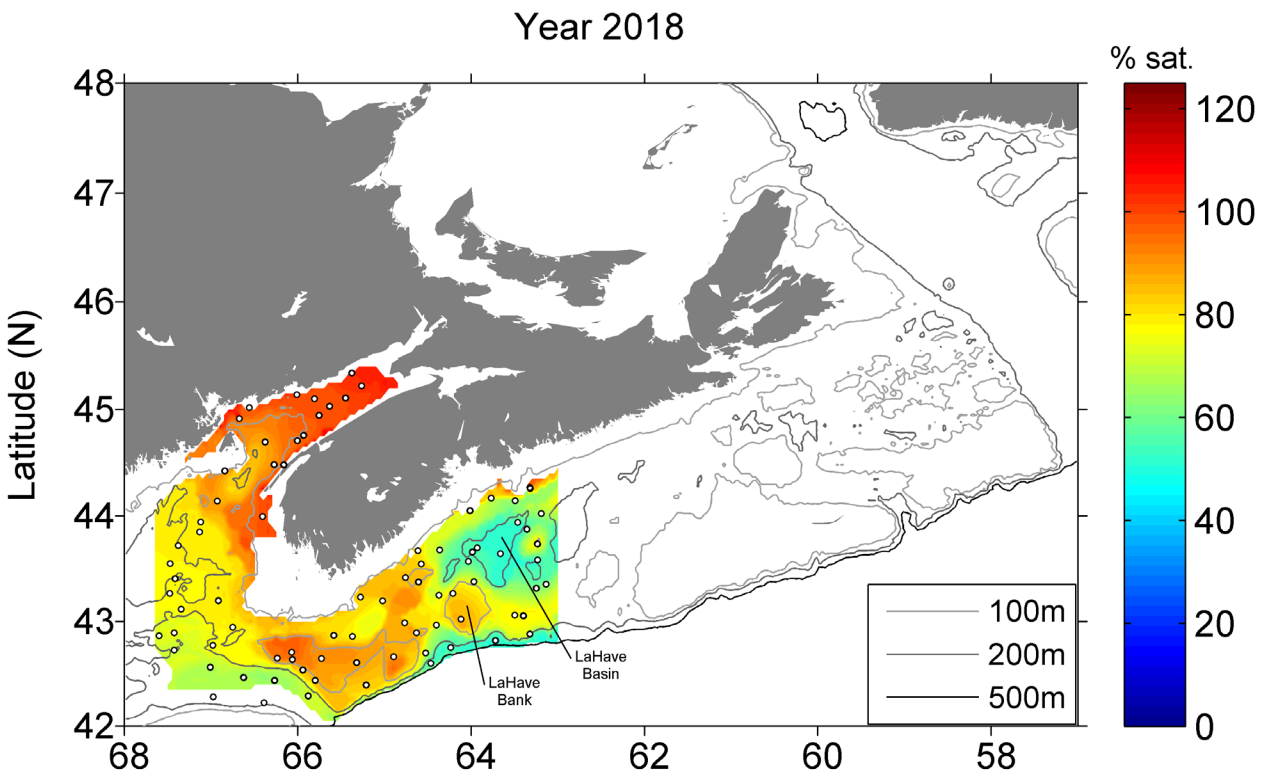

Figure 14. Bottom oxygen saturation level during the annual summer ecosystem trawl survey in 2018. Markers represent the sampling locations.

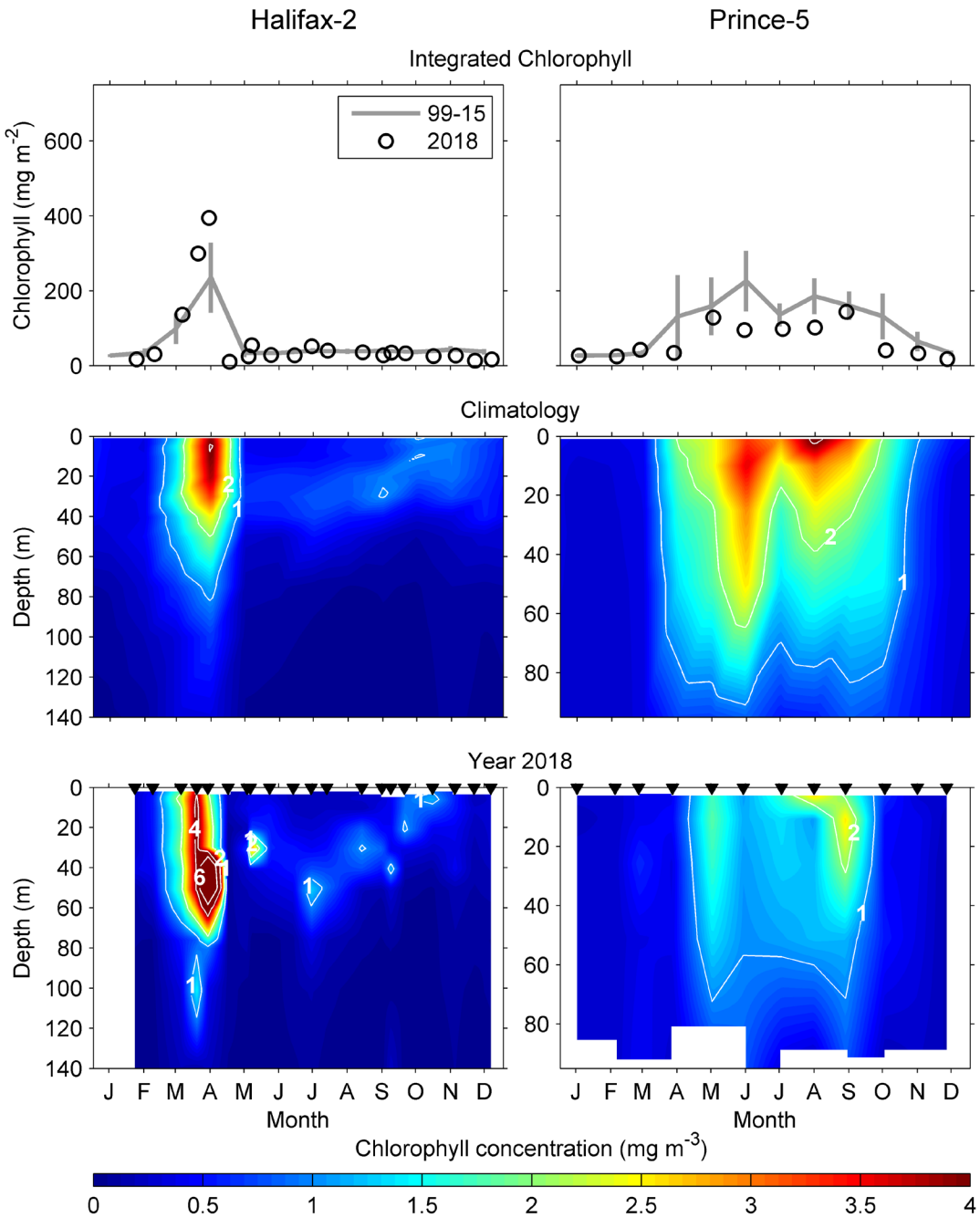

Figure 15. Annual variability in chlorophyll concentration at the Maritimes time series stations (left column: Halifax-2, right column: Prince-5). Top row: chlorophyll inventories (0–100 m at Halifax-2, 0–95 m at Prince-5) in 2018 (open circle) and mean values 1999–2015 (solid line). Vertical lines are 95% confidence intervals of the monthly means. Middle row: mean (1999–2015) seasonal cycle of the vertical structure of chlorophyll concentration (mg m^{-3}). Bottom row: seasonal cycle of the vertical structure of chlorophyll concentration in 2018. Colour scale chosen to emphasize changes near the estimated food saturation levels for large copepods. Black triangles in the bottom panels indicate sampling dates.

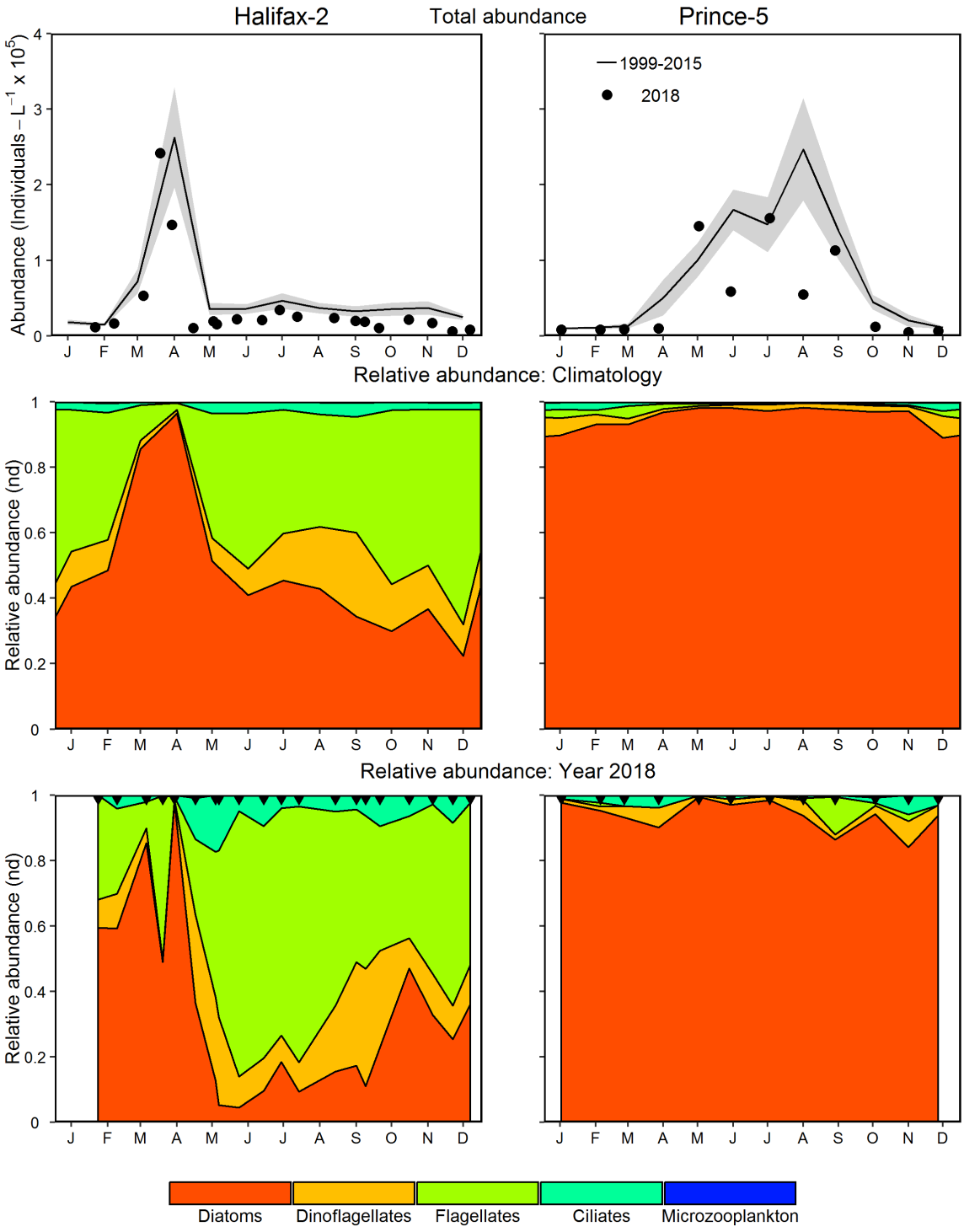

Figure 16. Comparison of 2018 microplankton (phytoplankton and protists) abundance and community composition with mean conditions from 1999–2015 at the Maritimes high frequency sampling stations (Halifax-2 right panels; Prince-5 left panels). Upper panels: 2018 microplankton abundance (solid circle) and mean conditions from 1999–2015 (solid line). The gray shaded area represents the standard error of the monthly means. Middle panels: climatological microplankton relative abundance from 1999–2015. Lower panels: 2018 microplankton relative abundance. nd = no dimensions. Black triangles in the bottom panels indicate sampling dates.

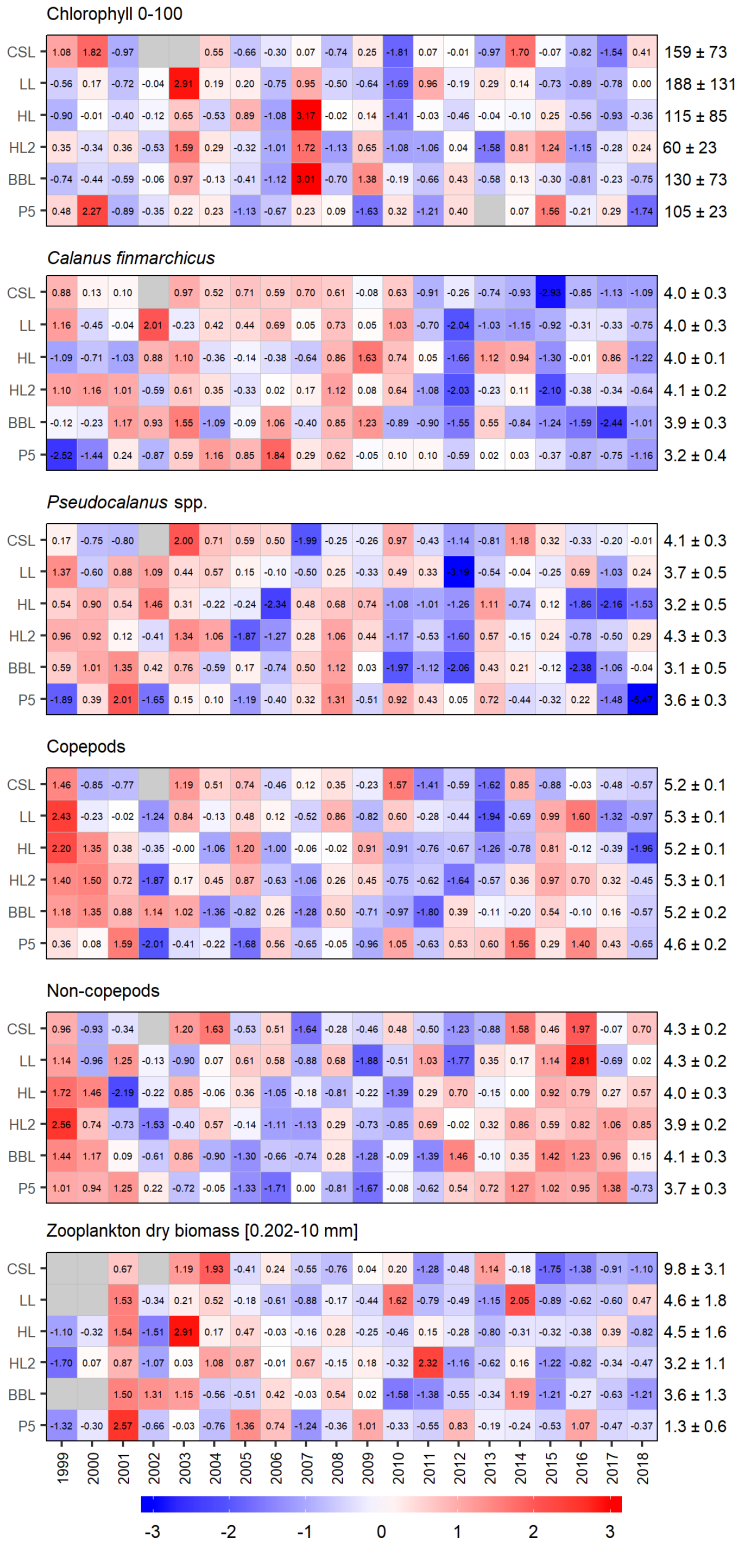

Figure 17. Annual anomaly scorecard for phytoplankton (chlorophyll) and zooplankton abundance and biomass. Values in each cell are anomalies from the mean for the reference period, 1999–2015, in standard deviation (sd) units (mean and sd listed at right). A grey cell indicates missing data. Red (blue) cells indicate higher (lower) than normal levels of the variable. CSL: Cabot Strait section; LL: Louisbourg section; HL: Halifax section; HL2: Halifax-2; BBL: Browns Bank section; P5: Prince-5.

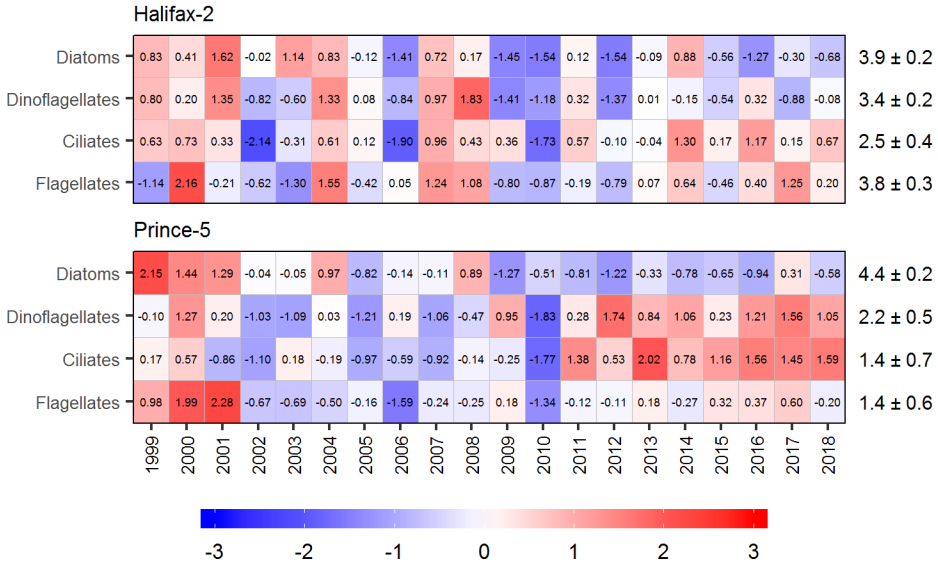

Figure 18. Annual anomaly scorecard for microplankton abundance at the Maritimes high frequency sampling stations. Values in each cell are anomalies from the mean for the reference period, 1999–2015, in standard deviation (sd) units (mean and sd listed at right). Red (blue) cells indicate higher (lower) than normal microplankton abundance levels.

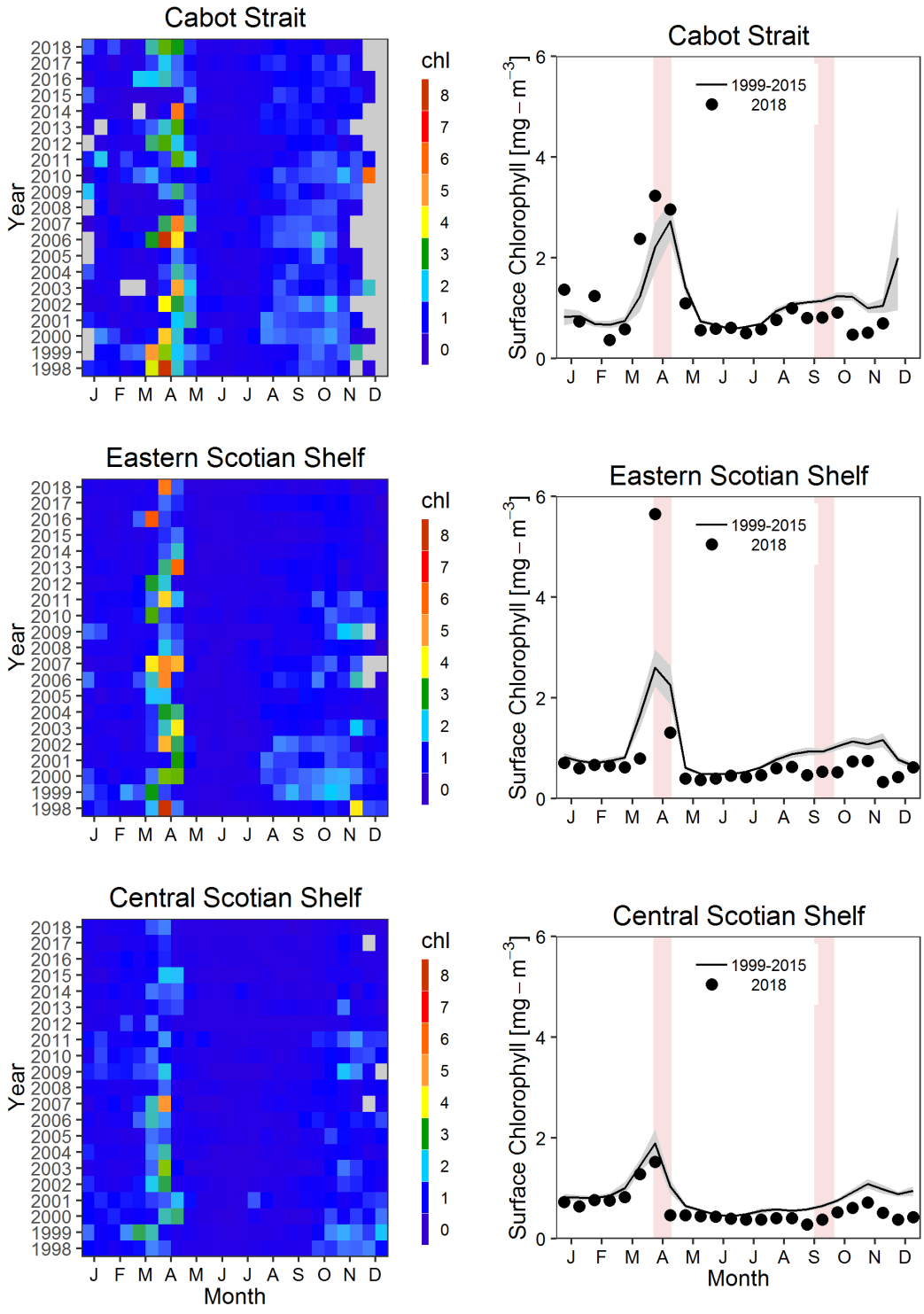

Figure 19a. Estimates of surface chlorophyll concentrations from semi-monthly remotely sensed ocean colour data in the Cabot Strait (top), Eastern Scotian Shelf (middle), and Central Scotian Shelf (bottom) statistical sub-regions (see Figure 4). Data from SeaWiFS 1998–2007; MODIS 2008–2011; VIIRS 2012–2017. Left panels: time series of annual variation in chlorophyll concentrations. Right panels: comparison of 2018 (solid circle) surface chlorophyll estimates with mean conditions from 1999–2015 (solid line) in the same sub-regions. Gray shaded area is the 95% confidence interval of the semi-monthly means. Pink vertical stripes indicate the timing of the seasonal missions.

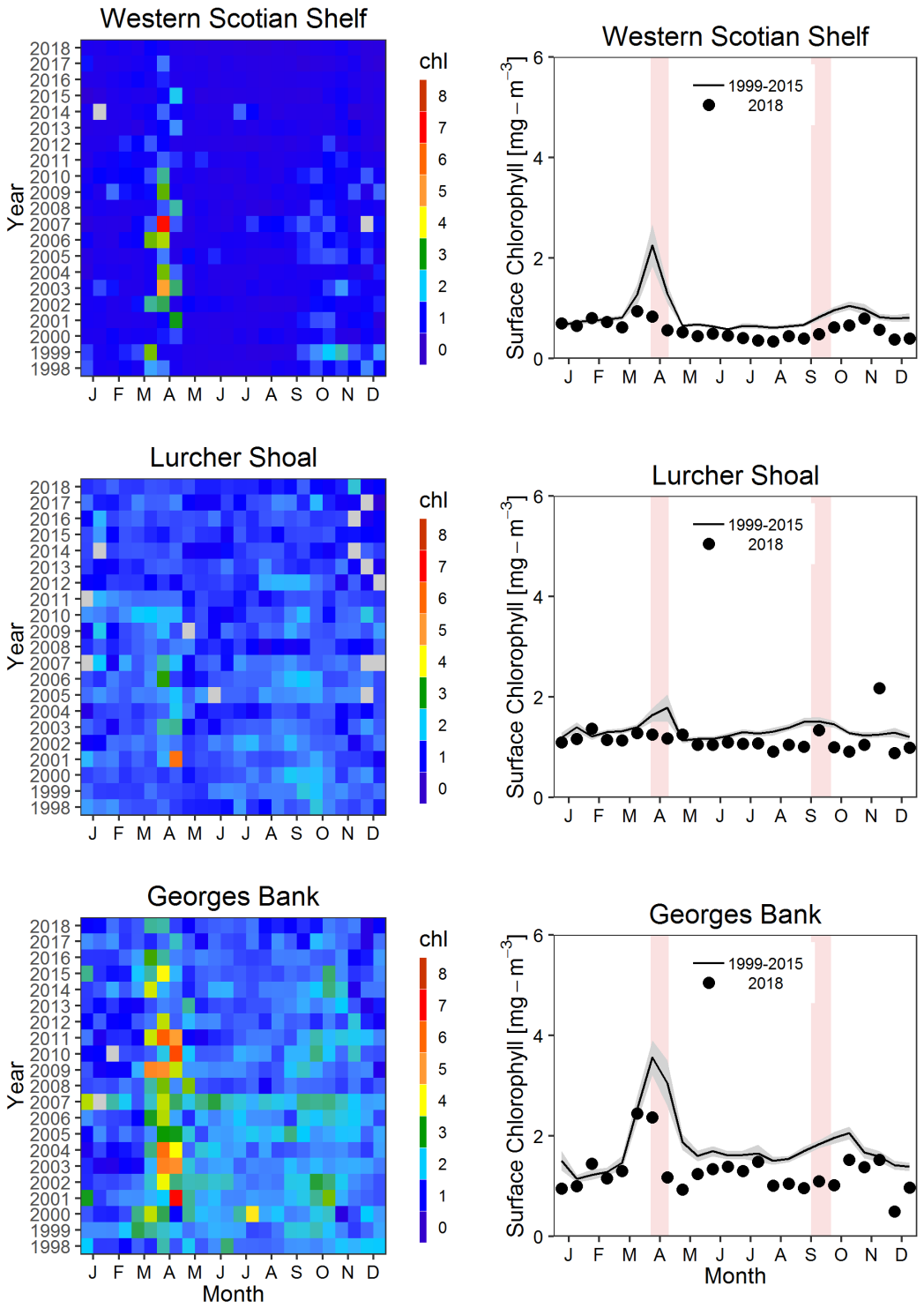

Figure 19b. Estimates of surface chlorophyll concentrations from semi-monthly remotely sensed ocean colour data in the Western Scotian Shelf (top), Lurcher Shoal (middle), and Georges Bank (bottom) statistical sub-regions (see Figure 4). Data from SeaWiFS 1998–2007; MODIS 2008–2011; VIIRS 2012–2017. Left panels: time series of annual variation in chlorophyll concentrations. Right panels: comparison of 2018 (solid circle) surface chlorophyll estimates with mean conditions from 1999–2015 (solid line) in the same sub-regions. Gray shaded area is the 95% confidence interval of the semi-monthly means. Pink vertical stripes indicate the timing of the seasonal missions.

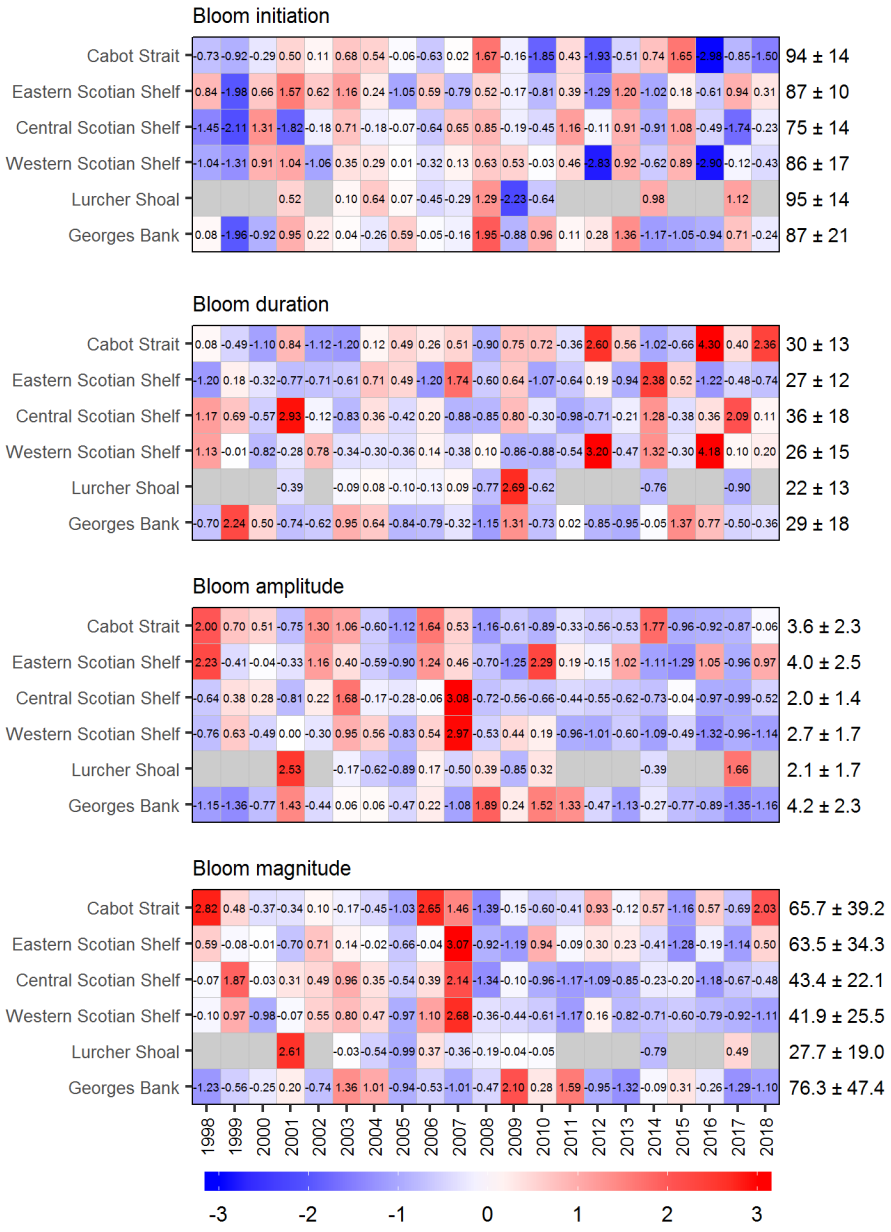

Figure 20. Annual anomaly scorecard for spring bloom parameters. Values in each cell are anomalies from the mean for the reference period, 1999–2015, in standard deviation (sd) units (mean and sd listed at right). A grey cell indicates missing data. Red (blue) cells indicate later (earlier) initiation, longer (shorter) duration or higher (lower) amplitude or magnitude than normal.

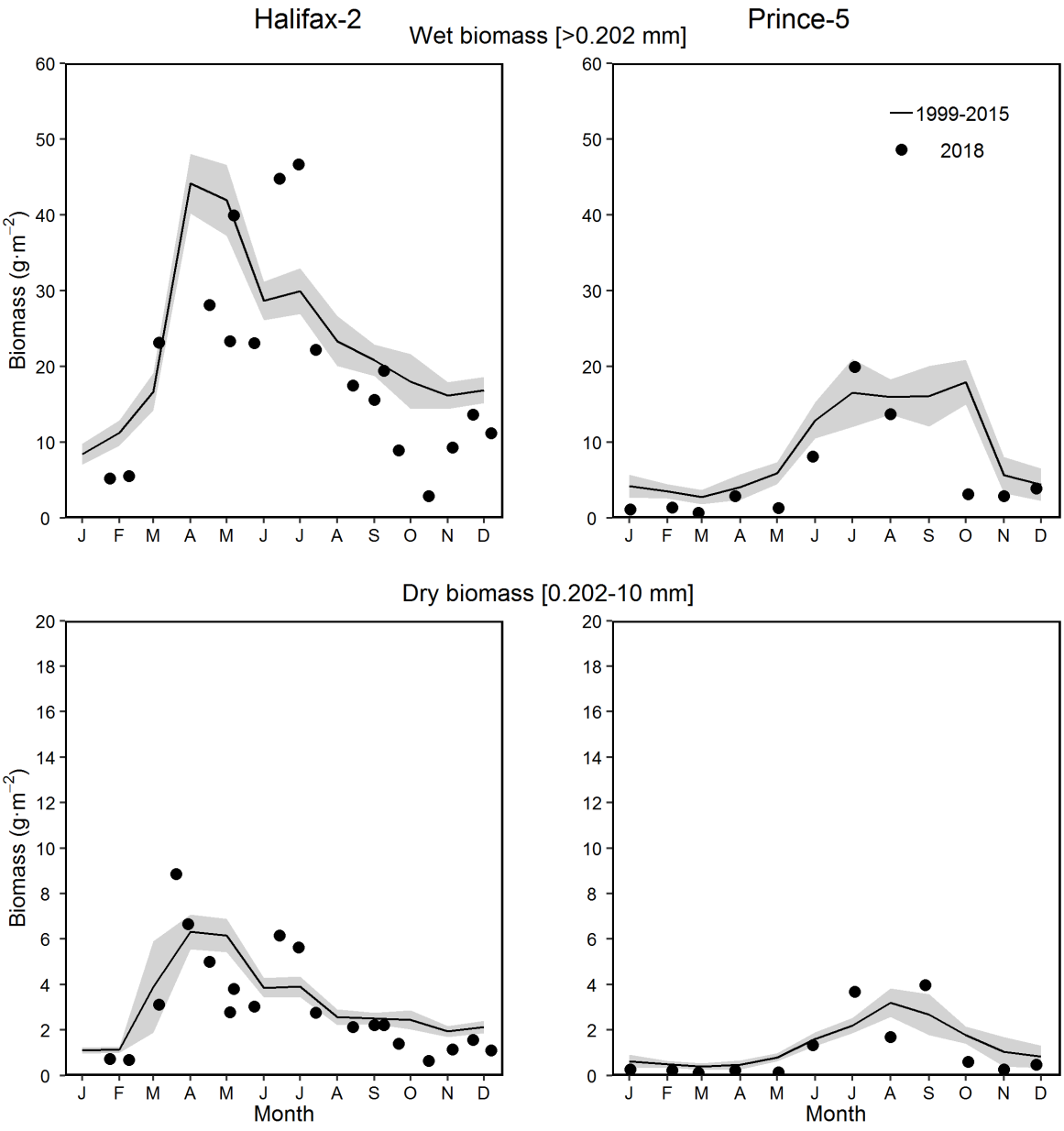

Figure 21. Zooplankton total wet biomass (upper panels) and mesozooplankton dry biomass (bottom panels) (integrated surface to bottom) in 2018 (solid circle) and mean conditions 1999–2015 (solid line) at the Maritimes high frequency sampling stations. The gray shaded area represents the standard error of the monthly means. Left panels: Halifax-2; right panels: Prince-5.

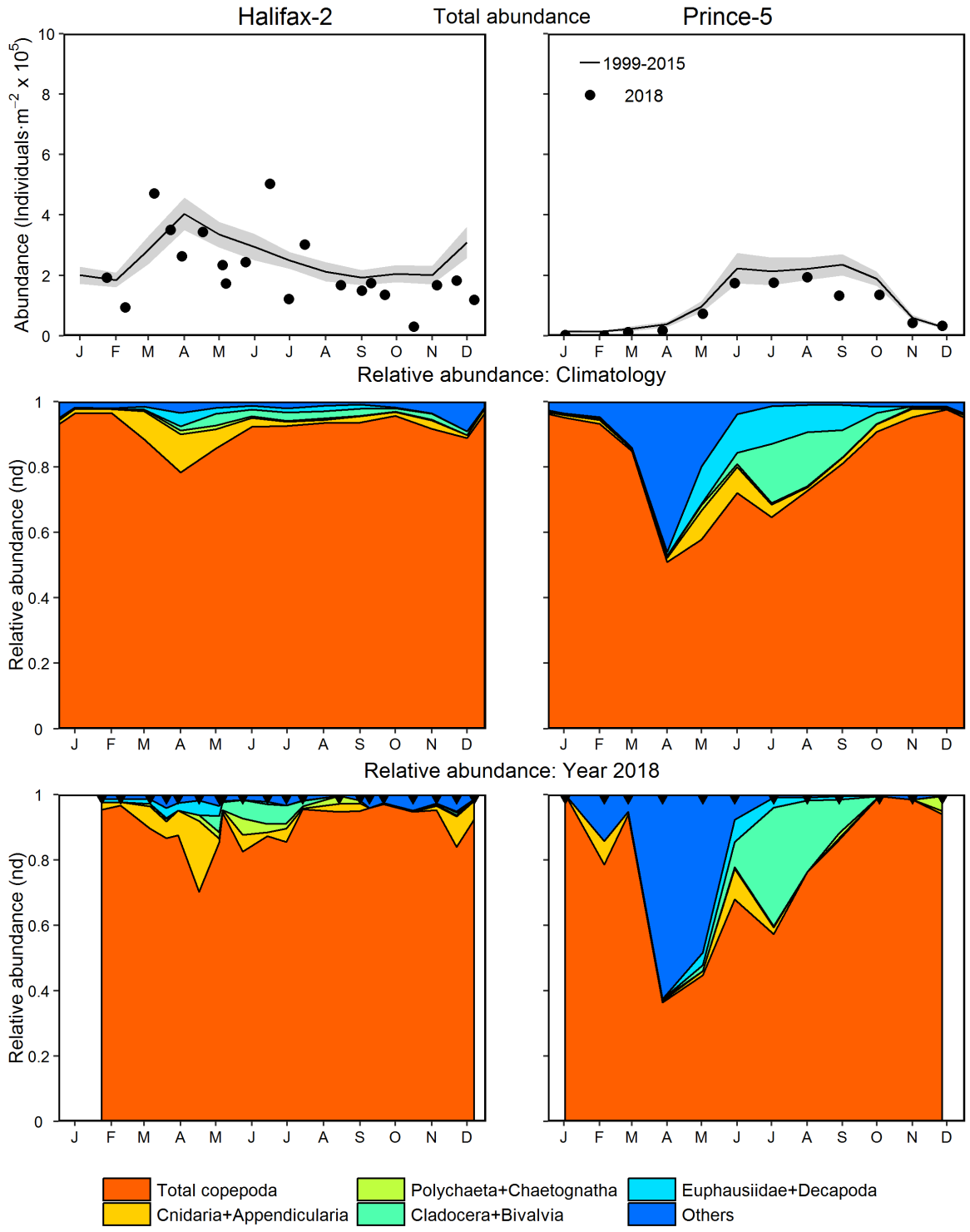

Figure 22. Zooplankton (>200 µm) abundance and community composition in 2018 and mean conditions 1999–2015 at the Maritimes high frequency sampling stations (Halifax-2, left panels; Prince-5, right panels). Upper panels: zooplankton abundance in 2018 (solid circle) and mean conditions 1999–2015 (solid line). The gray shaded area represents the standard error of the monthly means. Middle panels: climatology of major group relative abundances 1999–2015. Lower panels: major group relative abundances in 2018. nd = no dimensions. Black triangles in the bottom panels indicate sampling dates.

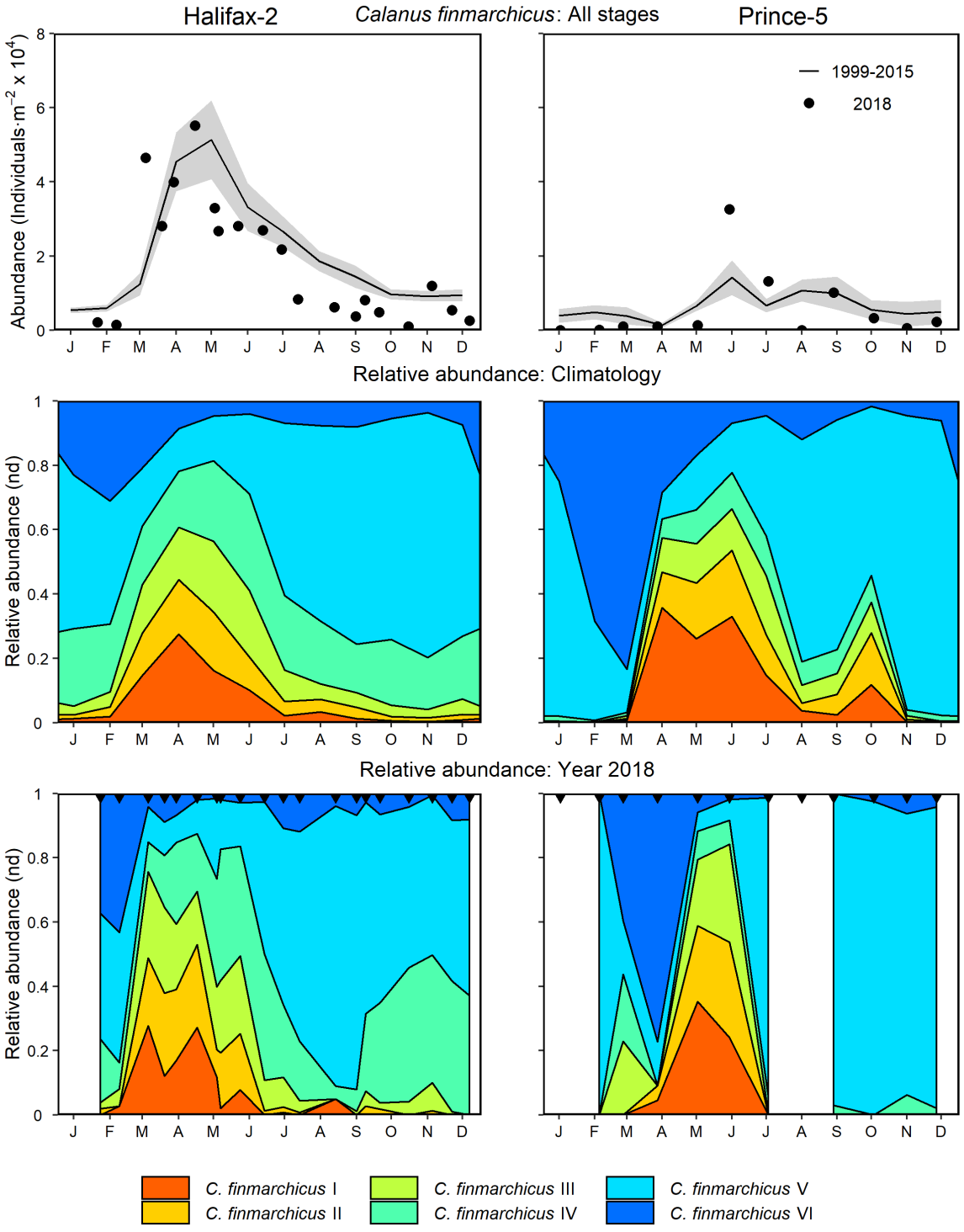

Figure 23. Calanus finmarchicus abundance and developmental stage distributions in 2018 and mean conditions 1999–2015 at the Maritimes high frequency sampling stations (Halifax-2, left panels; Prince-5, right panels). Upper panels: C. finmarchicus abundance in 2018 (solid circle) and mean conditions 1999–2015 (solid line). The gray shaded area represents the standard error of the monthly means. Middle panels: climatological C. finmarchicus stage relative abundances, 1999–2015. Lower panels: C. finmarchicus stage relative abundances in 2018. nd = no dimensions. Black triangles in the bottom panels indicate sampling dates.

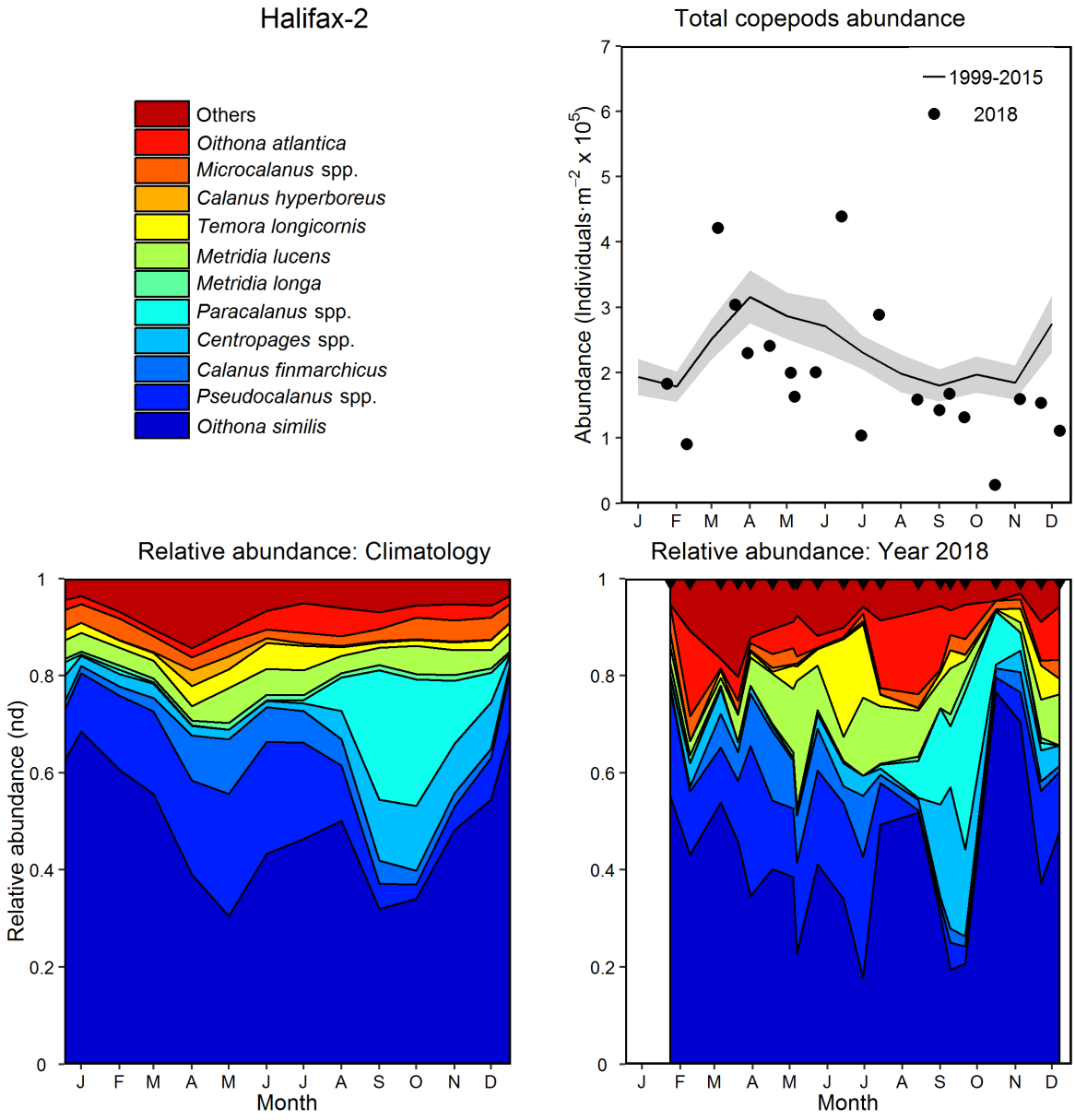

Figure 24a. Seasonal variability of dominant copepods at Halifax-2. The top 95% of identified copepod taxa by abundance, 1999–2015, are shown individually; others, including unidentified copepods (mostly nauplii) are grouped as "others." Upper right panel: copepod abundance in 2018 (solid circle) and mean conditions, 1999–2015 (solid line). The gray shaded area represents the standard error of the monthly means. Lower left panel: climatology of copepod relative abundances, 1999–2015. Lower right panel: copepod relative abundance in 2018. nd = no dimensions. Black triangles in the bottom right panel indicate sampling dates.

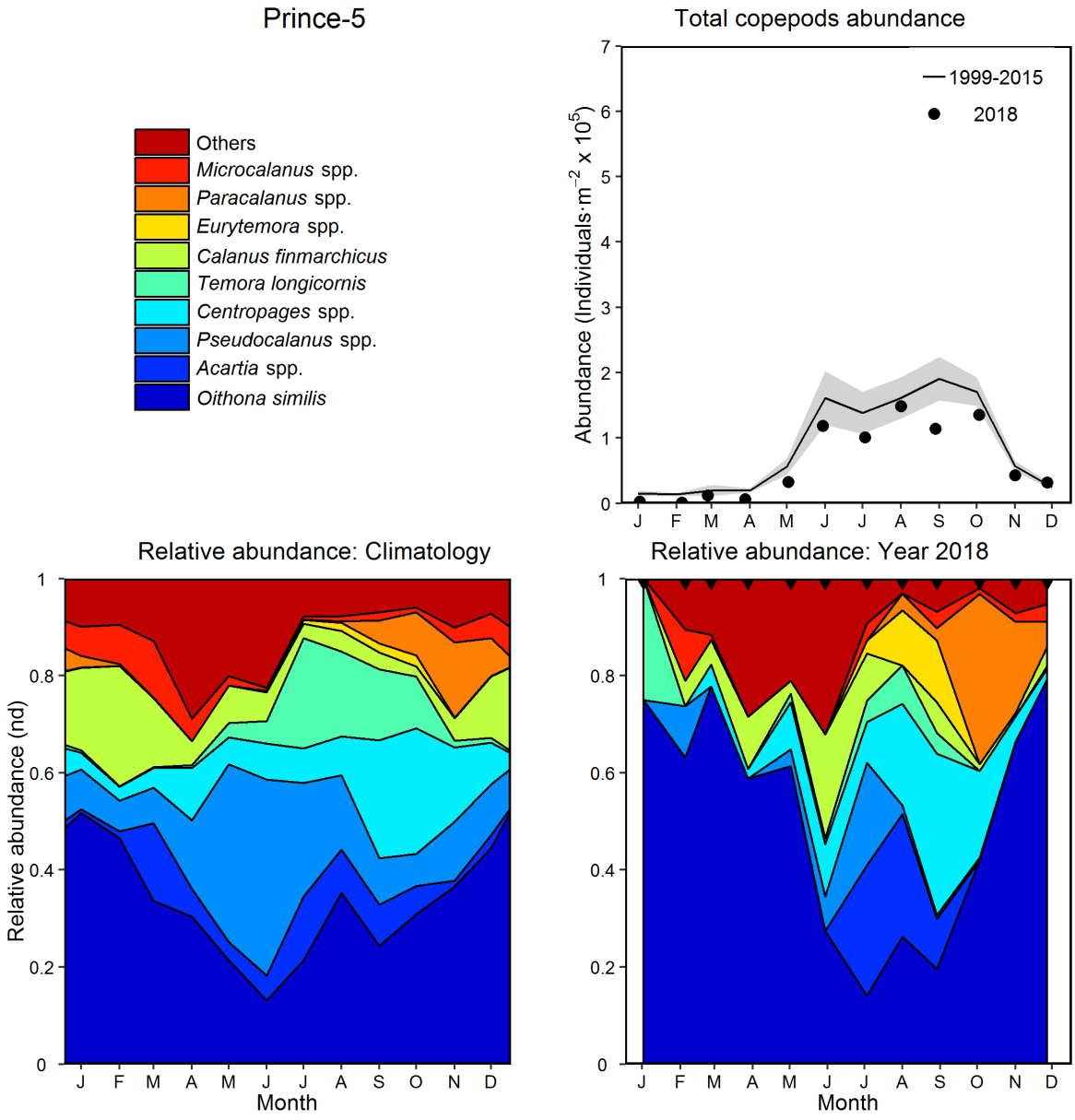

Figure 24b. Seasonal variability of dominant copepods at Prince-5. The top 95% of identified copepod taxa by abundance, 1999–2015, are shown individually; others, including unidentified copepods (mostly nauplii) are grouped as "others." Upper right panel: copepod abundance in 2018 (solid circle) and mean conditions, 1999–2015 (solid line). The gray shaded area represents the standard error of the monthly means. Lower left panel: climatology of copepod relative abundances, 1999–2015. Lower right panel: copepod relative abundances in 2018. nd = no dimensions. Black triangles in the bottom right panel indicate sampling dates.

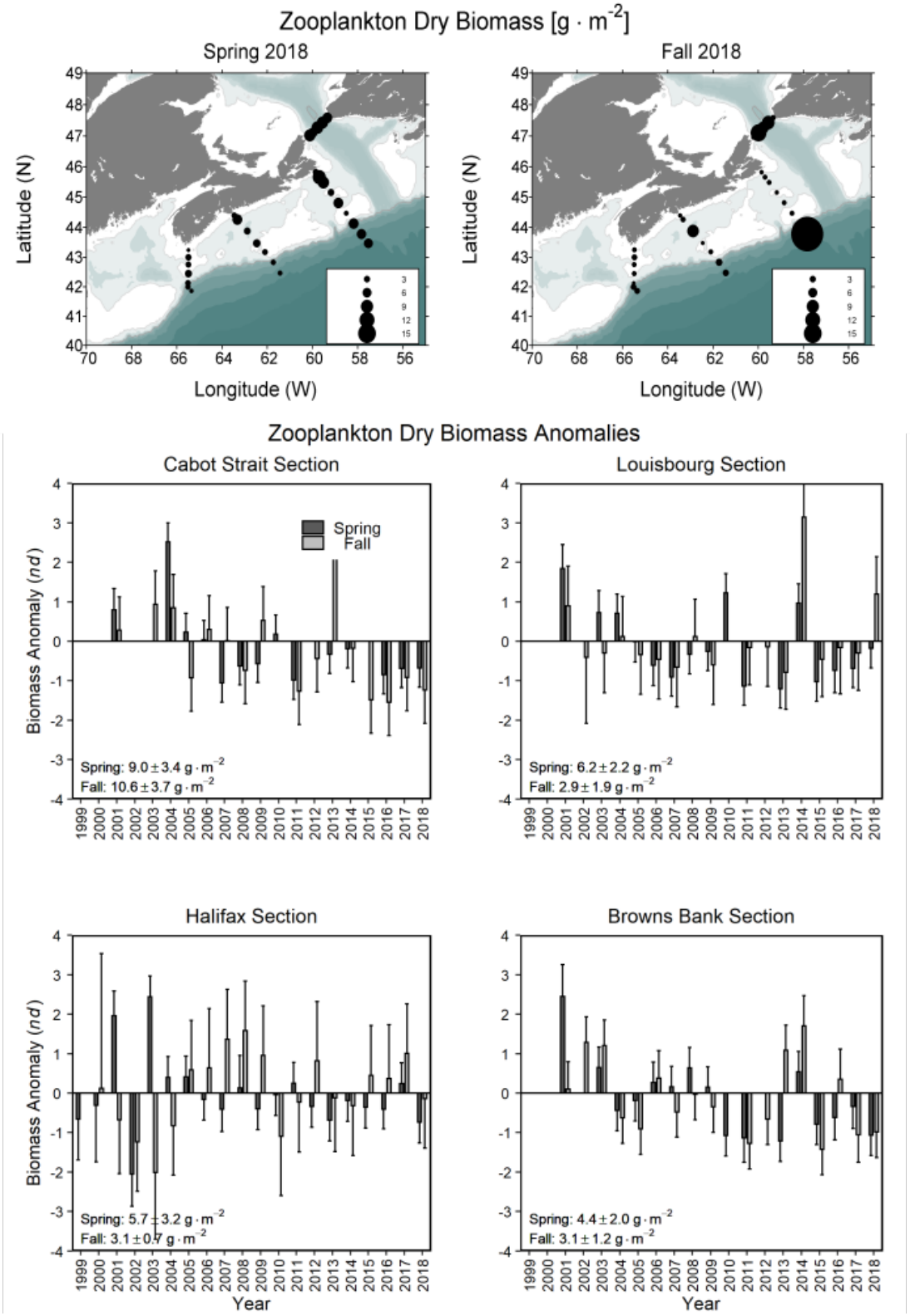

Figure 25. Spatial distribution of zooplankton dry biomass in 2018 (upper panels) and time series of zooplankton dry biomass anomalies on Scotian Shelf sections (middle and lower panels) in spring and fall, 1999–2018. Vertical lines in lower panels represent standard errors.

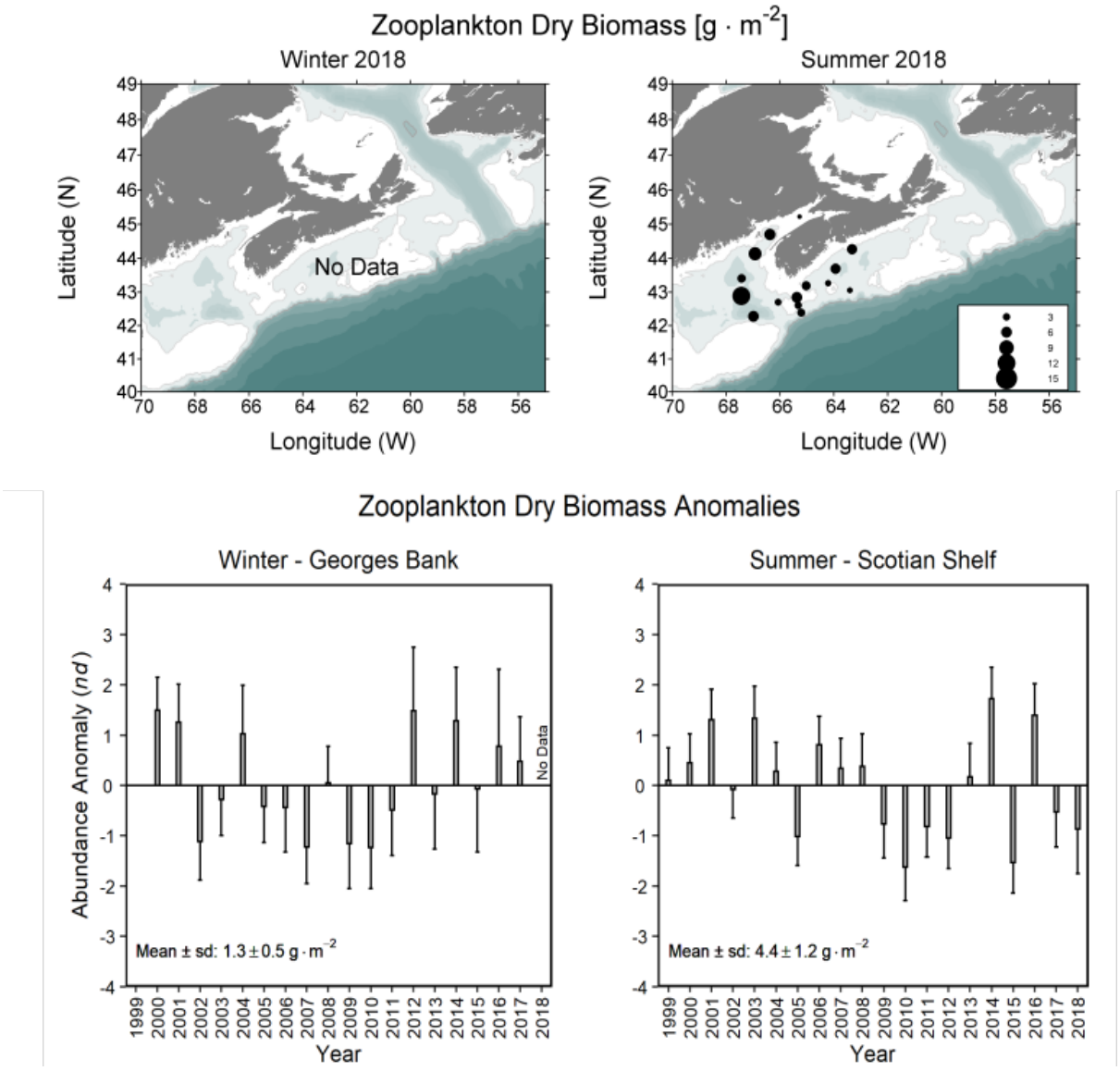

Figure 26. Spatial distribution of zooplankton dry biomass in 2018 (upper panels) and time series of zooplankton dry biomass anomalies (lower panels) from ecosystem trawl surveys on Georges Bank (winter) and the Scotian Shelf and eastern Gulf of Maine (summer), 1999–2018. Vertical lines in lower panels represent standard errors.

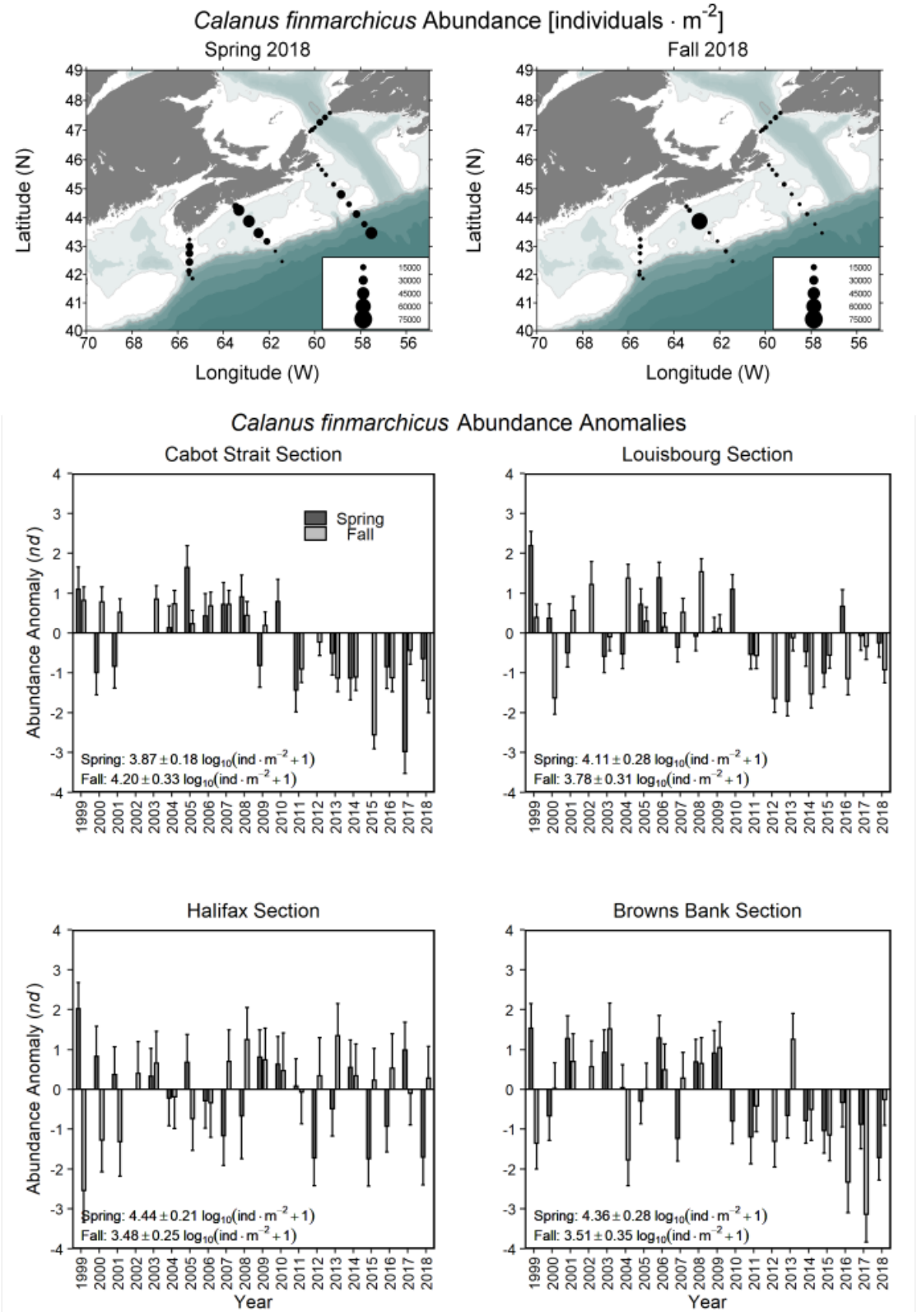

Figure 27. Spatial distribution of Calanus finmarchicus abundance in 2018 (upper panels) and time series of C. finmarchicus abundance anomalies on Scotian Shelf sections (middle and lower panels) in spring and fall, 1999–2018. Vertical lines in lower panels represent standard errors.

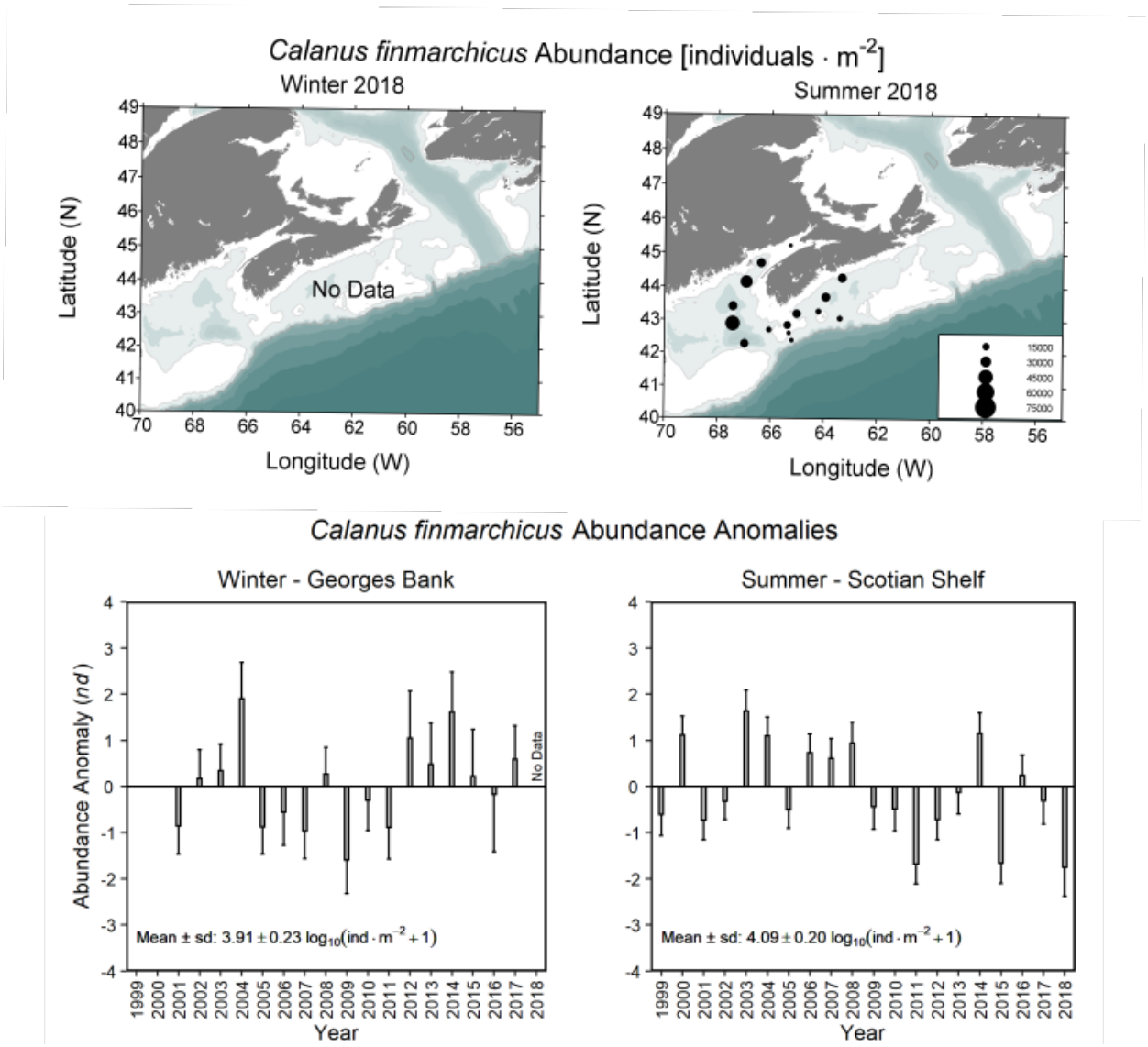

Figure 28. Spatial distribution of Calanus finmarchicus abundance in 2018 (upper panels) and time series of C. finmarchicus abundance anomalies (lower panels) from ecosystem trawl surveys on Georges Bank (winter) and the Scotian Shelf and eastern Gulf of Maine (summer), 1999–2018. Vertical lines in lower panels represent standard errors.

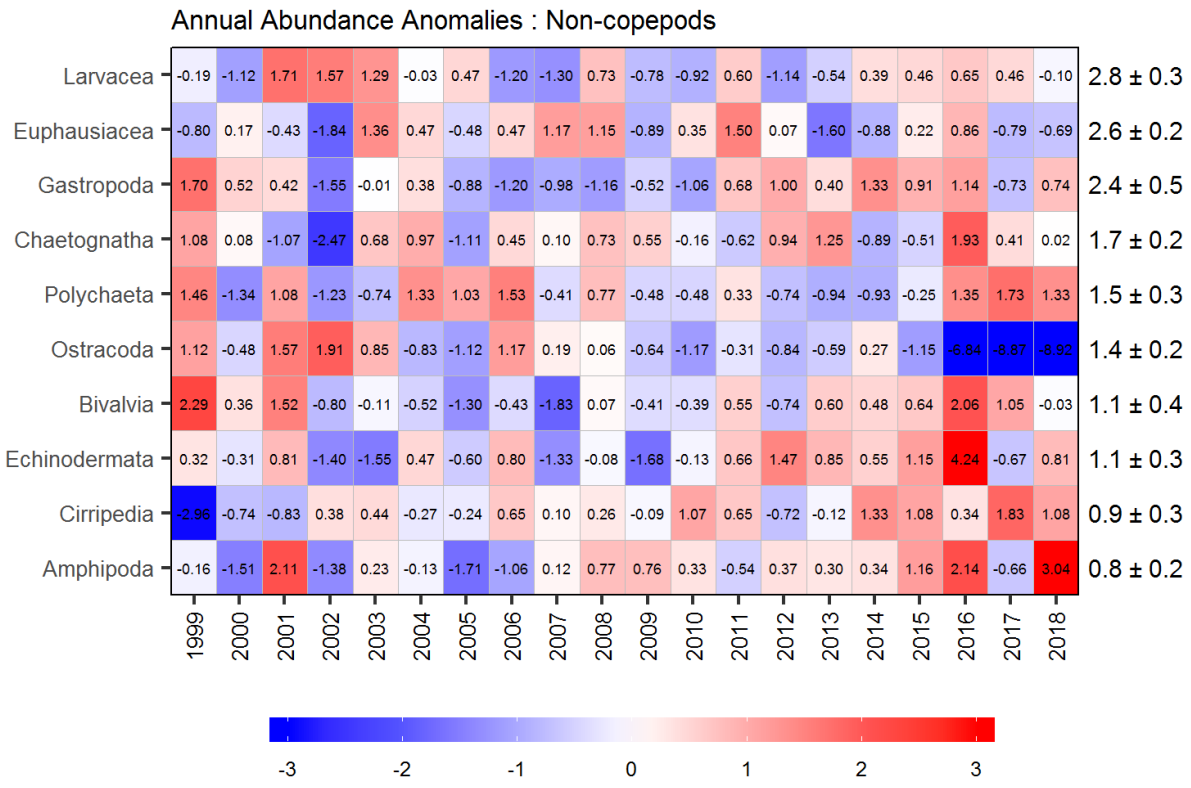

Figure 29. Annual anomaly scorecard for non-copepod group abundances on the Scotian Shelf sections, ordered from higher to lower abundance groups. Values in each cell are anomalies from the mean for the reference period, 1999–2015, in standard deviation (sd) units (mean and sd listed at right). A grey cell indicates missing data. Red (blue) cells indicate higher (lower) than normal abundance levels.

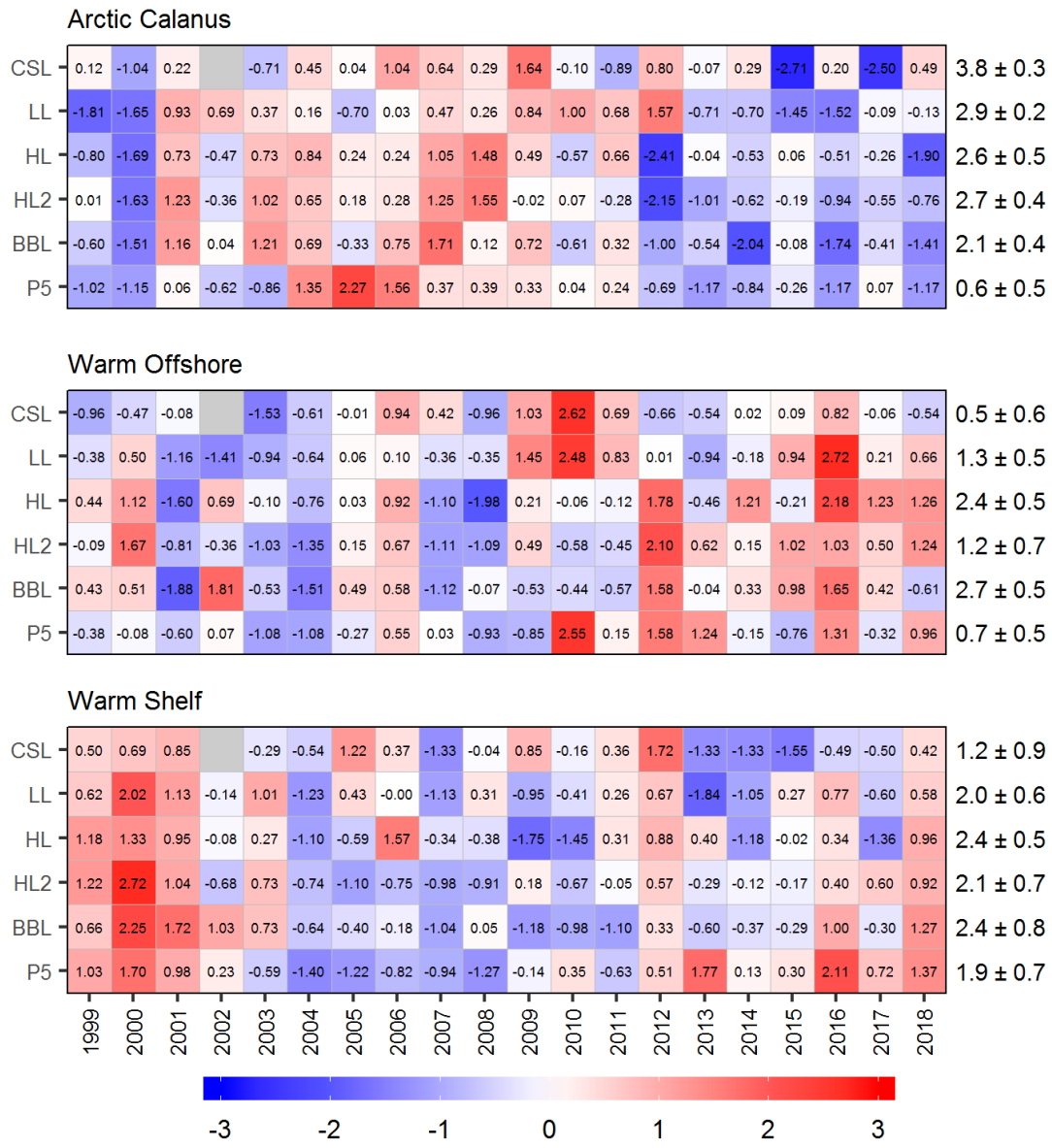

Figure 30. Annual anomaly scorecard for copepod indicator species group abundances. Values in each cell are anomalies from the mean for the reference period, 1999–2015, in standard deviation (sd) units (mean and sd listed at right). A grey cell indicates missing data. Red (blue) cells indicate higher (lower) than normal abundance levels. CSL: Cabot Strait section; LL: Louisbourg section; HL: Halifax section; HL2: Halifax-2; BBL: Browns Bank section; P5: Prince-5.

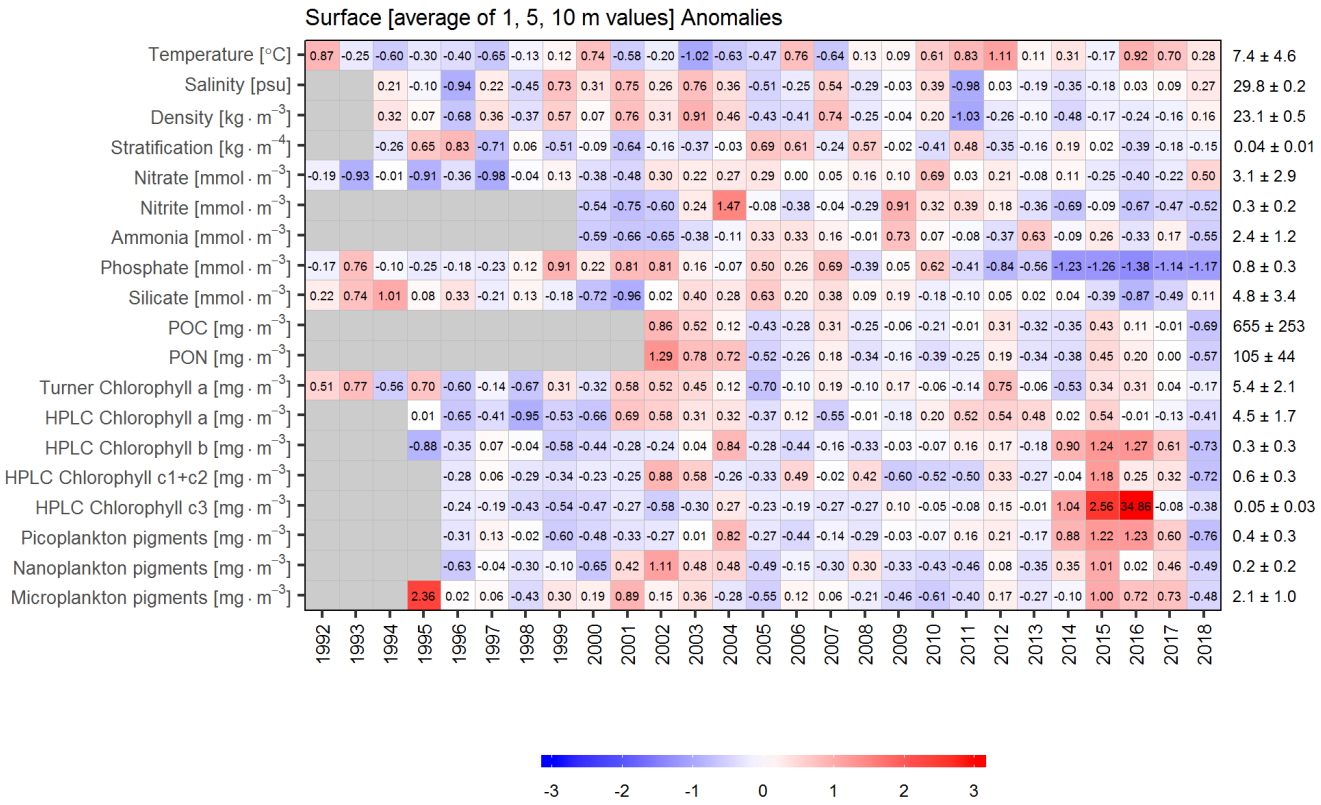

Figure 31. Annual anomaly scorecard for environmental and phytoplankton conditions at 2, 5, and 10 m in Bedford Basin. Values in each cell are anomalies from the mean for the reference period, 2000–2015, in standard deviation (sd) units (mean and sd listed at right). A grey cell indicates missing data. Red (blue) cells indicate higher (lower) than normal abundance levels.

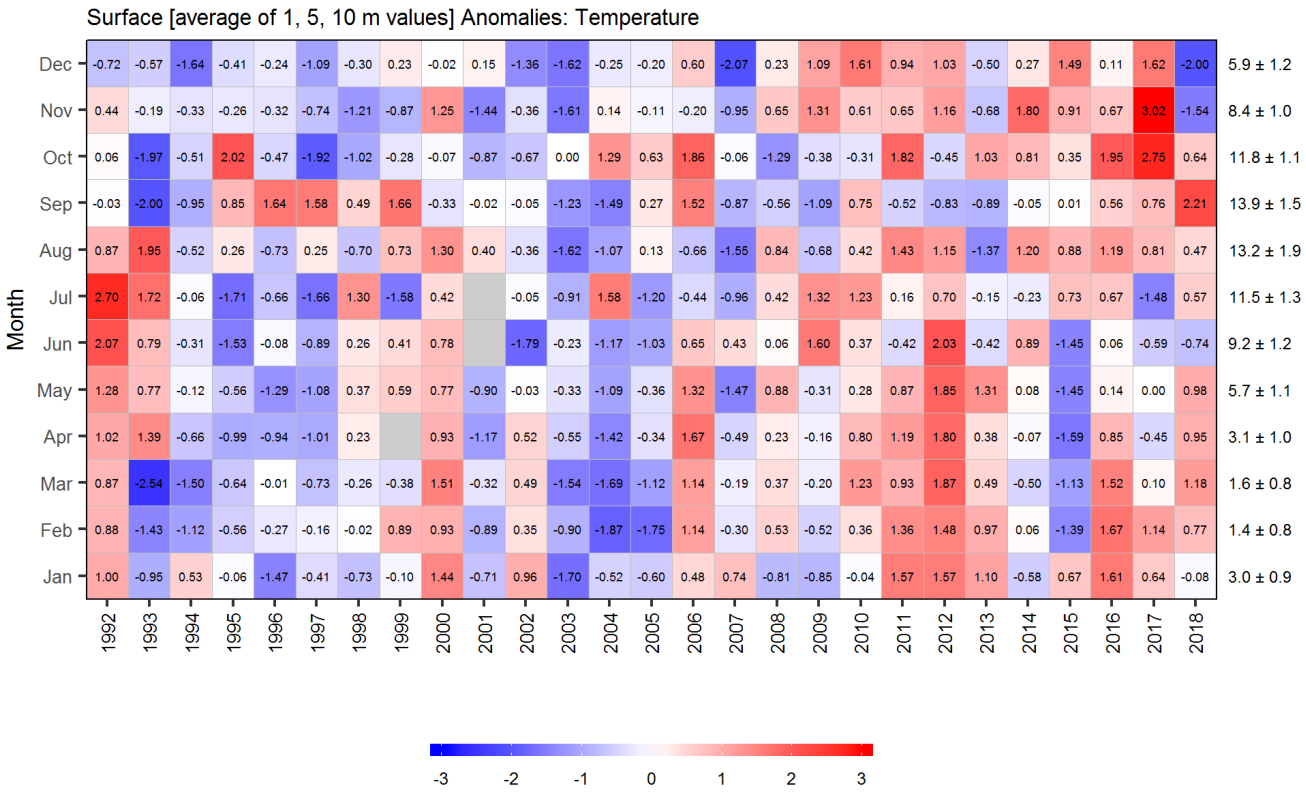

Figure 32. Average monthly temperature anomalies at 2, 5, and 10 m in Bedford Basin. Values in each cell are anomalies from the monthly means for the reference period, 2000–2015, in standard deviation (sd) units (mean and sd listed at right). A grey cell indicates missing data. Red (blue) cells indicate higher (lower) than normal abundance levels.

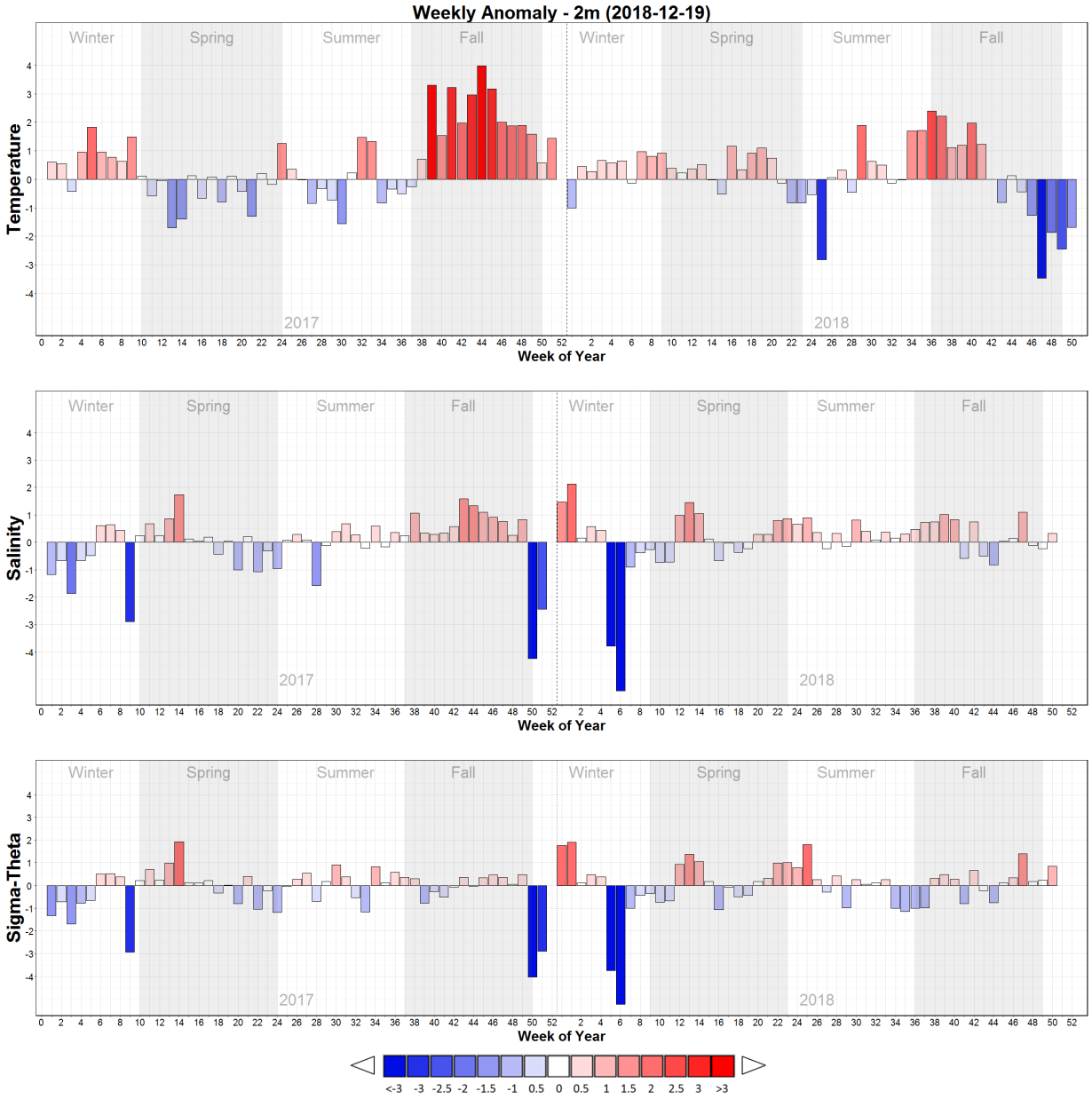

Figure 33. Weekly bottom temperature, salinity and density anomalies in Bedford Basin. Values are anomalies from the weekly mean for the reference period, 2000–2015, in standard deviation (sd) units (mean and sd listed at right). A grey cell indicates missing data. Red (blue) cells indicate higher (lower) than normal abundance levels.

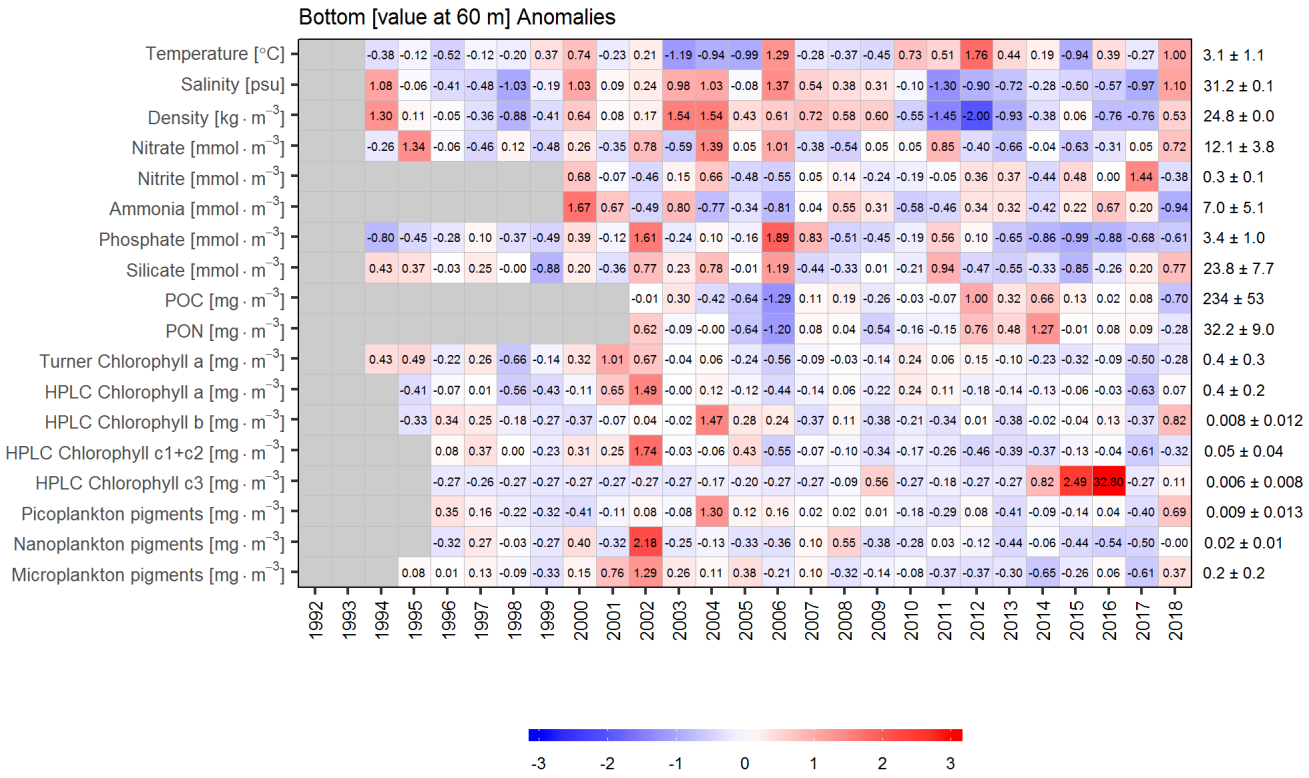

Figure 34. Annual anomaly scorecard for environmental and phytoplankton conditions at 60 m in Bedford Basin. Values in each cell are anomalies from the mean for the reference period, 2000–2015, in standard deviation (sd) units (mean and sd listed at right). A grey cell indicates missing data. Red (blue) cells indicate higher (lower) than normal abundance levels.

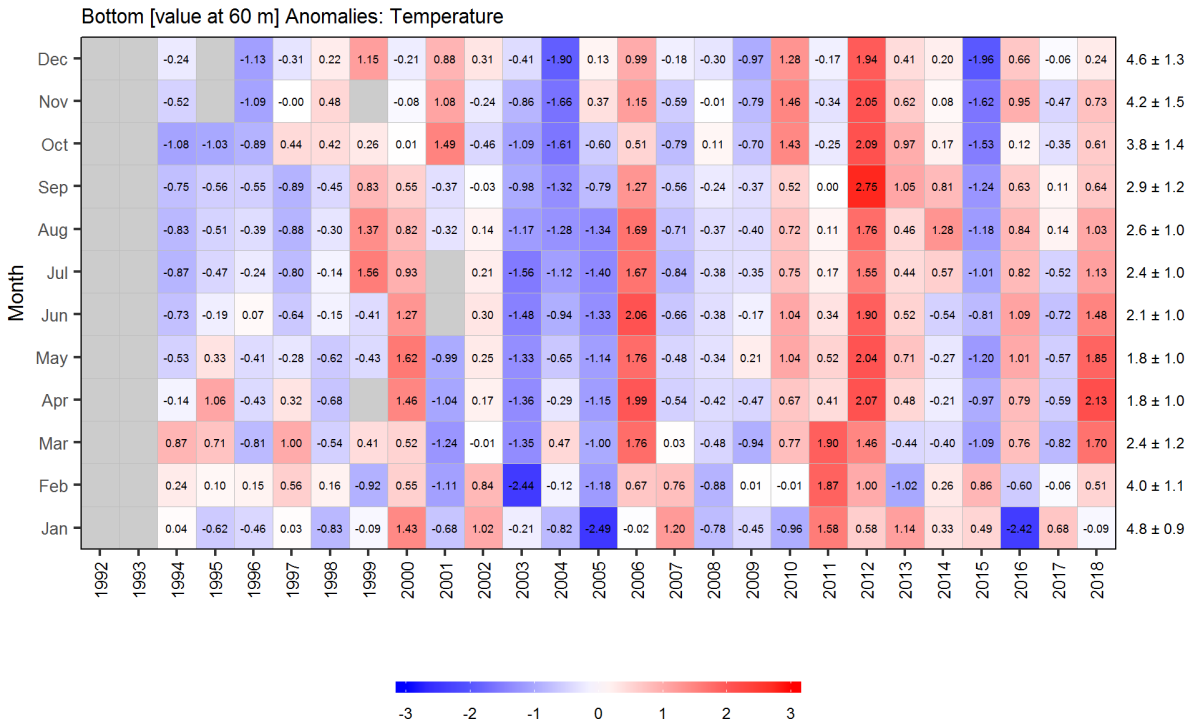

Figure 35. Bottom monthly temperature anomalies at 60 m in Bedford Basin. Values in each cell are anomalies from the monthly means for the reference period, 2000–2015, in standard deviation (sd) units (mean and sd listed at right). A grey cell indicates missing data. Red (blue) cells indicate higher (lower) than normal abundance levels.

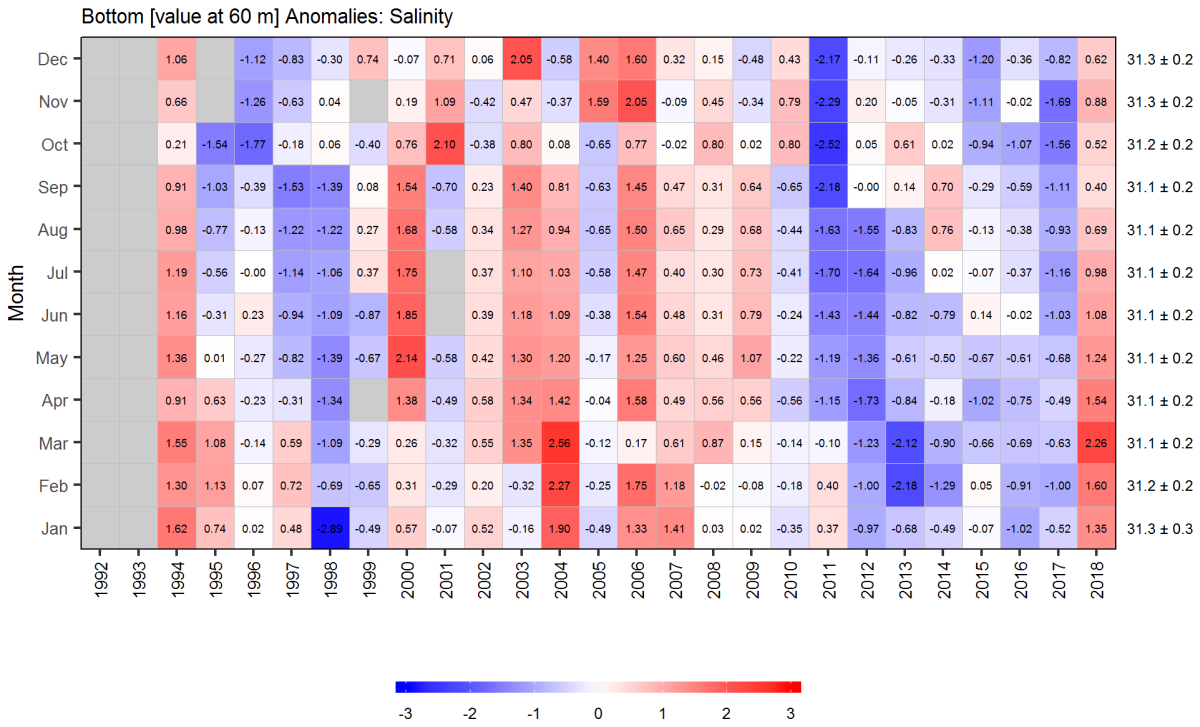

Figure 36. Bottom monthly salinity anomalies at 60 m in Bedford Basin. Values in each cell are anomalies from the monthly means for the reference period, 2000–2015, in standard deviation (sd) units (mean and sd listed at right). A grey cell indicates missing data. Red (blue) cells indicate higher (lower) than normal abundance levels.

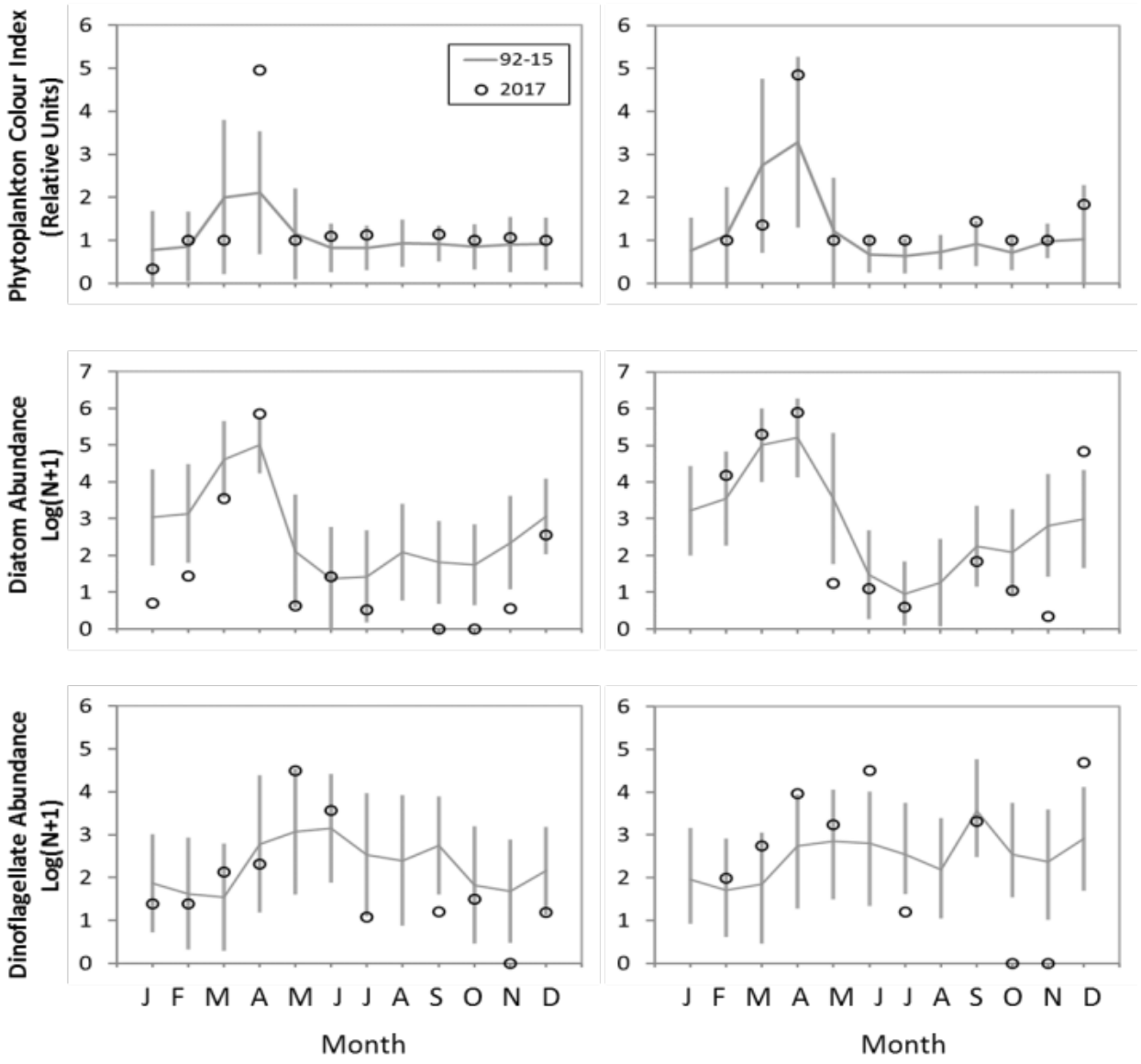

Figure 37. Continuous Plankton Recorder (CPR) phytoplankton abundance indices in 2017 and mean conditions, 1992–2015 (solid line) on the Western Scotian Shelf (left-hand column) and Eastern Scotian Shelf (right-hand column). Vertical lines show the standard deviations of the monthly averages.

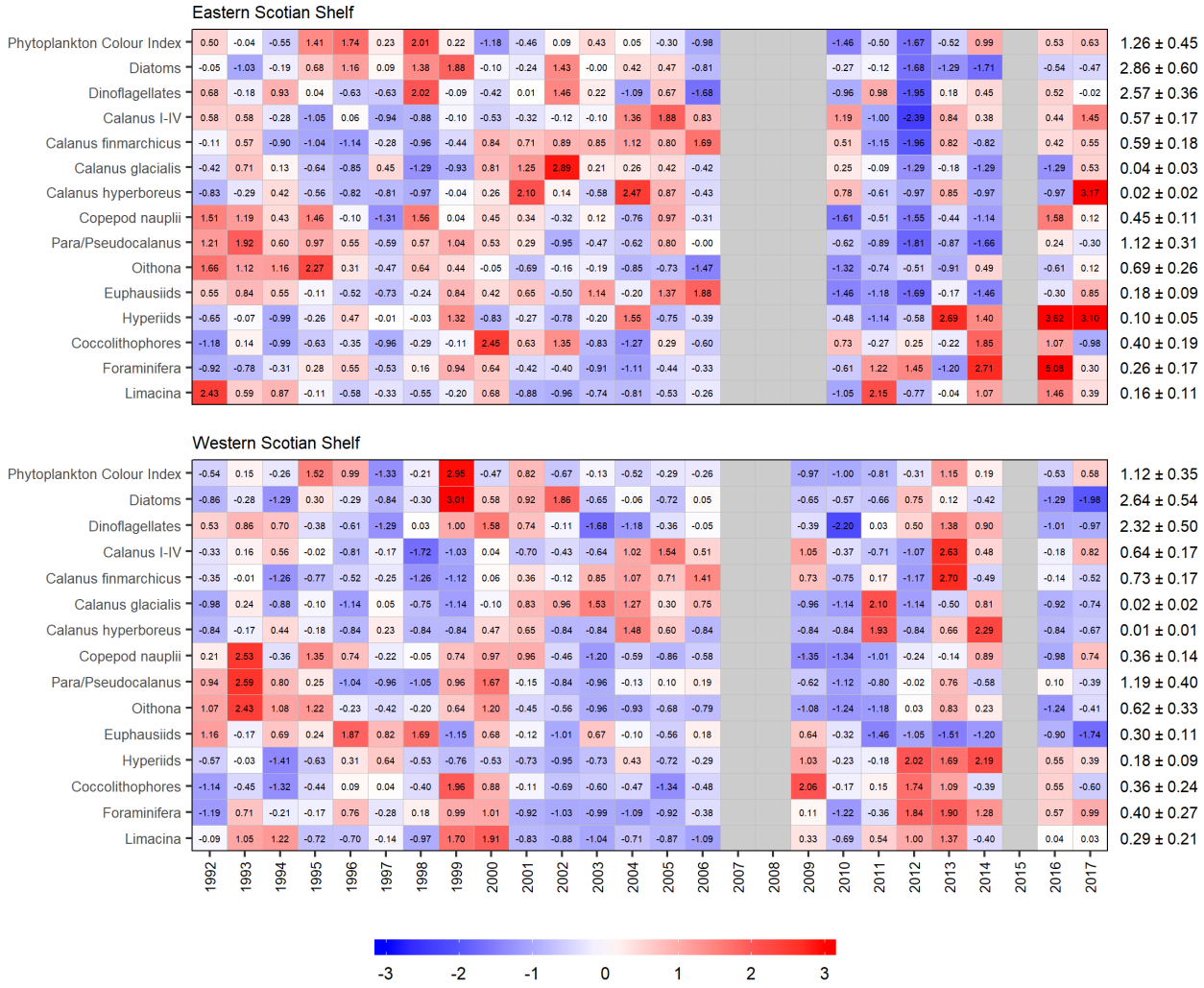

Figure 38. Annual anomaly scorecard for the abundances of phytoplankton and zooplankton taxa observed with the Continuous Plankton Recorder (CPR) on the Eastern Scotian Shelf (upper panel) and Western Scotian Shelf (lower panel). Blank cells correspond to years where either there was sampling in 8 or fewer months, or years where there was a gap in sampling of 3 or more consecutive months. Red (blue) cells indicate higher (lower) than normal values. The reference period is 1992–2015. The numbers in the cells are the standardised anomalies.

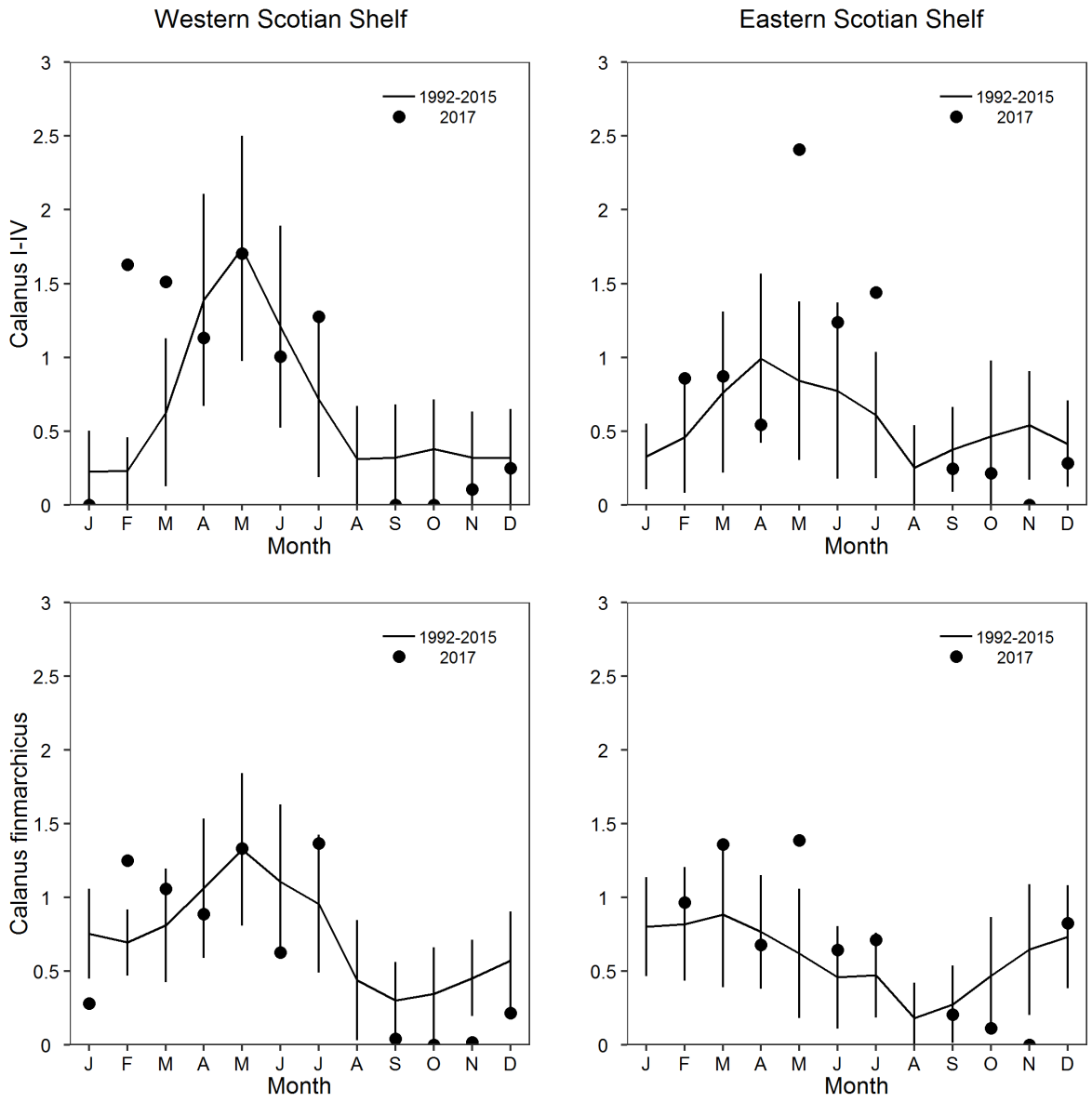

Figure 39. CPR abundance indices for Calanus I–IV (mostly Calanus finmarchicus, upper row) and C. finmarchicus V–VI (lower row) in 2017 and mean conditions, 1992–2015 (solid line) on the Western Scotian Shelf (left-hand column) and Eastern Scotian Shelf (right-hand column). Vertical lines represent standard deviations of the monthly averages.